

Acoustofluidics 2014



Book of Abstracts

Started in 2003 and originally called USWNet, the Acoustofluidics conference series offers an annual international meeting place for researchers interested in all aspects of ultrasound in microfluidics. It covers topics including ultrasonic standing wave technology and surface acoustic wave devices for particle, bubble and fluid manipulation, and ranges from fundamental theory and physics to biomedical and industrial applications. In 2014 there will be attendees from Australia, Denmark, England, France, Germany, Italy, Japan, the Netherlands, Scotland, Spain, Sweden, Switzerland and the United States of America.

Organising Committee:

Adrian Neild, Monash University

Thomas Franke, University of Glasgow

Scientific Committee:

Henrik Bruus, Technical University of Denmark

Jurg Dual, ETH Zurich

Thomas Franke, University of Glasgow

Peter Glynne-Jones, University of Southampton

Itziar Gonzalez, CSIC

Jeremy Hawkes, University of Manchester

Martyn Hill, University of Southampton

Thomas Laurell, Lund University

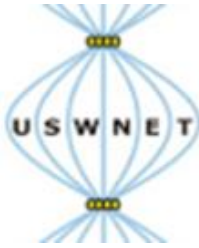
Andreas Lenshof, Lund University

Adrian Neild, Monash University

Johan Nilsson, Lund University

Stefan Radel, TU Wien

Martin Wiklund, Royal Institute of Technology (KTH)



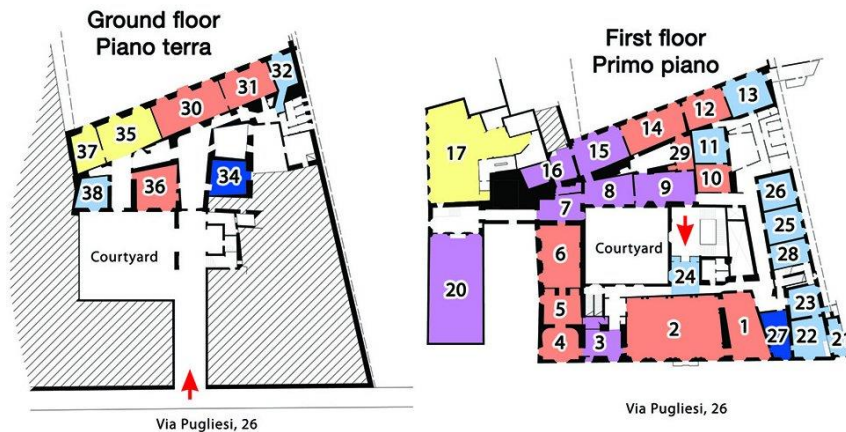
Acoustofluidics 2014

MONASH University

Conference Program

Venue: Monash University Prato Centre, Palazzo Vaj, Via Pugliesi 26, Prato

Presentations will be held in the Sala Veneziana (Room 6), poster sessions will be in Rooms 4 and 5.



Time	Thursday 11 th September
10.30	USWnet Management Meeting (open to all who are interested) – Room 15
13.00	Conference Opening
13.05 - 13.45	Keynote Lecture – Jonathan Cooper Fluidic microcircuits using Phononic Lattices and Surface Acoustic Waves University of Glasgow
	Session 1: Biological Applications
13.50 - 14.10	3D Cell Culture Using a Temperature Controlled Ultrasound Actuated Multi-Well Chip Device Mathias Ohlin, Athanasia E. Christakou, Björn Önfelt, Martin Wiklund Royal Institute of Technology (KTH)
14.10 - 14.30	Removal of proteins from blood using acoustophoresis Andreas Lenshof, Maria Tenje, Maria N. Lundgren, Ann-Margret Svärd-Nilsson, Jens Kjeldsen-Kragh, Lena Åberg and Thomas Laurell Lund University
14.30 - 14.50	Engineering composite tissue sheets with acoustic levitation Angela Tait, Peter Glynn-Jones, Emily Swindle, Adam Fisher, Martin Grossel, Martyn Hill, and Donna Davies University of Southampton
14.50 - 15.10	On-Chip Ultrasonic Sample Preparation For DNA-Based Diagnostics Ida Iranmanesh, Harisha Ramachandriah, Mathias Ohlin, Aman Russom, and Martin Wiklund Royal Institute of Technology (KTH)

15.10 - 15.30	Coffee and Posters
Session 2: Modelling and Numerical Analysis	
15.30 – 15.50	Thermoviscous theory of ultrasound scattering on microparticles and droplets Jonas T. Karlsen, Mads J. H. Jensen, and Henrik Bruus Technical University of Denmark
15.50 - 16.10	Effects of surface profile on a boundary-driven acoustic streaming field Junjun Lei, Martyn Hill, and Peter Glynne-Jones University of Southampton
16.10 - 16.30	Numerical analysis of particles undergoing acoustophoresis in a PDMS channel driven by surface acoustic waves Nitesh Nama, R. Barnkob, C. J. Kähler, F. Costanzo, and T. J. Huang The Pennsylvania State University
16.30 - 16.50	Hydrodynamic interactions in microfluidic acoustophoresis at high particle concentrations Mikkel W. H. Ley and Henrik Bruus Technical University of Denmark
16.50 - 17.00	Coffee Break
Session 3: Acoustic Microbubbles	
17.00 – 17.25	Invited Lecture – Michel Versluis StemBells: a novel stem cell delivery platform using microbubbles and acoustic radiation force University of Twente
17.25- 17.45	Sono-optical tweezers: an instrument for microbubble characterisation Gianluca Memoli, Chris Fury National Physical Laboratory, University College London
17.45 - 18.05	Acoustic bubble sorting for ultrasound contrast agent enrichment Tim Segers, Michel Versluis, University of Twente
18.05 – 18.25	Live demonstration: Some acoustic properties of cooked spaghetti Jeremy J Hawkes, Jorge A Yescas Hernandez, Sara Baldock, Kenji Yasuda University of Manchester, Tokyo Medical and Dental University
19.00	Conference Banquet, Ristorante Tonio



Time	Friday 12 th September
	Session 4: Droplets
9.00 - 9.20	On-Chip Biochemistry: Droplet Generation and Merging Adrian Neild, Monash University
9.20 – 9.40	Ultrasonic Atomization of sessile drop in an Acoustic levitator Marina Reissenweber, Gerhard Lindner Coburg University
9.40 – 10.00	Droplet handling with acoustophoresis in bulk acoustic wave devices Peter Reichert, Ivo Leibacher, and Jürg Dual ETH Zurich
10.00 – 10.30	Coffee and Posters
10.30 – 11.10	Keynote Lecture – James Friend Beyond SAW in Acoustic Microfluidics RMIT University
	Session 5: SAW Technologies
11.10 - 11.30	Towards high efficient SAW-based microfluidic actuators Raimund Brüning, Andreas Winkler, Florian Kiebert, and Hagen Schmidt IFW Dresden
11.30 - 11.50	Interaction-free phononic crystal droplet sensing for portable surface acoustic-wave driven microfluidic devices M. Agostini, M. Travagliati, G. De Simoni, R. J. Shilton, V. Piazza, M. Cecchini Scuola Normale Superiore and Istituto, Istituto Italiano di Tecnologia
11.50 - 12.10	SAW-based fluid atomization using mass-producible chip devices Andreas Winkler, Stefan Harazim, and David J. Collins IFW Dresden, Monash University
12.10 - 12.55	Lunch
	Session 6: SAW Devices
12.55 – 13.20	Invited Lecture – Richie Shilton Ultra high frequency surface acoustic wave driven microfluidics Istituto Italiano di Tecnologia
13.20 – 13.40	Acoustic and dielectrophoretic particle sorting using virtual deterministic lateral displacement (vDLD) David J Collins, Tuncay Alan and Adrian Neild Monash University
13.40 - 14.00	Combined acoustic torques and forces on spherical particles obtained by the leakage of two standing orthogonal surface acoustic waves Janis Bernard, Philippe Marmottant, David Rabaud, Cédric Poulain, and Pierre Thibault Univ. Grenoble Alpes
14.20 - 14.40	Cell and droplet sorting with surface acoustic waves Thomas Franke University of Glasgow
14.40 - 15.10	Coffee Break

Session 7: Particle Manipulation	
15.10 - 15.30	<p>Cell trapping on acoustofluidic edge structures</p> <p>Ivo Leibacher and Jürg Dual ETH Zurich</p>
15.30 - 15.50	<p>Engineering single-vortex acoustic streaming for sub-micrometer particle handling</p> <p>P. B. Muller, M. Antfolk, P. Augustsson, T. Laurell, and H. Bruus Technical University of Denmark, Lund University</p>
15.50 - 16.10	<p>Efficiency Assessment of Acoustic Solid-Particle Separation in Gases</p> <p>Ramin J. Imani, Etienne Robert Royal Institute of Technology (KTH), Polytechnique Montréal</p>
16.10 – 16.30	<p>A novel combination of an optical trap with an acoustofluidic device to provide direct acoustic force measurements</p> <p>Andreas Lamprecht, Stefan Lakämper, Iwan Schaap, and Jurg Dual ETH Zurich, Georg-August Universität</p>
16.30 – 16.50	<p>Acoustic trapping for sepsis diagnosis using MALDI-MS</p> <p>B. Hammarström, B. Nilson, T. Laurell, J. Nilsson and S. Ekström Lund University, Dongguk University</p>
16.50 – 17.10	<p>SAW induced particle deflection in a microchannel using PDMS posts</p> <p>Richard Rambach and Thomas Franke University of Glasgow, Augsburg University</p>
17.10 – 17.15	Announcing “Acoustofluidics 2015” and closing remarks

13.00	Conference Opening
13.05 - 13.45	Keynote Lecture – Jonathan Cooper Fluidic microcircuits using Phononic Lattices and Surface Acoustic Waves University of Glasgow
	Session 1: Biological Applications
13.50 - 14.10	3D Cell Culture Using a Temperature Controlled Ultrasound Actuated Multi-Well Chip Device Mathias Ohlin, Athanasia E. Christakou, Björn Önfelt, Martin Wiklund Royal Institute of Technology (KTH)
14.10 - 14.30	Removal of proteins from blood using acoustophoresis Andreas Lenshof, Maria Tenje, Maria N. Lundgren, Ann-Margret Svärd-Nilsson, Jens Kjeldsen-Kragh, Lena Åberg and Thomas Laurell Lund University
14.30 - 14.50	Engineering composite tissue sheets with acoustic levitation Angela Tait, Peter Glynn-Jones, Emily Swindle, Adam Fisher, Martin Grosse, Martyn Hill, and Donna Davies University of Southampton
14.50 - 15.10	On-Chip Ultrasonic Sample Preparation For DNA-Based Diagnostics Ida Iranmanesh, Harisha Ramachandriah, Mathias Ohlin, Aman Russom, and Martin Wiklund Royal Institute of Technology (KTH)

Fluidic microcircuits using Phononic Lattices and Surface Acoustic Waves

Jonathan M. Cooper¹

¹ School of Engineering
University of Glasgow,
G12 8LT
Scotland
Email: Jon.Cooper@glasgow.ac.uk

The development of point of care systems is often constrained by the integration of different technologies involved in sample preparation, amplification and detection. Surface acoustic wave (SAW) devices have previously shown some promise in sample manipulation, although designing complex fluid manipulations involves using mixed acoustic signals with multiple transducers.

We now demonstrate a new and simple interface between a low cost SAW device and a disposable chip, involving a new concept in microfluidics using phononic metamaterial as acoustic holograms. Further, we demonstrate the application of this new technology in a number of analytical procedures, including e.g., the implementation of digital microfluidics. We show how to create a "tool-box" of different diagnostic functions each of which requires a different phononic structure, and demonstrate the concept of using these methods to deliver integrated Nucleic Acid Testing using PCR amplification for malaria in blood and STI diagnosis from swabs.

Just as in electronics, where discrete components are combined to create a circuit, so we will use different combinations of phononic lattices to create fluidic microcircuits, each of which provides a unique diagnostic function.

3D Cell Culture Using a Temperature Controlled Ultrasound Actuated Multi-Well Chip Device

Mathias Ohlin¹, Athanasia E. Christakou¹, Björn Önfelt^{1,2}, Martin Wiklund¹

¹Department of Applied Physics
Royal Institute of Technology
KTH - Albanova
SE-10691 Stockholm, Sweden
Email: mathias.ohlin@biox.kth.se
URL: www.biox.kth.se

²Department of Microbiology, Tumor and Cell Biology
Karolinska Institute
SE-17177 Stockholm, Sweden

Introduction

3D cell culture systems are an important part of both organs-on-chips and human-on-chips [1]. Both of these on-chips solutions have potential to revolutionize the drug testing industry and eventually replace animal testing altogether. Furthermore, 3D culture of solid tumors can be particularly important for cancer drug screening [2] and potentially for cancer diagnosis. In this paper we present a novel method to form many 3D spheroids in parallel using ultrasound.

Experiment

The multi-well chip device [3-5] was placed inside a small tabletop cell incubator for maintaining the correct CO₂ and humidity levels. The temperature in the multi-well device was regulated using an in-house built liquid heat exchanger capable of both cooling and heating, see Fig. 1. Human hepatocellular carcinoma (HCC) HepG2 cells as well as fibroblasts were used as cell models. 3D solid spheroids were formed with both cell models using the ultrasound actuated multi-well device, see Fig. 2B dashed circle. Two different microscope systems were employed: confocal and bright field. The resulting images were analyzed using MATLAB to calculate tumor size (projected area) and fluorescence intensity of the viability probe calcein-AM (from the surface towards the center). Furthermore, experiments without ultrasound actuation were performed for both cell models with the multi-well device.

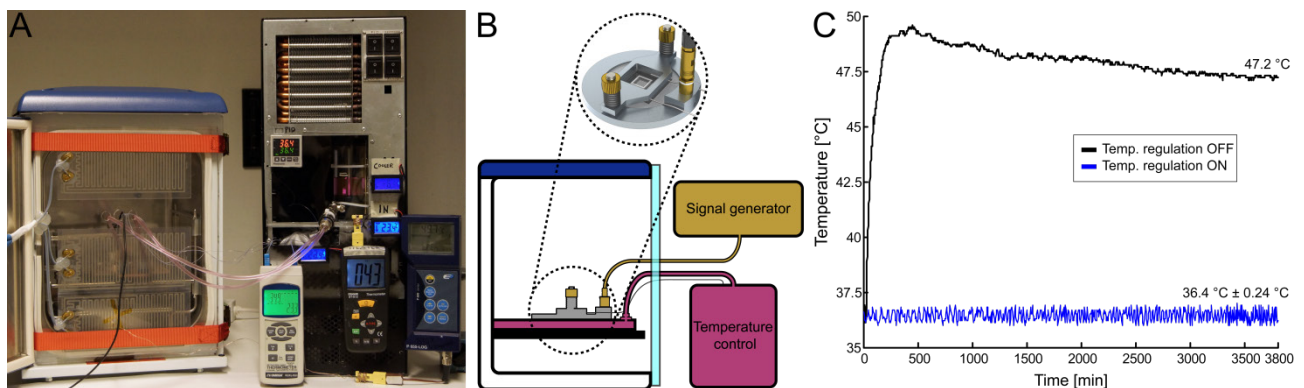


Fig. 1. (A) Photo of the experimental setup with the cell incubator to the left and the temperature control and liquid heat exchanger to the right. (B) Sketch showing the different parts of the setup. The multi-well device can be seen in the dashed circle. The temperature inside the multi-well device is regulated by controlling the temperature on the pink-colored plate inside the incubator. Heat is conducted away from the multi-well device via the plate to the liquid heat exchanger. The device is driven using a signal generator and an RF amplifier here shown in gold color. The driving frequency is 1.96 MHz with frequency modulation (span 100 kHz, rate 1 kHz) and with an amplitude exceeding 100 V. (C) Shows the difference between temperature regulation ON and OFF. The regulation set-value was set to 36.4 °C. The temperature is measured on the multi-well chip using a thermocouple T-type probe.

Results

We show that 3D spheroids of HepG2 cells and fibroblasts were successfully formed during continuous ultrasound actuation, Fig. 2 (A and C). On the contrary, the same cells grow into monolayers (2D) without ultrasound actuation (Fig. 2B and D). Figure 2E show the multi-well chip and its 100 wells containing calcein-AM stained HepG2 cell aggregates after 7 days of continuous ultrasound exposure. Furthermore, Fig. 2F show the correlation between the penetration depths of the viability dye calcein-AM and three different manually sorted cell aggregate categories (data from Fig. 2E): Spheroids (59%), inconclusive (26%), and no spheroids (14%). Here, the length of each curve (up to 120 μm) corresponds approx. to the radius of the spheroid. When there are tight contacts formed between cells calcein cannot penetrate far into the spheroid, which we use as a spheroid formation indicator. The spheroid formation efficiency, i.e. how many spheroids out of the 100 wells that are formed, depends on which type of cells we use. For HepG2 cells we have a formation efficiency of 59% and for fibroblasts the efficiency is decreased to 22 % under the same approx. level of ultrasonic actuation. It is clear that fibroblasts are more difficult to persuade to form spheroids than HepG2 cells. One reason could be the different set of adhesion proteins fibroblasts have compared to HepG2 cells.

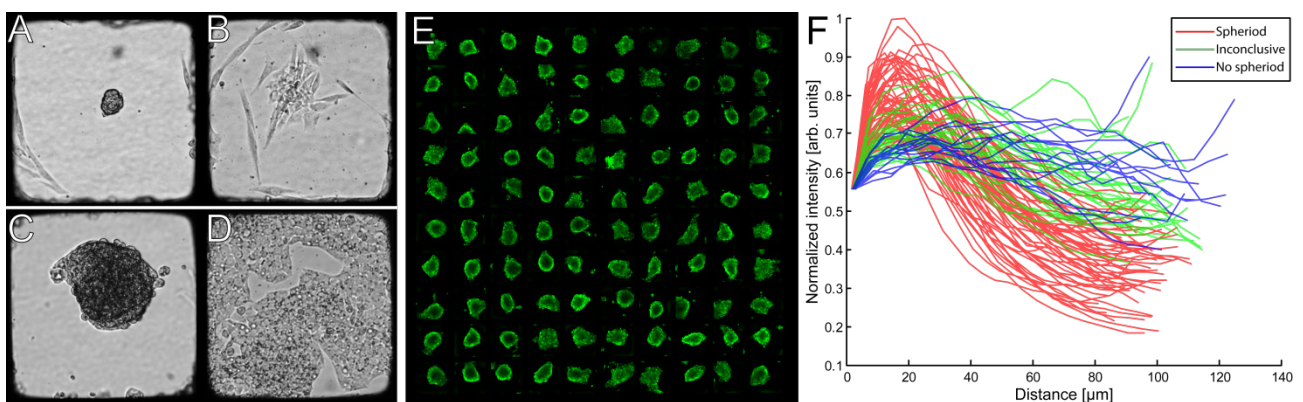


Fig. 2. (A) A typical example of a solid 3D spheroid of fibroblasts formed under the effect of ultrasound. (B) The same spheroid in (A) but 20 hours later without ultrasound actuation, the spheroid starts to grow in 2D. (C) When the ultrasound is turned ON the HepG2 cells form a solid tumor spheroid. (D) HepG2 cells grow in a 2D layer when the ultrasound is turned OFF. (E) Calcein-AM stained HepG2 cell aggregates after 7 days of continuous ultrasound exposure (average projected area of spheroids: $3 \cdot 10^4 \pm 5 \cdot 10^3 \mu\text{m}^2$). (F) Calcein-AM fluorescence intensity variations from the surface towards the center of each of the aggregates seen in (E).

Conclusion

We have demonstrated our temperature controlled multi-well device and the effective 3D growth of HepG2 cells and fibroblasts into cell spheroids, in parallel. These spheroids can be important in cancer research for example drug screening. Moreover, in the future our system could be a valuable part in the organ-on-chips and ultimately human-on-chips platforms.

References

- [1] D. Huh, G. A. Hamilton, and D. E. Ingber, "From 3D cell culture to organs-on-chips," *Trends Cell Biol.*, vol. 21, pp. 745-54, Dec 2011.
- [2] J. Haycock, "3D Cell Culture: A Review of Current Approaches and Techniques," in *3D Cell Culture*. vol. 695, J. W. Haycock, Ed., ed: Humana Press, 2011, pp. 1-15.
- [3] B. Vanherberghen, O. Manneberg, A. Christakou, T. Frisk, M. Ohlin, H. M. Hertz, B. Onfelt, and M. Wiklund, "Ultrasound-controlled cell aggregation in a multi-well chip," *Lab on a Chip*, vol. 10, pp. 2727-2732, 2010.
- [4] M. Ohlin, A. E. Christakou, T. Frisk, B. Onfelt, and M. Wiklund, "Influence of acoustic streaming on ultrasonic particle manipulation in a 100-well ring-transducer microplate," *Journal of Micromechanics and Microengineering*, vol. 23, Mar 2013.
- [5] A. E. Christakou, M. Ohlin, B. Vanherberghen, M. A. Khorshidi, N. Kadri, T. Frisk, M. Wiklund, and B. Onfelt, "Live cell imaging in a micro-array of acoustic traps facilitates quantification of natural killer cell heterogeneity," *Integr Biol (Camb)*, vol. 5, pp. 712-9, Apr 2013.



Removal of proteins from blood using acoustophoresis

Andreas Lenshof¹, Maria Tenje¹, Maria N. Lundgren², Ann-Margret Svärd-Nilsson², Jens Kjeldsen-Kragh², Lena Åberg² and Thomas Laurell¹

¹Department of Biomedical Engineering
Lund University
S-221 00 Lund, Sweden
Email: Andreas.Lenshof@bme.lth.se

²Division of Clinical Immunology and Transfusion Medicine
Skåne University Hospital
S-221 00 Lund, Sweden

This work presents the development of a miniaturised system developed for removing plasma proteins and other low-molecular-weight compounds from erythrocyte concentrate in a simple one-step-process using ultrasound in a microfluidic system.

Introduction

IgA is the dominating immunoglobulin in human external secretion with the role to protect us from bacterial and viral infections in the mucous lining of the mouth, eyes, airways, gastrointestinal tract and urinary tract. Individuals lacking IgA have a tendency to develop antibodies against IgA even without previous exposure to plasma IgA.¹ The presence of these antibodies is connected with high risk of severe, potentially life-threatening, anaphylactic transfusion reactions upon treatment with blood components containing IgA. There is therefore a need within the health care system to have access to IgA free blood components quickly and in abundance, especially to accommodate blood transfusions in acute situations when it is not possible to test for IgA deficiency of the patient. Currently used technique of washing red blood cells consists of repeated dilutions and centrifugation steps. It is a very time-consuming and labour intensive process. This work presents a lab-on-a-chip system utilizing integrated acoustophoresis to prepare IgA-free red blood cells in an efficient manner.

Experiment

A standard silicon wash chip with two inlets and two outlets was used (Figure 1).² Erythrocyte concentrate diluted 1:20 in NaCl entered through the side inlets at a flow rate of 100 $\mu\text{L}/\text{min}$ and clean SAGMAN solution used as wash buffer was injected through the centre inlet at 300 $\mu\text{L}/\text{min}$. The washed erythrocytes were recovered at 100 $\mu\text{L}/\text{min}$ through the centre outlet and the original plasma containing solution and additional SAGMAN solution was eluted at 300 $\mu\text{L}/\text{min}$ through the side outlets as waste. All fluid flows were controlled via a custom-made pressure driven system based on Sensirion flow sensors and a pressure control feedback loop. Besides the measuring of IgA protein, albumin was also measured as it is the most abundant protein in blood plasma.

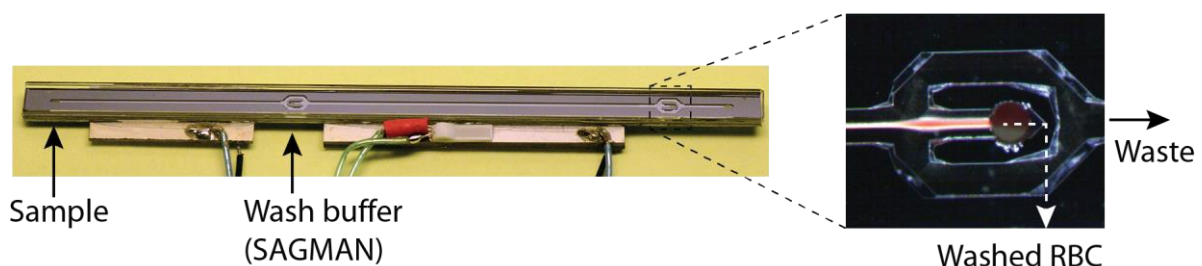


Figure 1. Picture of the wash chip. Wash buffer (SAGMAN solution) enters through the center inlet while blood sample enters through the side inlets. The acoustic standing wave transfers the RBCs from the original medium into the wash buffer in the center of the channel. The washed RBCs exit through the center outlet while the original medium with solved proteins exit through side outlets.

Results

The processed erythrocyte fractions were analysed by a Coulter Counter, and an erythrocyte recovery of 98% was achieved. This should be compared with the manual wash recovery which is about 92%. Further, the wash efficiency for albumin was 100% which can be seen in Figure 2. Also, the wash efficiency of IgA was shown to be in the same range as the manual wash (96% or higher). Preliminary data indicates that the wash efficiency of IgA is at a sufficient level from a clinical perspective and thus comparable to the manual centrifugal wash.

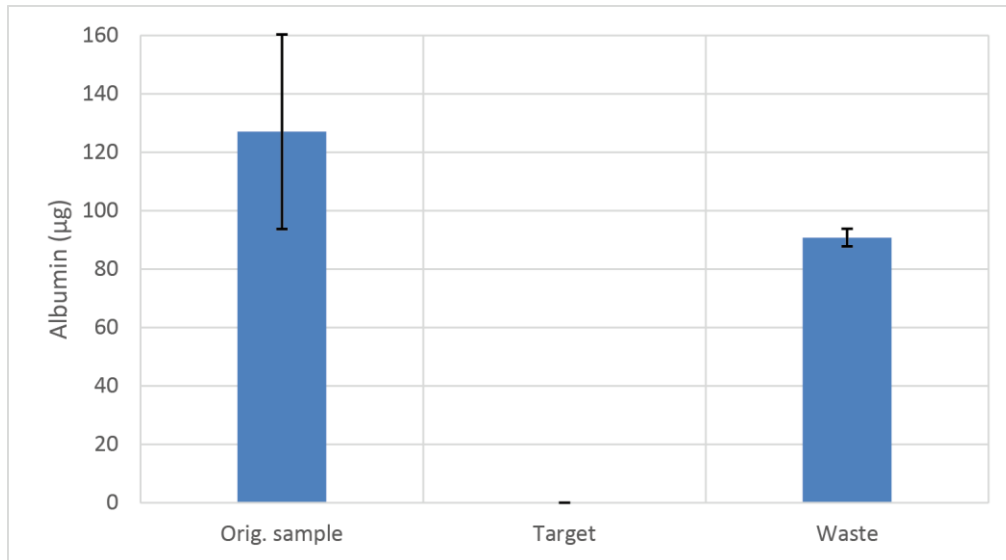


Figure 2. The wash efficiency of albumin.

Conclusion

Both the recovery of erythrocytes and the preliminary data on the wash efficiency of Albumin and IgA protein indicates the potential of acoustophoresis based cell wash for IgA depletion of blood samples. Previous findings also states that the use of acoustophoresis for cell manipulation does not harm the cells and show that it is a viable way of processing clinical samples.³

References

- [1]. SLIPI (Swedish physicians society for primary immune deficiency). http://www.slipi.nu/klinik/Riktlinjer_V4.pdf
- [2]. Augustsson, P., et al., *Microfluidic, label-free enrichment of prostate cancer cells in blood based on acoustophoresis*. Analytical Chemistry, 2012. **84**(18): p. 7954-62
- [3]. Burguillos, M.A., et al., *Microchannel acoustophoresis does not impact survival or function of microglia, leukocytes or tumor cells*. PLOS ONE, 2013. 8(5): p. e64233

Engineering composite tissue sheets with acoustic levitation

Angela Tait^{1*}, Peter Glynn-Jones^{2*},
Emily Swindle², Adam Fisher³, Martin Grosse³, Martyn Hill², and Donna
Davies¹

* These two authors have contributed equally to this work

¹ Brooke Laboratories, Clinical and Experimental Sciences, University of Southampton Faculty of Medicine, UK

² Engineering Science, Faculty of Engineering and the Environment, University of Southampton, UK

³ Chemistry, Faculty of Natural & Environmental Sciences, University of Southampton, UK

Email: P.Glynn-Jones@soton.ac.uk

Introduction

Creating layered constructs of human cells that mimic those found *in-vivo* in epithelial structures is challenging. Cell culture models are important in understanding the fundamentals of diseases as well as normal cellular physiology. We aim to create a multi-layered cell culture model to investigate the interactions of the different cells in the airways for a better insight into asthma.

Using thermo-responsive polymers to grow then subsequently release cell sheets for layering has previously been demonstrated with cardiomyocytes¹ [ref], however the process of detaching the layers has several drawback including the difficulty of detaching the more adherent epithelial cells, and the stresses induced in cells through this mechanical handling.

We demonstrate a new technique that takes advantage of the propensity of cells in a planar resonator to form sheets that are one cell in thickness, and investigate the progress of junctional formation, and the factors that cause cells to preserve their layered structure once they have been deposited on underlying cell layers. Previous studies² have shown that levitating sheets of PZ-PHV-7 prostate epithelial cells for 1 hour allows formation of their adherens junctions, which is important for preserving morphological structure.

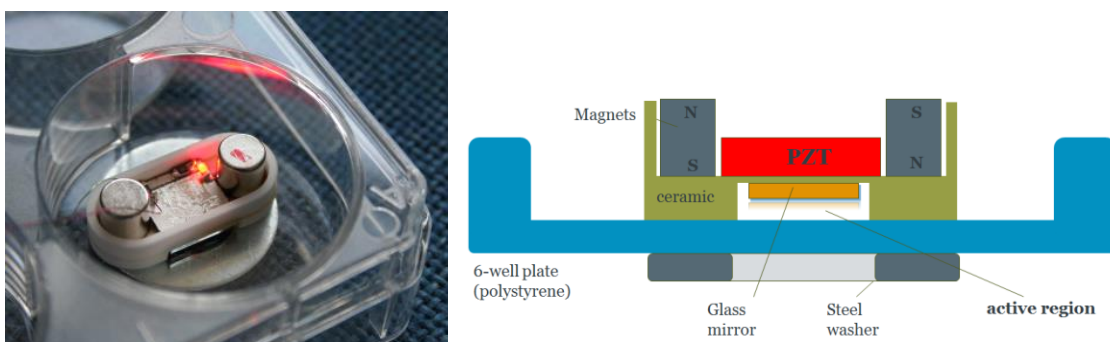


Figure 1: 6-well plate mounted planar resonator, with a resonant (half-wave) cavity of 0.3mm height.

Experiments and Results

The device shown in figure 1 was created to allow levitation within a conventional 6-well plate. It incorporates magnets to enable easy mounting, and a mirror to create a dark background during fluorescent imaging. We investigated the formation of adherens junctions between levitated 16HBE cells, staining for F-actin and E-cadherin at regular intervals over 24 hours. Figure 2 shows results at 2 hours. We find that initially cells do not form a perfect monolayer (the layer is often two cells thick), but re-arrange themselves so that by 2-hours the layer has single cell thickness. At around 6-hours, the cell aggregate is seen to begin to contract becoming pellet shaped.

We will report on detailed investigations into the junction formation, and demonstrate that this contraction results from F-actin filaments creating tension in the monolayer.

We will show that seeding 16HBE cells, on a confluent layer of MRC5 cells does not lead to a layered structure (figure 3a), and that through suitable initial levitation (details not yet published) a sheet of 16HBE cells can form a sheet that preserves its morphology when deposited on confluent MRC5 cells to form the structure seen in figure 3b.

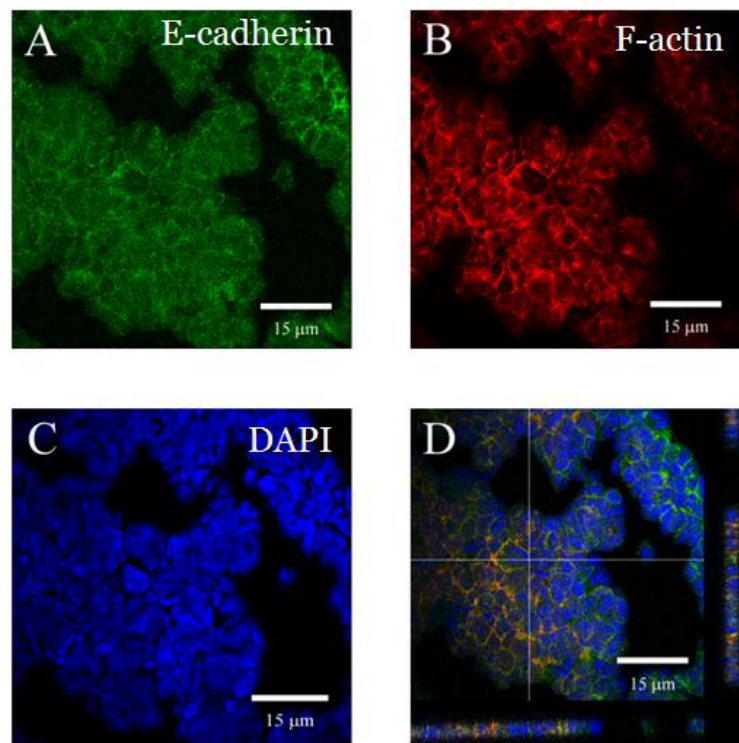


Figure 2: Immunofluorescent staining of 16HBE cells after 2 hours of levitation. Localisation of E-cadherin and F-actin at cell membranes indicates an early stage of adherens junction formation.

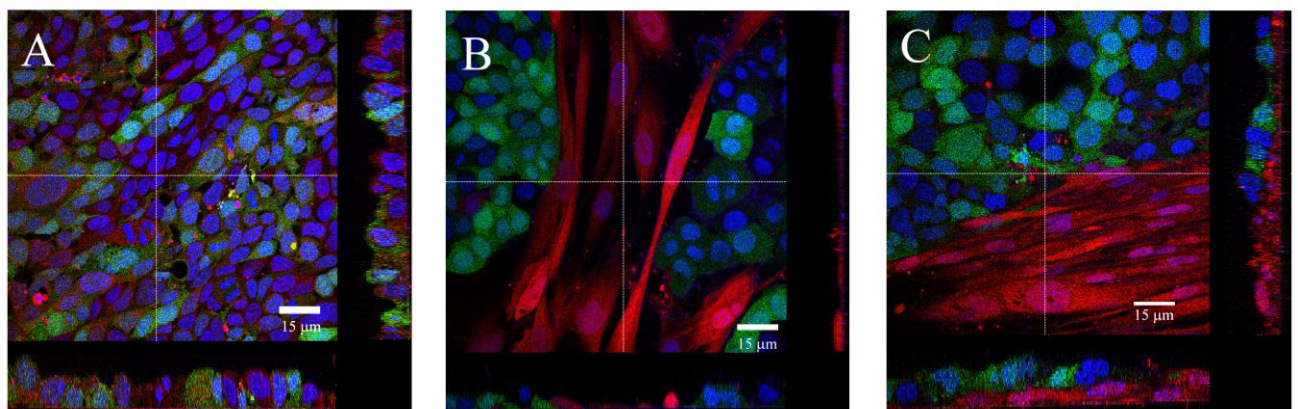
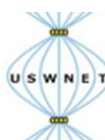


Figure 3: Composite structures of cells 24 hours after seeding using three different methods: (A) 16HBE and MRC5 cells added together (B) 16HBE cells added onto a confluent MRC5 layer; (C) 16HBE cells allowed to form junctions during acoustic levitation prior to deposition onto a confluent MRC5 layer. Top and RHS of each image show cross sectional views along the white lines.

References

- ¹ T. Kikuchi, T. Shimizu, M. Wada, M. Yamato, and T. Okano, *Biomaterials* **35** (8), 2428 (2014).
- ² D. Bazou, G. Davies, W. G. Jiang, and T. Coakley, *Cell Commun Adhes* **13** (5-6), 279 (2006).



ON-CHIP ULTRASONIC SAMPLE PREPARATION FOR DNA-BASED DIAGNOSTICS

Ida Iranmanesh¹, Harisha Ramachandriah²,
Mathias Ohlin¹, Aman Russom², and Martin Wiklund¹

¹Division of Biomedical and X-ray Physics
Department of Applied Physics
Royal Institute of Technology (KTH)
AlbaNova University Center,
SE-10691 Stockholm, Sweden
Email: isir@kth.se
URL: www.biox.kth.se

²Division of proteomics and nanotechnology
Department of Biotechnology
Royal Institute of Technology (KTH)
SciLifeLab
SE-17165 Solna, Sweden
Email: harisha.r@scilifelab.se

Introduction

Sample preparation is a crucial step in many analytical and diagnostic methods. In particular, there is a growing need for fast and simple methods for isolating and up-concentrating a certain pathogen or cell from a complex sample containing a mixture of different cell types for further analysis. In addition, molecular detection methods, such as DNA-detection by PCR, are typically based on analysis of a lysed cell sample. Therefore, an automated, on-chip sample preparation method combining cell isolation/purification, up-concentration and lysis would be an attractive alternative to conventional procedures involving several steps and manual handling.

In the present paper we combine for the first time kHz- and MHz-frequency ultrasonic actuation for on-chip size-based isolation, up-concentration and lysis of cells. As proof of concept, we demonstrate MHz-frequency ultrasonic isolation and trapping of $\sim 10\text{-}\mu\text{m}$ (4H4b) breast cancer cells from $\sim 5\text{-}\mu\text{m}$ RBCs, and we investigate the kHz-frequency ultrasonic lysis effect on isolated cancer cells.

Experiments

Ultrasonic cell isolation: A modified design of the acoustofluidic chip described in Ref. 1 was fabricated and is shown in Fig. 1. A. mixture of 4H4b breast cancer cells and red blood cells (RBCs) was acoustophoretically pre-aligned into two nodes at 4.43-MHz actuation, followed by size-selective focusing of the larger breast cancer cells into the main channel using a second transducer operating at 1.40 MHz, while guiding the RBCs into the side channels (*cf.* Fig. 2A).

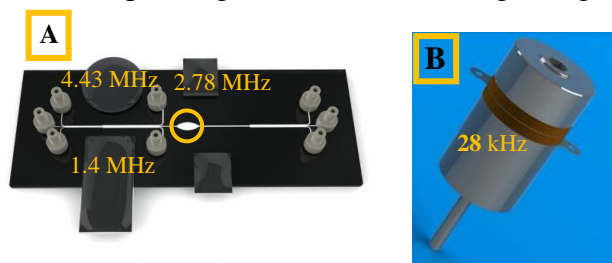


Fig.1. (A) Illustration of the glass-silicon-glass microchip with ultrasonic transducers. The yellow circle around the expansion chamber shows the position of the tip of the ultrasonic horn that is used for cell lysis. (B) Ultrasonic horn operating at 28 kHz.

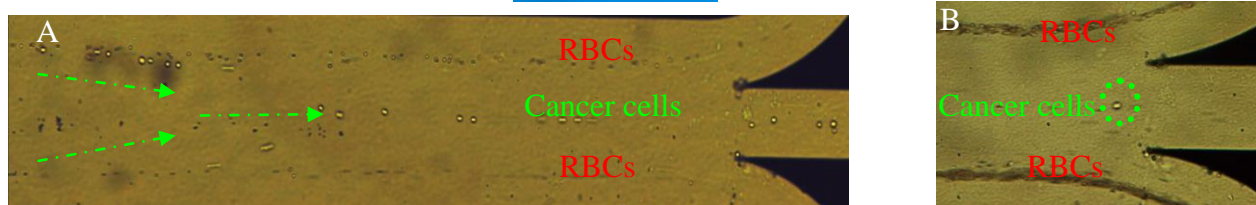


Fig.2. (A) Separation of cancer cells ($C=270 \times 10^4$ cells/mL) from low concentration of RBCs (10^6 times diluted from whole blood). (B) Separation of cancer cells ($C=95 \times 10^4$ cells/mL) from high concentration of RBCs (10^3 times diluted from whole blood).

Ultrasonic cell lysis: After the isolation and trapping procedure, a 28-kHz transducer was attached to the chip and operated for 80 seconds at 100 W for lysing the trapped cell aggregates. For quantifying lysis we used the viability probe calcein-AM (green) and the DNA probe Hoechst (blue). During the lysis operation, the temperature on the chip increased from 22.5 °C to 38 °C, which indicates that acoustic cavitation and not heating is the most likely reason for the cell disruption.

Results

The separation efficiency is quantified in Fig. 3 and compared with the corresponding efficiency when separating polystyrene beads with similar sizes. In Fig.4 the cell separation efficiency at different flow rates are compared. Fig. 5 shows the trapping efficiency for isolated cancer cells that were trapped up-streams and concentrated in an expansion chamber with 93.1% efficiency (at the flow rate 1 μm/min for all of the two middle outlets, 0.5 μl/min of the end outlet) and ultrasound actuation at 2.78 MHz and 10 V_{pp}). Finally the cells were lysed in the chamber using kHz-frequency horn transducer (*cf.* Fig. 6).

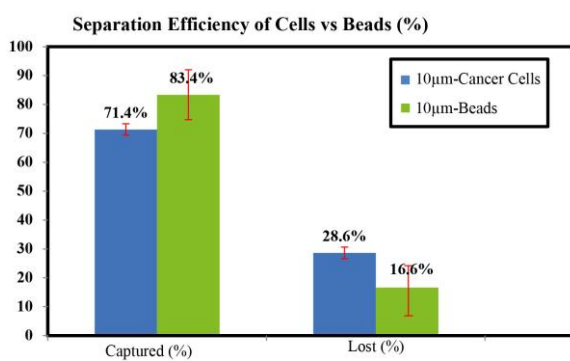


Fig.3. Quantification of the separation efficiency (percentage of captured and lost cells). Comparison between separating cancer cells from RBCs (blue), and separating 10-μm polystyrene beads from 5-μm polystyrene beads (green). Each experiment was repeated 3 times, and the selected concentrations were the same for the cells and the beads (using the concentrations in Fig. 2A).

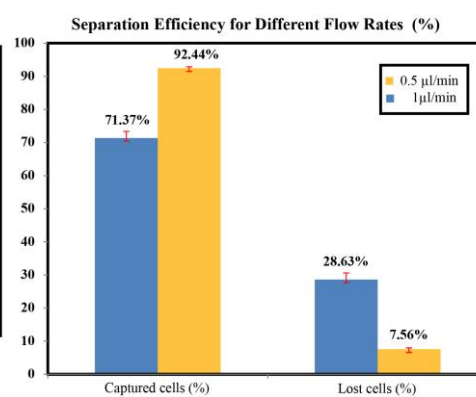


Fig.4. Quantification of the separation efficiency (percentage of captured and lost cells). Comparison between different flow rates from the end outlet. Error bars correspond to 3 times repetition of the same experiment.

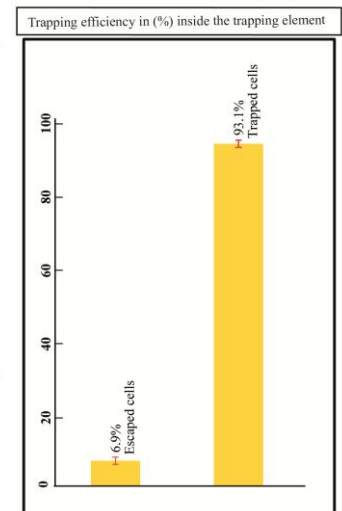


Fig.5. Trapping efficiency of the 4H4b-cancer cells inside the trapping element.

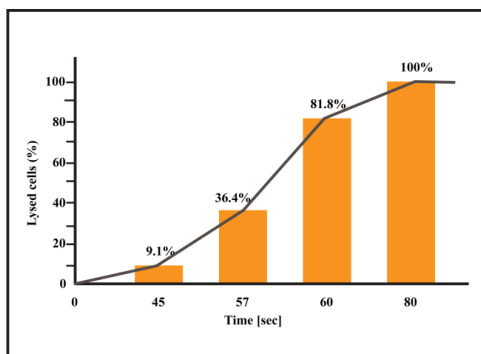


Fig.6. Quantification of the lysis experiment. The diagram shows the fraction of lysed cells as a function of ultrasonic exposure time (28 kHz operation). During the 80 seconds, the temperature on the chip increased from 22.5 °C to 38 °C. In this quantification, the bright field microscopy mode was turned off which facilitated the classification of live and lysed cells (green and blue, respectively).

Conclusion

Our experiment demonstrates that an acoustofluidic chip operated with five different ultrasonic transducers (from kHz to MHz) can be used for on-chip sample preparation, by performing in a sequence the following cell manipulation functions: Pre-alignment, size-selective separation, isolation, up-concentration and lysis.

References

[1] J. Svennebring *et al.*, “Selective Bioparticle Retention and Characterization in a Chip-Integrated Confocal Ultrasonic Cavity”, *Biotechnol. Bioeng.* **103**, 323-328, 2009.

Session 2: Modelling and Numerical Analysis	
15.30 – 15.50	<p>Thermoviscous theory of ultrasound scattering on microparticles and droplets</p> <p>Jonas T. Karlsen, Mads J. H. Jensen, and Henrik Bruus Technical University of Denmark</p>
15.50 - 16.10	<p>Effects of surface profile on a boundary-driven acoustic streaming field</p> <p>Junjun Lei, Martyn Hill, and Peter Glynne-Jones University of Southampton</p>
16.10 - 16.30	<p>Numerical analysis of particles undergoing acoustophoresis in a PDMS channel driven by surface acoustic waves</p> <p>Nitesh Nama, R. Barnkob, C. J. Kähler, F. Costanzo, and T. J. Huang The Pennsylvania State University</p>
16.30 - 16.50	<p>Hydrodynamic interactions in microfluidic acoustophoresis at high particle concentrations</p> <p>Mikkel W. H. Ley and Henrik Bruus Technical University of Denmark</p>

Thermoviscous theory of ultrasound scattering on microparticles and droplets

Jonas T. Karlsen¹, Mads J. H. Jensen², and Henrik Bruus¹

¹Department of Physics
 Technical University of Denmark
 DTU Physics, Building 309
 DK-2800 Kongens Lyngby, Denmark
 URL: www.fysik.dtu.dk/microfluidics

²COMSOL A/S
 Diplomvej 373
 DK-2800 Kongens Lyngby, Denmark

Introduction

The acoustic radiation force is the time-averaged force experienced by a particle in an acoustic field due to scattering of the acoustic waves on the particle. It depends on the scattering coefficients particular to the given particle and fluid. For particles of radius a much smaller than the acoustic wavelength λ , only the monopole and dipole scattering coefficients f_0 and f_1 , respectively, are necessary to evaluate the force. These scattering coefficients are known for compressible spheres in ideal [1] and viscous [2] fluids, but not in general for thermoviscous fluids. In this work we apply the mode method developed for acoustic attenuation in emulsions [3] and suspensions [4], and we derive a general analytical theory of scattering from microparticles and droplets suspended in a real fluid including both viscous and thermal dissipation.

Theory

The physical mechanisms responsible for scattering of acoustic waves on a microparticle in a thermoviscous fluid are sketched in Fig. 1, indicating the relevant parameters, namely compressibility κ_s , thermal expansion coefficient α_p , specific heat capacity C_p , heat capacity ratio γ , thermal conductivity k_{th} , density ρ_0 , and viscosity η_0 . The scattering depends on the particle-to-fluid ratios of the material parameters, and these ratios are denoted by a tilde. For example, a contrast $\tilde{\alpha}_p = \alpha_p^{\text{particle}} / \alpha_p^{\text{fluid}} \neq 1$ in thermal expansion, combined with the oscillatory thermal field, leads to a "breathing mode" as the particle contracts and expands relative to the fluid, thus contributing to the monopole scattering coefficient f_0 . This scattering problem is solved using linear scattering theory, where all physical fields are expressed in terms of the compressional scalar potential ϕ_c , the thermal scalar potential ϕ_t , and the shear-viscous vector potential Ψ_s , each a solution to a wave equation with corresponding wavenumbers k_c , k_t , and k_s ,

$$\nabla^2 \phi_c + k_c^2 \phi_c = 0, \quad \nabla^2 \phi_t + k_t^2 \phi_t = 0, \quad \nabla^2 \Psi_s + k_s^2 \Psi_s = \mathbf{0}, \quad (1)$$

$$k_c \simeq \frac{\omega}{c} \left[1 + \frac{i}{2} [\Gamma_s + (\gamma - 1)\Gamma_t] \right], \quad k_t \simeq \frac{(1+i)}{\delta_t} \left[1 + \frac{i}{2} (\gamma - 1)(\Gamma_s - \Gamma_t) \right], \quad k_s = \frac{(1+i)}{\delta_s}. \quad (2)$$

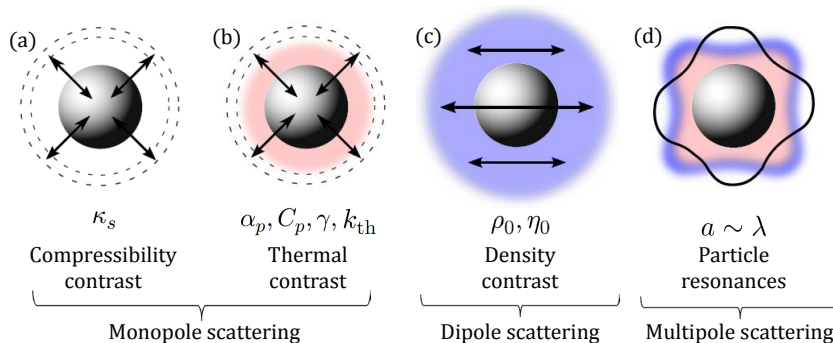


Figure 1: Sketch of acoustic scattering mechanisms. (a) Monopole scattering due to contrast in compressibility between fluid and particle. (b) Monopole scattering and thermal boundary layer (pink) due to contrast in thermal properties (e.g. thermal expansion). (c) Dipole scattering and viscous boundary layer (blue) due to contrast in density (inertia). (d) Multipole scattering due to shape changes for large particles (not studied in this work).

Here, ω is the angular frequency, c the speed of sound, while the characteristic viscous and thermal lengths $\delta_s = \sqrt{2\nu_0/\omega}$ and $\delta_t = \sqrt{2D_{\text{th}}/\omega}$ are given in terms of the momentum and thermal diffusivities $\nu_0 = \eta_0/\rho_0$ and $D_{\text{th}} = k_{\text{th}}/\rho_0 C_p$, respectively. The dimensionless viscous and thermal damping factors $\Gamma_s = (1+\beta)\nu_0\omega/c^2$ and $\Gamma_t = D_{\text{th}}\omega/c^2$ are much smaller than unity.

Analytical results

In brief, the above wave equations are solved analytically using a partial-wave expansion applying the appropriate boundary conditions at the fluid-particle interface (continuous velocity, stress, temperature, and heat-fluxes) as well as imposing outgoing scattered waves. For the case of a small fluid droplet ($a \ll \lambda$), we find the scattering coefficients f_0 and f_1 to be

$$f_0 = 1 - \tilde{\kappa}_s + 3(\gamma - 1) \left[1 - \frac{\tilde{\alpha}_p}{\tilde{\rho}_0 \tilde{C}_p} \right]^2 H, \quad f_1 = \frac{2(\tilde{\rho}_0 - 1)(1 + F - G)}{(2\tilde{\rho}_0 + 1)(1 + F) - 3G}, \quad (3)$$

where H , F , and G are known analytical functions of the droplet radius a as well as the wavenumbers, viscosity and thermal conductivity of the fluid and the droplet. We note that an additional term corresponding to the thermal mechanism of Fig. 1(b) is added to the usual expression $f_0 = 1 - \tilde{\kappa}_s$ [1,2]. Moreover, in the limit of small boundary layers, $\delta_s, \delta_t \ll a$ and $\delta_t \ll a$, we recover the known results for f_0 and f_1 in Refs. [1] and [2], respectively.

For a horizontal standing wave, we have the acoustic contrast factor $\Phi_{\text{ac}} = \frac{1}{3}\text{Re}[f_0] + \frac{1}{2}\text{Re}[f_1]$, which in Fig. 2 is calculated using ideal, viscous, and thermoviscous theory, respectively. We note that for small particles, the thermal effects are significant and can even cause a tunable sign change in Φ_{ac} , which may be used in size-based particle sorting.

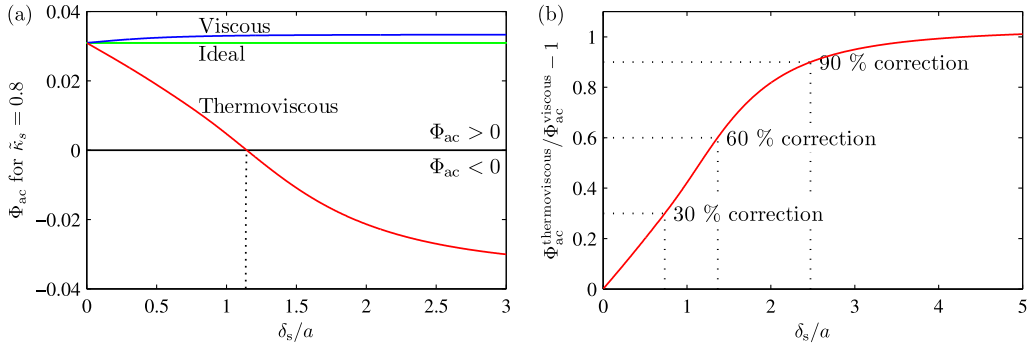


Figure 2: (a) Analytical results (Ideal, Viscous, and Thermoviscous) for the acoustic contrast factor Φ_{ac} in a halfwave standing wave field versus the viscous boundary layer thickness δ_s in units of the droplet radius a , using realistic parameter ratios corresponding to a droplet in water. $\tilde{\kappa}_s = 0.8$ was chosen to illustrate that Φ_{ac} may change sign at a critical value of δ_s/a due to the thermal correction term. (b) Relative deviation of Φ_{ac} for the thermoviscous theory from that of the viscous theory for the case of a vegetable oil droplet in water. The thermoviscous theory introduces corrections of more than 100% compared to the viscous theory.

Conclusion and outlook

We have developed a complete analytical thermoviscous theory of ultrasound scattering on microparticles and droplets. We find that for small droplets with a radius comparable to the thickness of the thermal and viscous boundary layer, respectively 0.2 μm and 0.4 μm in water at 2 MHz, the corrections due to thermal effects may be as large as 100%. Under properly tuned conditions, this means that submicrometer particles with the same acoustical properties, may be separated according to size at nodes and anti-nodes, a feature relevant for the design of devices for sorting bacteria and vira. We are currently establishing numerical validation of the thermoviscous theory by extending our prior numerical analysis of the acoustic radiation force using COMSOL Multiphysics from the viscous to the thermoviscous case.

References

- [1] L. P. Gorkov, Sov. Phys. Dokl. **6**, 773-775 (1962).
- [2] M. Settnes and H. Bruus, Phys. Rev. E **85**, 16327 1-12 (2012).
- [3] P. S. Epstein and R. R. Carhart, J. Acoust. Soc. Am. **25**, 553-665 (1953).
- [4] J. R. Allegra and S. A. Hawley, J. Acoust. Soc. Am. **51** 1545-1564 (1972).
- [5] M. J. H. Jensen and H. Bruus, Proc. Meet. Acoust. **19**, 045001 1-8 (2013).

Effects of surface profile on a boundary-driven acoustic streaming field

Junjun Lei¹, Martyn Hill¹, and Peter Glynne-Jones¹

¹Faculty of Engineering and the Environment
 University of Southampton
 University Road, Southampton
 SO17 1BJ, UK
 Email: j.lei@soton.ac.uk

Introduction

Control of boundary-driven streaming in acoustofluidic systems is vital for various microfluidic applications either to generate it as a positive mechanism (e.g. microfluidic mixing, heat/mass transfer and fluid pumping) or suppressing it as an undesired disturbance (e.g. particle/cell focusing). It has been shown that two-dimensional (2D) and three-dimensional (3D) boundary-driven streaming can be solved from the limiting velocity method as long as the curvature of the surface is small compared to the viscous penetration depth, δ_v . [1, 2] In this work, acoustic streaming fields in 2D rectangular enclosures that have structured textures, which do not satisfy this condition are numerically studied by full modelling of Reynolds stresses and the effects of surface profile amplitude on a boundary-driven acoustic streaming field are investigated. Specifically, a sine-wave shaped profile on a boundary parallel to the particle oscillations is considered, which is found to have large influences on both the magnitude of acoustic streaming velocities and streaming patterns.

Model description

Fig. 1(a) & (b) show respectively the model and a magnified view of A on the top wall of the fluid chamber, where a sine wave shaped boundary is considered. It is determined by two parameters, h_0 and λ_s , which are respectively the amplitude and wavelength of this sine-wave. The standing wave field in this chamber is generated by the vibration of its left wall, which is driven at $f = 1$ MHz and a half-wavelength resonance in the x direction of fluid chamber is established. Only half of the chamber is modelled for the numerical efficiency so in both steps the bottom wall of the fluid chamber is considered as a symmetric boundary. The results presented here are for $\lambda_s = 3.3 \mu\text{m}$.

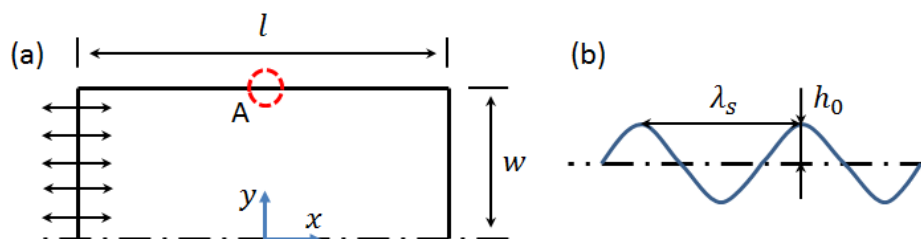


Fig. 1 Illustration of the model: (a) excitation, coordinates and dimensions of the model; (b) showing a magnified view of A in (a), where λ_s and h_0 represent respectively its wavelength and amplitude.

Results

In the first step the linear wave equation is solved in the frequency domain. Then, the Reynolds stress force can be calculated and with it the driving force for the second step, creeping flow, solved by the stationary solution. A series of surface profiles with diverse h_0 ranging from 0.1 nm to 20 μm were studied. The modelled results in two cases respectively with $h_0 = 0.1$ nm and $h_0 = 0.53 \mu\text{m}$ are shown and compared in Fig. 2, where acoustic pressure field, acoustic streaming field and a magnification of acoustic streaming field near the viscous boundary are presented. It can be seen from Fig. 2 (a) & (c) that half wavelength resonances are formed in the x direction of the fluid chamber for both cases and the pressure magnitudes of them are similar, which means that the

amplitude of the surface profile has little effect on the first-order acoustic pressure field. However, a significant difference is found for these cases in both magnitudes of acoustic streaming velocities and streaming patterns. It is found that in cases where h_0 are extremely small, e.g. Fig. 2 (b), the modelled streaming fields are the classical boundary-driven streaming patterns. When h_0 reaches to a certain value (around 10 nm), the number of inner vortices is found to be dependent on λ_s such that there are two inner streaming vortices within each wavelength, Fig. 2 (f). However, there is less impact on the pattern of outer streaming, Fig. 2 (d). With a further increase of h_0 , some interesting phenomena are observed (graphs not shown): (1) a global growth trend is obtained for the maximum inner streaming velocity, which grows less quickly after h_0 exceeds δ_v ; (2) the maximum outer streaming velocities firstly increase rapidly to its peak when h_0 is approximately half of δ_v and then decreases to the maximum streaming velocity in an enclosure with flat boundaries when h_0 reaches close to δ_v . With a further increase of h_0 , the maximum outer streaming velocity further decrease and then reverses in direction.

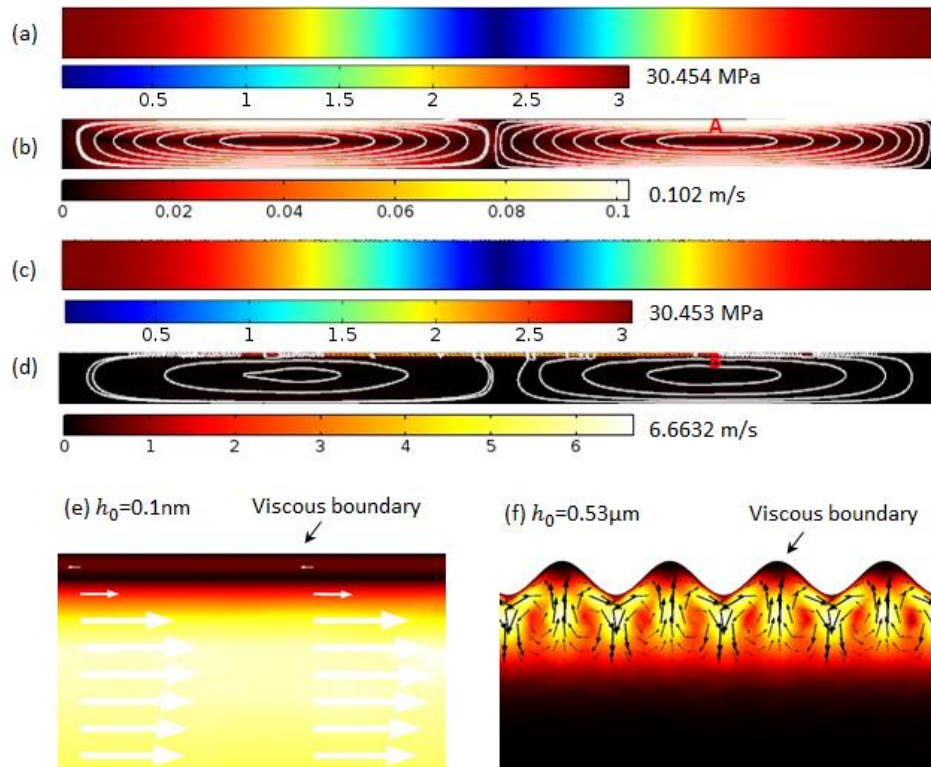


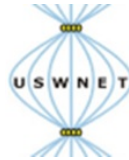
Fig. 2 Modelled acoustic pressure and acoustic streaming fields: (a) acoustic pressure field in an enclosure with $h_0 = 0.1$ nm; (b) acoustic streaming field in an enclosure with $h_0 = 0.1$ nm; (c) acoustic pressure field in an enclosure with $h_0 = 0.53$ μ m; (d) acoustic streaming field in an enclosure with $h_0 = 0.53$ μ m; (e) magnification of A in (b) with arrow plot of streaming velocity field; (f) magnification of B in (d) with arrow plot of streaming velocity field, where A and B are local areas close to the boundary.

Conclusions

The effects of surface profile on a boundary-driven acoustic streaming field have been numerically investigated for the case of a sine wave shaped profile on the boundary that is parallel to the direction of acoustic oscillations in rectangular enclosures. It was found that this kind of surface has significant influence not only on the magnitude of streaming velocities, but also on the streaming patterns. The dramatic increase of the number of inner vortices and magnitude of streaming velocity could significantly enhance mass transfer in acoustofluidic devices, which is of potential use in applications where acoustic streaming has a positive effect, such as microfluidic mixing, fluid-pumping and battery systems that are diffusion limited.

References

- [1] Lei, J., P. Glynne-Jones, and M. Hill, Acoustic streaming in the transducer plane in ultrasonic particle manipulation devices. *Lab Chip*, 2013. 13(11): p. 2133-43.
- [2] Lei, J., M. Hill, and P. Glynne-Jones, Numerical simulation of 3D boundary-driven acoustic streaming in microfluidic devices. *Lab Chip*, 2013. 14(3): p. 532-41.



Numerical analysis of particles undergoing acoustophoresis in a PDMS channel driven by surface acoustic waves

Nitesh Nama⁽¹⁾, R. Barnkob⁽²⁾, C. J. Kähler⁽²⁾, F. Costanzo⁽¹⁾, and T. J. Huang⁽¹⁾

¹Dept. of Engineering Science and Mechanics
The Pennsylvania State University
State College, PA, USA
nxn144@psu.edu

²Inst. of Fluid Mechanics and Aerodynamics
Bundeswehr University Munich
Neubiberg, Germany
barnkob@unibw.de

Introduction

Surface Acoustic Wave (SAW) based systems have gained prominence in recent years for various applications including particle and fluid manipulation. However, the theoretical and numerical work is rather limited and so is the full understanding of the fundamental physical mechanisms, e.g. what is the mechanisms behind the vertical focusing of particles in PDMS channels driven by SAW¹ and what is the critical particle size for the transition between radiation-dominated and streaming-dominated acoustophoresis in these systems? The latter has been extensively studied for Bulk Acoustic Wave (BAW) driven systems numerically by Muller *et al.*² and experimentally by Barnkob *et al.*³ In this work, we present a numerical analysis along the lines of that by Muller *et al.*, but where the model differs in the actuation mechanism and the wall conditions.



Figure 1: (a) Cross-sectional sketch of the SAW device with a microfluidic PDMS channel of width $w = 600 \mu\text{m}$ and height $h = 150 \mu\text{m}$. (b) Two-dimensional computational domain subject to impedance boundary conditions (water/PDMS interfaces) and actuation condition (water/substrate interface).

Numerical analysis

Figure 1 shows a schematic of a typical device for SAW separation in a PDMS microchannel¹. We model the fluid using compressible Navier-Stokes equations without making any a priori assumptions about specific flow regimes. We employ a perturbation approach where the solution of the first-order equations is used to calculate the source terms in the time-averaged second-order equations, which are then solved to obtain the acoustic streaming field. Combining information from these two solutions, it is possible to estimate the mean trajectory of particles in the flow. The particle motion inside the flow is governed by two forces: acoustic radiation force, \mathbf{F}^{rad} , and the hydrodynamic drag force from the acoustic streaming. In many acoustofluidics problems the inertia of the bead can be neglected and thus, the velocity of the particles can be obtained using Newton's second law as: $\mathbf{v}^{\text{bead}} = \langle \mathbf{v}_2 \rangle + \mathbf{F}^{\text{rad}}/(6\pi\mu a)$. We apply impedance boundary conditions to model the PDMS channel walls, while the bottom surface of the channel is subjected to a standing SAW. This actuation displacement is obtained via superposition of two SAWs traveling in opposite directions using the traveling SAW displacement

profile as used by Köster⁵. The numerical solution was obtained via an in-house finite element code based on the `deal.II` finite element library.

Results

Figure 2 shows the plots of the first-order and second-order pressure and velocity fields. These fields are significantly different from those obtained by Muller *et al.* for BAW systems, which can be attributed to the large differences in acoustic impedance of the channel wall material (PDMS for SAW systems versus typically glass or silicon for BAW systems).

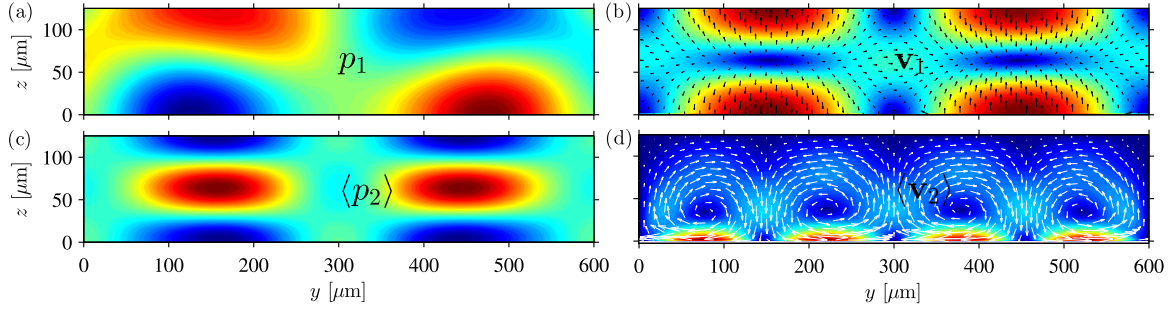


Figure 2: (a) First-order pressure p_1 (from blue -5.7 kPa to red 5.7 kPa). (b) First-order velocity v_1 (magnitude from blue 0 to red 8.4 mm/s). (c) Second-order time-averaged pressure $\langle p_2 \rangle$ (from blue -16.4 mPa to red 18.8 mPa). (d) Second-order time-average velocity $\langle v_2 \rangle$ (magnitude from blue 0 to red 2.5 $\mu\text{m/s}$).

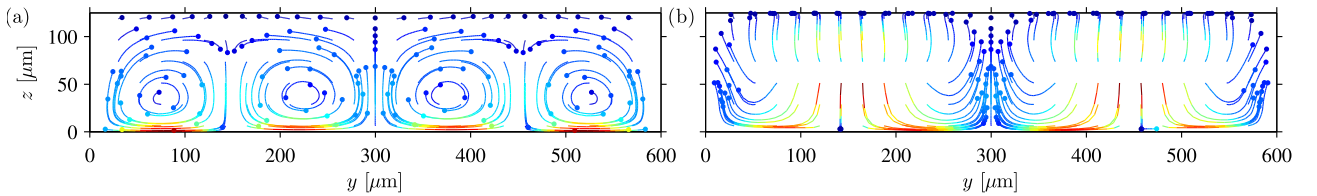


Figure 3: Plot of trajectories of polystyrene beads of diameter (a) 3 μm , and (b) 12 μm . The dots indicate the final position of the beads. Streaming-induced drag force dominates the motion of the smaller beads resulting in their advection along streaming flow patterns while the motion of the bigger beads is dominated by the acoustic radiation force which moves them to the pressure node.

Figure 3 shows the trajectories of polystyrene particles of diameter (a) 3 μm , and (b) 12 μm . It can be seen that while the motion of the smaller particles is dominated by the hydrodynamic drag force, the motion of the large particles is radiation force driven and large particles are moved to the pressure node by the acoustic radiation force. The critical size for transition from streaming dominated motion to radiation force dominated motion obtained from our numerical model is similar to those reported by experiments which have shown the ability of SAW devices to separate particles of size around 9 μm due to the radiation force. We also observe vertical focusing of larger beads, which in combination with gravity (neglected in this work), may explain the results obtained by Shi *et al.*¹ Future investigations will aim at more comprehensive validation of our numerical model using 3D astigmatic particle tracking measurements to gain a better understanding of the acoustophoretic phenomena in SAW devices.

References

- [1] J. Shi, S. Yazdi, S. C. S Lin, X. Ding, I. K. Chiang, K. Sharp, and T. J. Huang. *Lab Chip*, **11**, 2319-2324 (2011).
- [2] P. B. Muller, R. Barnkob, M. J. H. Jensen, and H. Bruus. *Lab Chip* **12**, 4617-4627 (2012).
- [3] R. Barnkob, P. Augustsson, T. Laurell, H. Bruus. *Phys. Rev. E* **86**, 056307 (2012).
- [4] M. Settnes and H. Bruus. *Phys. Rev. E* **85**, 016327 (2012).
- [5] D. Köster. PhD thesis, Universität Augsburg, Germany, 2006.

Hydrodynamic interactions in microfluidic acoustophoresis at high particle concentrations

Mikkel W. H. Ley and Henrik Bruus

Department of Physics
 Technical University of Denmark
 DTU Physics, Building 309
 DK-2800 Kongens Lyngby, Denmark
 URL: www.fysik.dtu.dk/microfluidics

Introduction

For many biological applications of acoustophoresis, the particles or cells to be handled are at so high concentrations that hydrodynamic interactions are significant. However, in the majority of theoretical studies, these interactions are neglected to allow for a simplified single-particle approach. In this work we present a theoretical and numerical analysis of the interaction effects in terms of an effective particle mobility and an effective viscosity of the entire suspension.

Theory

We consider hard monodisperse spherical particles of radius a suspended in a Newtonian liquid with viscosity η . At position \mathbf{r} at time t , we introduce the local *number concentration* $c(\mathbf{r}, t)$ of particles and the local particle-to-liquid *volume fraction* $\phi(\mathbf{r}, t) = (4\pi/3) a^3 c(\mathbf{r}, t)$. As $\phi(\mathbf{r}, t)$ increases, so does the viscous stress in the liquid between the particles. This hydrodynamic interaction results in an increase of both the effective viscosity $\eta_{\text{eff}} = \psi(\phi)\eta$ of the suspension, and the particle mobility (force-to-velocity ratio) $\mu = -6\pi\eta a/\chi(\phi)$. Brenner proposed analytical models for the non-dimensional pre-factors $\psi(\phi)$ and $\chi(\phi)$ [1], which we use in the conservation equations for the particle concentration, fluid momentum (Navier–Stokes), and mass

$$\partial_t c = -\nabla \cdot \left[-D\nabla c + \mathbf{v}c + \frac{\chi(\phi)}{6\pi\eta a} \mathbf{F}_{\text{ac}} c \right], \quad \rho \partial_t \mathbf{v} = -\nabla p + \psi(\phi) \eta \nabla^2 \mathbf{v} + c \mathbf{F}_{\text{ac}}, \quad 0 = \nabla \cdot \mathbf{v}, \quad (1)$$

where D is the effective particle diffusion constant, \mathbf{F}_{ac} is the acoustic radiation force on a single particle, while ρ , p and \mathbf{v} is the density, pressure and velocity of the liquid, respectively.

Model and numerical simulation

We consider the standard situation of a standing halfwave resonance in a microchannel with hard walls [2], see Fig. 1(a). The analytical expression for the acoustic radiation force \mathbf{F}_{ac} on a single particle is known [3]. It is inserted into the governing equations Eq. (1), which then are solved numerically using the COMSOL Multiphysics implementation, described in Ref. [3], for an initial uniform particle distribution with volume fraction ϕ_0 .

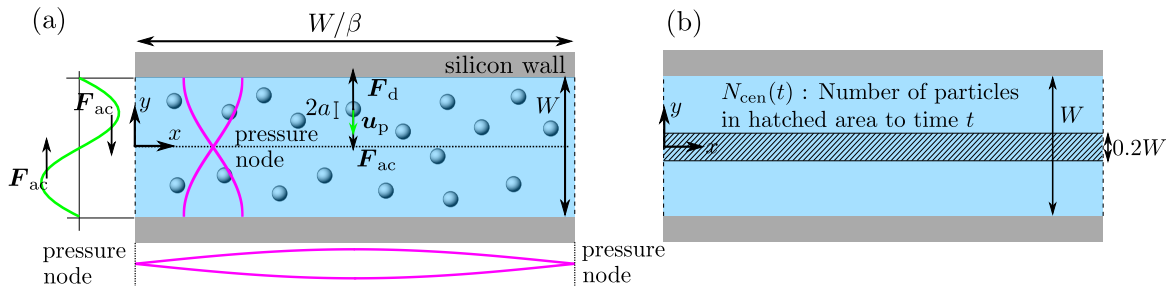


Figure 1: (a) Top view of the microchannel with hard (horizontal gray) walls and periodic (vertical dashed) boundaries. Initially, the suspended particles (circles) are uniformly distributed with volume fraction ϕ_0 (from 0.001 to 0.1). (b) The number of particles at time t in the center region of width $0.2W$ is denoted $N_{\text{cen}}(t)$.

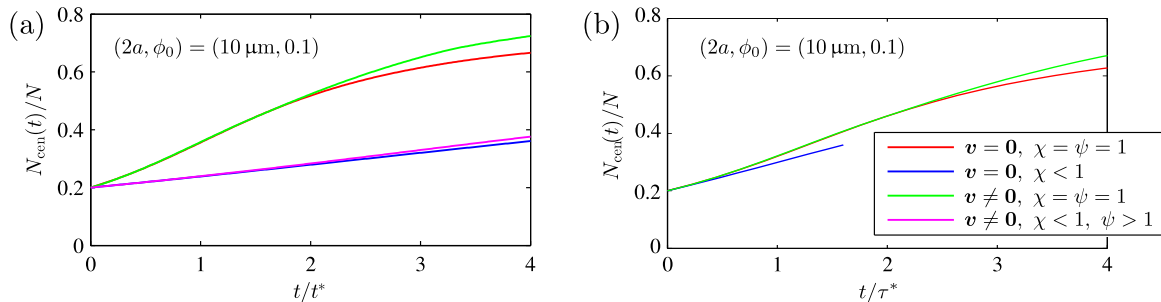


Figure 2: (a) Numerical simulation of the ratio of focused particles $N_{\text{cen}}(t)/N$ defined in Fig. 1(b) versus time t scaled by the single-particle migration time t^* . The four combinations of with/without advection and with/without hydrodynamic interaction effects are presented, see legends. (b) Same as (a) but re-scaling time by the interacting-particle migration time τ^* , resulting in a near-collapse of the curves on a single curve.

Results

It is of practical relevance to study how quickly the suspended particles can be focused near the center of the channel. We therefore calculate numerically the ratio $N_{\text{cen}}(t)/N$ of particles, which at time t are collected in the center region defined in Fig. 1(b), relative to the total number of particles. In Fig. 2(a) we plot $N_{\text{cen}}(t)/N$ versus t/t^* , where t^* is the timescale set by the non-interacting migration time from the edge to the center of the channel for a single particle subject to an external force \mathbf{F}_{ac} and no interaction effects, $\mathbf{v} = \mathbf{0}$ and $\chi = \psi = 1$. To study the role of the effective mobility χ and viscosity ψ , four cases are shown in Fig. 2(a): (i) Neglecting both advection and hydrodynamic interaction effects ($\mathbf{v} = \mathbf{0}$, $\chi = \psi = 1$). (ii) Neglecting advection but including effective mobility ($\mathbf{v} = \mathbf{0}$ and $\chi < 1$). (iii) Including advection but neglecting interaction effects ($\mathbf{v} \neq \mathbf{0}$, $\chi = \psi = 1$). (iv) Including both advection and interaction effects ($\mathbf{v} \neq \mathbf{0}$, $\chi < 1$, $\psi > 1$).

The main result extracted from Fig. 2(a) is that the effective mobility χ dominates and slows down the particle focusing significantly (blue and magenta curves). Clearly, t^* is not the relevant timescale, and we therefore introduce the new timescale $\tau^* = t^*/\chi(\phi_0)$, which is a simple rescaling of t^* taking the effective mobility χ (at the initial particle concentration) into account. In Fig. 2(b) we re-plot $N_{\text{cen}}(t)/N$ now versus t/τ^* , which (nearly) leads to a collapse of the four curves. In the specific example we have used $\phi_0 = 0.1$ which implies $\tau^* = 3.1 t^*$.

Conclusion and Outlook

The above analysis of hydrodynamic interaction effects shows that the effective mobility χ is an important parameter. For high particle concentrations we have shown that the characteristic migration time in acoustophoresis increases significantly for volume fractions ϕ above 0.01. For $\phi_0 = 0.01$ and $\phi_0 = 0.10$ we obtain $\tau^* = 1.5t^*$ and $\tau^* = 3.1t^*$, respectively. This has consequences for high-concentration experiments. In Fig. 3 we show a promising, qualitative comparison between our numerical simulations and preliminary acoustophoretic focusing experiments on polystyrene microparticle suspensions at low and high initial concentration.

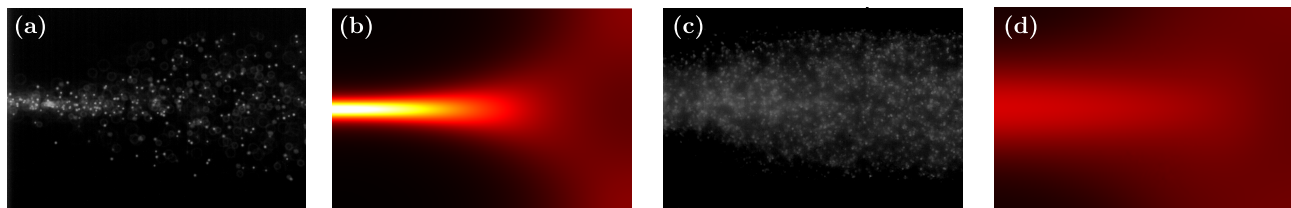


Figure 3: Comparison between preliminary acoustophoretic experiments (micrographs courtesy K. Cushing and T. Laurell, Lund University) and numerical simulations (color-plots). (a) Partially focused, fluorescent 5- μm -diameter polystyrene particles at time $20t^*$ for $\phi_0 = 0.001$ (dilute suspension). (b) Numerical simulation of panel (a). (c) Same as (a) but for $\phi = 0.1$ (concentrated suspension). (d) Numerical simulation of panel (c).

References

- [1] J. Happel and H. Brenner, *Low Reynolds Number Hydrodynamics: With Special Applications to Particulate Media*. Mechanics of Fluids and Transport Processes Series (Prentice-Hall) (1965).
- [2] P. Augustsson, R. Barnkob, ST Wereley, H Bruus, T Laurell. *Automated and temperature-controlled micro-PIV measurements enabling stable microchannel acoustophoresis characterization*, Lab Chip **11**, 4152 (2011).
- [3] P. B. Muller, R. Barnkob, M. J. H. Jensen, and H. Bruus. *A numerical study of microparticle acoustophoresis driven by acoustic radiation forces and streaming-induced drag forces*. Lab Chip **12**, 4617-4627 (2012).

Session 3: Acoustic Microbubbles	
17.00 – 17.25	Invited Lecture – Michel Versluis StemBells: a novel stem cell delivery platform using microbubbles and acoustic radiation force University of Twente
17.25- 17.45	Sono-optical tweezers: an instrument for microbubble characterisation Gianluca Memoli, Chris Fury National Physical Laboratory, University College London
17.45 - 18.05	Acoustic bubble sorting for ultrasound contrast agent enrichment Tim Segers, Michel Versluis, University of Twente
18.05 – 18.25	Live demonstration: Some acoustic properties of cooked spaghetti Jeremy J Hawkes, Jorge A Yescas Hernandez, Sara Baldock, Kenji Yasuda University of Manchester, Tokyo Medical and Dental University

StemBells: a novel stem cell delivery platform using microbubbles and acoustic radiation force

Michel Versluis¹, Tom Kokhuis², Ilya Skachkov², Benno Naaijken³, Lynda Juffermans³, Otto Kamp³, Antonius van der Steen², and Nico de Jong²

¹Physics of Fluids group
University of Twente
Enschede, The Netherlands
Email: m.versluis@utwente.nl
URL: <http://pof.tnw.utwente.nl>

²Biomedical Engineering,
Erasmus Medical Center
Rotterdam, The Netherlands
Email: n.dejong@erasmusmc.nl
URL: <http://www.erasmusmc.nl/thoraxcenterbme>

³Dept. of Physiology and Cardiology
VU Medical Center
Amsterdam, The Netherlands
Email: l.juffermans@vumc.nl
URL: <http://www.vumc.nl>

Introduction

Cardiac regenerative therapy is currently hampered by the low number of stem cells that are delivered at the site of infarction [1]. To improve the homing of stem cells, we are currently investigating a novel delivery platform in which stem cells are conjugated with targeted microbubbles (tMBs), creating echogenic complexes dubbed StemBells. In this study we investigate the feasibility of manipulating the position of StemBells within the blood vessels of a chicken embryo (150–400 μm in diameter) using acoustic radiation force (ARF). Translational dynamics were measured for different saturation grades (i.e. bare stem cells, unsaturated StemBells with < 5 tMBs/cell and saturated StemBells with > 30 tMBs/cell) and peak acoustic pressures ($P_{\text{max}} = 200$ kPa and $P_{\text{max}} = 450$ kPa).

Experiment

Stem cells were cultured in platelet lysate enriched medium. Next, cells were fluorescently labeled (Hoechst), trypsinized, washed and mixed with CD90-targeted microbubbles for 30 min under continuous rotation at room temperature to create StemBells. The mixing ratios (stem cell : tMBs) used to get unsaturated and saturated StemBells were 1:10 and 1:200 respectively. For the experiment, the embryo (5 days old) was taken out of the eggshell, transferred to a cup and embedded in a heated water bath which was connected to a microscope equipped with a color camera. The water tank was also holding the 1 MHz ultrasound (US) transducer. Samples were infused into one of the vitelline veins upstream from the optical field of view. The radial displacement of the fluorescent stem cells following acoustic forcing (1 MHz, $P_{\text{max}} = 200$ kPa or $P_{\text{max}} = 450$ kPa, 10 seconds, 10% duty cycle) was studied using intravital time-lapse fluorescence microscopy.

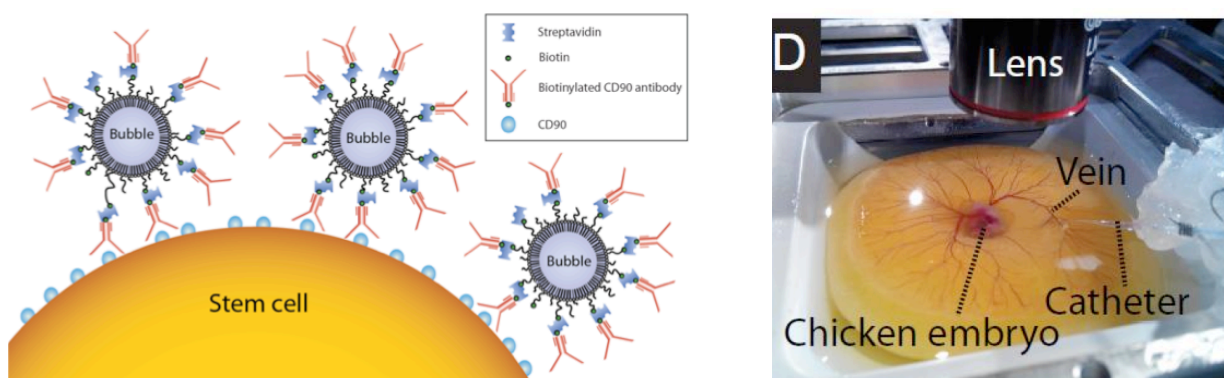


Fig. 1. (left) Coated bubbles are targeted to stem cells through biotinylated CD90 antibody binding. (right) The stem cell/bubble complex is injected into one of the vitelline veins of a 5-day old chicken-egg embryo model.

Results

StemBells were found to be highly susceptible to acoustic radiation force; this acoustic force can then be used after injection to deliver the StemBells locally at the treatment site. The dynamics of StemBells during ultrasound insonification was characterized using high-speed optical imaging in an in-vitro setup (see panel Fig. 2(left)). Using a simple hydrodynamic model the resonant radial dynamics of the complexes could then be used to predict the acoustic radiation forces to manipulate the StemBells. StemBells were also injected in a chicken embryo model, allowing for the real-time optical observation of the effects of acoustic radiation force on the StemBells *in vivo*. Bare stem cells ($n = 21$) or unsaturated StemBells ($n = 11$) did not respond to US application. However, saturated StemBells ($n = 12$) could be propelled toward and arrested at the vessel wall. The mean translational velocities measured are $61 \mu\text{m/s}$ and $177 \mu\text{m/s}$ for $P_- = 200 \text{ kPa}$ and $P_- = 450 \text{ kPa}$ respectively. Fig. 2 (right) shows a typical radial displacement-time curve of a saturated StemBell in response to US (200 kPa , black); the curve of a non-responding bare stem cell (red) is also shown. The StemBell- technique offers potential to increase the homing of stem cells to their target tissue in a well-controlled and minimally invasive manner.

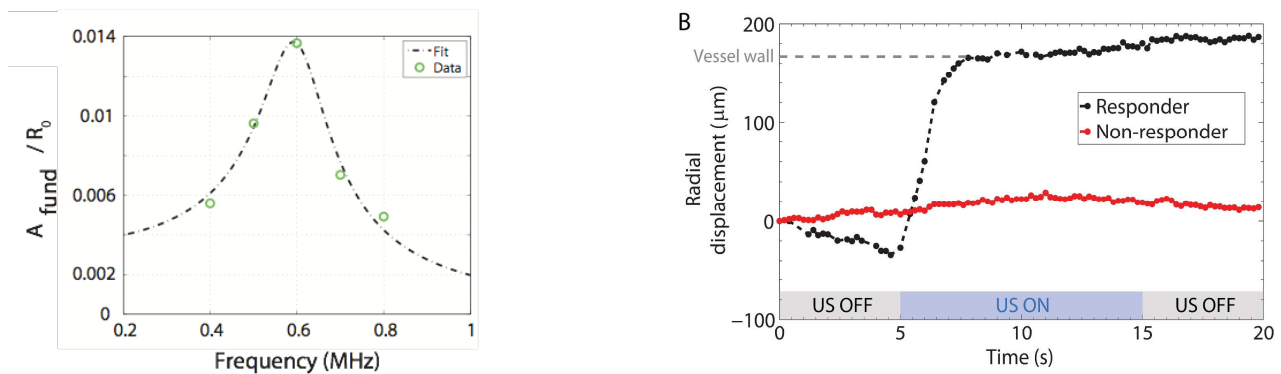


Fig. 2. (left) The StemBells resonate to the driving ultrasound field at a much lower resonance frequency than those known for single bubbles. A simple Rayleigh-Plesset type equation predicts the resonance behaviour of the stemcell/bubbles complex. (right) Typical radial displacement-time curves obtained for responders (black) and non-responders (red), both obtained using $P_- = 200 \text{ kPa}$. The blue bar indicates the time window of ultrasound (US) application.

Conclusion

We have developed a new method for localized stem cell delivery using ultrasound radiation force and StemBells: stem cells decorated with targeted microbubbles. As proof of concept, StemBells were successfully delivered at the endothelium of microvessels in a chicken embryo. This ultrasound-mediated stem cell delivery technique therefore offers potential to increase the homing of stem cells to their target tissue in a minimally invasive manner.

References

- [1] M. Hofmann, K. C. Wollert, G. P. Meyer, A. Menke, L. Arseniev, B. Hertenstein, A. Ganser, W. H. Knapp, and H. Drexler. Monitoring of bone marrow cell homing into the infarcted human myocardium. *Circulation*, 111(17):2198–2202 (2005).



Sono-optical tweezers: an instrument for microbubble characterisation

Gianluca Memoli¹, Chris Fury^{1,2}

¹ Acoustics and Ionising Radiation Division
National Physical Laboratory
Hampton Rd,
Teddington, TW11 0LW,
United Kingdom.
Email: gianluca.memoli@npl.co.uk

² Department of Physics and Astronomy
University College London
Gower Street,
London, WC1E 6BT,
United Kingdom.
Email: chris.fury@npl.co.uk

Introduction

Bubbles are ubiquitous in many modern technologies, which eventually rely on their size distribution and volume concentration. Diagnostic applications using lipid-coated microbubbles already require in addition a good knowledge of the acoustic emission of a single bubble, controlled by the shell parameters, but precise characterization of the coating becomes key for therapeutic developments as drug delivery and targeted microbubbles. If the acoustic emission is well known, bubbles' non-linear response to environmental changes makes them potentially extremely sensitive sensors, eventually used to stratify treatments. A team of researchers led by the National Physical Laboratory has been building a facility for bubble characterisation: NPL's sono-optical tweezers. Based on the simultaneous use of optical and acoustical tweezers, offering respectively a fine and a coarser manipulation tool, the instrument comprises of a microfluidic manifold designed to excite bubbles in a controlled metrological environment, where their acoustical emission can be fully characterised. This work summarises the recent results of this research, ending in December 2014.

Experiment

For optical tweezing we used a holographic set-up to impose a doughnut shape on the Nd:YAG trapping beam, and incorporated the microfluidic chip in a custom inverted microscope. The acoustic field in the glass chip was created using a PZT transducer bonded on its top surface. We used polymeric-coated bubbles (ExpancelTM, i.e. negligible volume oscillations) for calibrating the system and lipid-coated bubbles (resonant at a few MHz) to explore bubble dynamics [1].

During calibration, we scanned the top surface of the glass chip with a laser vibrometer (Polytec), allowing a preliminary identification of the presence of standing waves [2]. We then inserted the chip (with its holder) in the inverted microscope set-up and injected polymeric-coated bubbles (6-20 μm diam.) in the main microchannel. We trapped one bubble in the dark core of the laser beam (Fig. 1a) and we observed its dynamics in the optical potential using an 80 fps camera. The acoustic field was then switched on: its frequency was changed until stable aggregation in the centre of the manifold was observed (163-165 kHz). Trajectories of free bubbles for different transducer voltages (Fig. 1b) were recorded using a 25 fps camera and the *Particle Tracker* plugin in ImageJ.

An exponential horn (<300 μm tip), designed to have its main emission at $\sim 1\text{MHz}$ and characterised using hydrophone scans and acousto-optic vibrometry [3], was inserted in the channel to pilot the dynamics of lipid-coated bubbles closer to their acoustic resonance. In this case, we used the scattering of a probe He-Ne beam and an ultra-high speed camera (10 Mfps) to monitor dynamics.

Results

During calibration, we compared the acoustical pressure measured in the channel in three different ways. Detailed comparison of laser vibrometry data with FEM model (not presented in [2]) gave a first estimate of the pressure distribution and amplitude in the channel. We analysed the trajectories of isolated and optically-free Expancel bubbles to get a second, independent estimate of the acoustic pressure, using classical acoustophoresis theory [4].

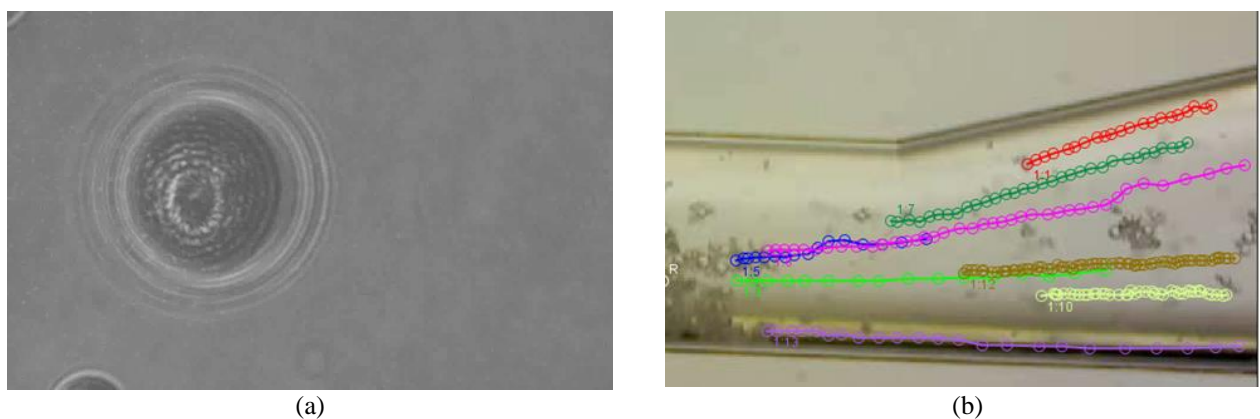


Fig. 1. (a) Bubble trapped in the optical tweezers. (b) Bubble trajectories after switching on the acoustic tweezers.

Finally, thanks to a full calibration of the optical tweezers set-up [5], we measured the acoustical forces acting on optically trapped bubbles by recording the average displacement in the trap for different transducer voltages (Fig. 2a) and assuming a harmonic potential. Repeating this measurement at different positions in the acoustic field (under classical acoustophoresis assumptions) gave a third independent estimate of pressure in the channel. The three methods showed good agreement, but different uncertainties.

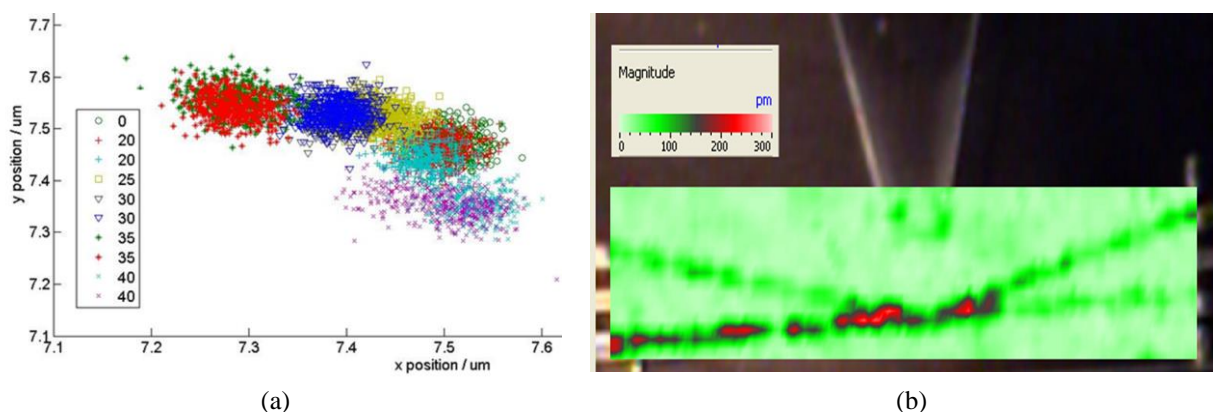


Fig. 2. (a) Position of the bubble in the optical trap for different values of the driving voltage (in mV): the centroid of each cloud gives the displacement used for force measurements. (b) Displacement on the top surface of the channel (RMS value) as determined by laser vibrometry during excitation with the horn (~ 1.2 MHz). This plot shows that the field reaches the central area of the chip.

Calibration methods were tested later on lipid-coated microbubbles, in presence of 1.2 MHz excitation (Fig 2b). We found that, even with the low exciting pressures used, the validity of Gorkov's assumptions were put to test. We also found that optical tweezers could be used to measure forces only off resonance, so it was necessary to rely on much quicker measurement methods (i.e. light scattering and high-speed cinematography) to measure the forces on the bubbles.

Conclusion

We presented a microfluidic chip designed for simultaneous acoustic and optic manipulation of microbubbles. During calibration, we have compared three different techniques to measure acoustic forces (i.e. optical tweezers, particle tracking, and laser vibrometry); in this work, we discussed advantages and challenges for each of them. Finally, we modified the set-up to allow for the acoustical excitation of lipid-coated microbubbles and discussed some preliminary results on methods to investigate bubble dynamics. Future studies will see other techniques for bubble characterisation tested in our environment, feeding results into standardisation (e.g. ISO-TC281).

References

- [1] T. G. Leighton, *The Acoustic Bubble*, Academic Press Limited, London (1994).
- [2] C Fury *et al.*, Laser vibrometry characterisation of a microfluidic lab-on-a-chip device: a preliminary investigation, *J. Phys.: Conf. Ser.* **498** 012002 (2014).
- [3] C Fury *et al.*, Design and Characterisation of a Microtransducer for Microbubble Excitation, Ultrasonic Industry Association Symposium, Madrid (2014).
- [4] H. Bruus, Acoustofluidics 7: The acoustic radiation force on small particles. *Lab Chip* **12**, 1014-1021 (2012).
- [5] C. Fury *et al.*, Experimental characterisation of holographic optical traps for microbubbles, Proc SPIE 9126 Nanophotonics V, 91263L (2014).

Acoustic bubble sorting for ultrasound contrast agent enrichment

Tim Segers¹, Michel Versluis²,

¹Physics of Fluids group
University of Twente
Enschede, The Netherlands
Email: t.j.segers@utwente.nl
URL: <http://pof.tnw.utwente.nl>

Introduction

An ultrasound contrast agent (UCA) suspension contains encapsulated microbubbles with radii ranging from 1 to 10 μm . Clinical ultrasound systems typically operate at a single frequency, therefore only a small fraction of the bubbles will resonate to the driving ultrasound pulse. Thus the sensitivity in diagnostic imaging can be improved by narrowing down the size distribution. Moreover, a fully resonant bubble population of drug-loaded agents will be much more efficient in the local delivery to target cells. Finally, for the use of targeted molecular imaging with ultrasound it would be highly beneficial to discriminate adherent bubbles from freely floating ones, which can be achieved through spectral differences through a resonance shift of the adherent bubbles of a single size. For all these reasons it is of great interest to devise a method to inject only the resonant bubbles [1].

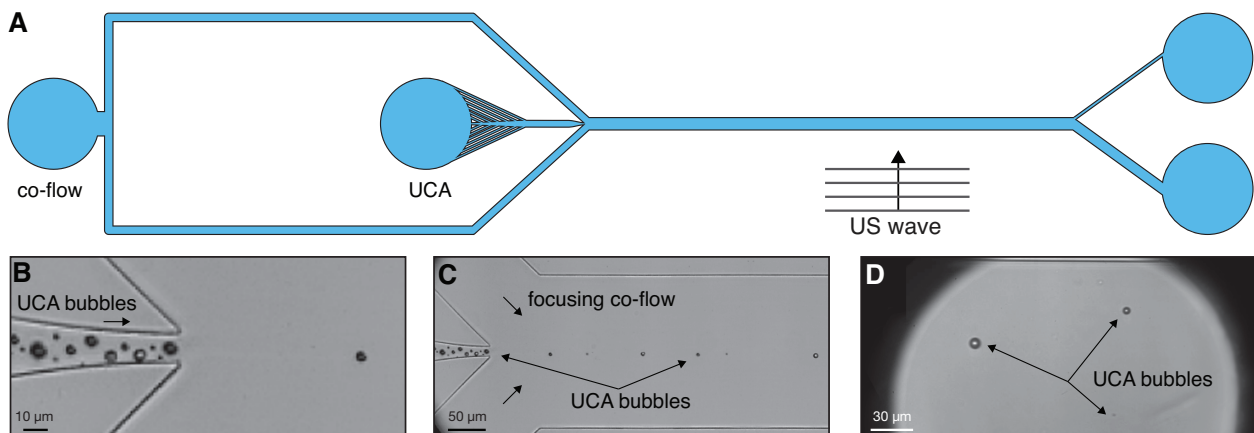


Fig. 1. Acoustic bubble sorter for the sorting of UCAs. (A) Shows the design. A microbubble suspension is hydrodynamically focused in between two liquid co-flows (B) forming a bubble train (C). A traveling acoustic wave pushes the bubbles in vertical direction downstream of the channel (D). Note: the channel lengths are not drawn to scale.

On-chip acoustic bubble sorting

Here, we present a simple lab on-a-chip method to sort a population of microbubbles on-chip using a traveling ultrasound wave. A bubble in a traveling pressure wave experiences a net acoustic radiation force that pushes the bubble in the direction of wave propagation [2]. The magnitude of the radiation force is bubble size-dependent through resonance; bubbles close to resonance experience the largest force. We use the radiation force to sort bubbles in a microfluidic channel made in polydimethylsiloxane (PDMS) with an embedded piezo transducer. The use of a low-pressure travelling continuous ultrasound wave allows for a finite net displacement of the bubbles during multiple cycles, whereas the ultrasound frequency allows for size-selectivity through resonance. We quantify the physical parameter space of the bubble-sorting device first by scaling up the problem by one order of magnitude to minimize the effects of diffraction and Mie scattering typically experienced in contrast bubble sizing. We do this by connecting a flow focusing geometry to the sorting channel to produce and sort bubbles in a 12 – 25 μm size range. Next, we connect a smaller flow focusing geometry to the inlet of the sorting channel and show that sorting of bubbles

with sizes similar to those of UCA is feasible. Finally, we show that UCA bubbles can be sorted with this novel sorting strategy. We focus them hydrodynamically between two co-flows to produce a bubble train with large enough spacing between the bubbles to minimize bubble-bubble interactions. The acoustic pressure employed during the experiments was measured by subdividing the sorting chip in two pieces along the sorting channel. A calibrated hydrophone measured the acoustic pressure along the sorting channel, which served as input for the displacement model.

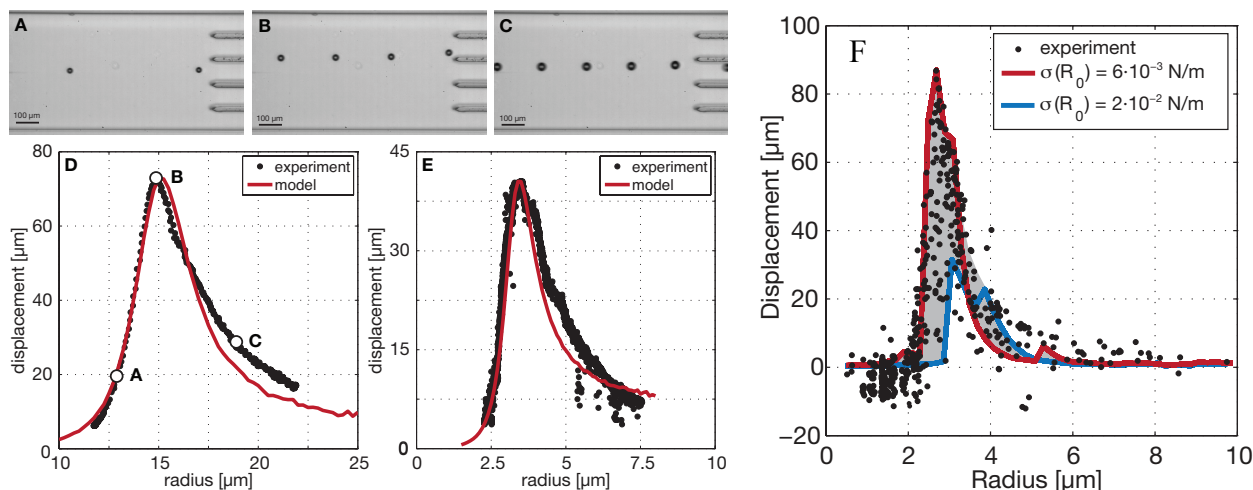


Fig. 2. The acoustic bubble sorter in operation for bubbles produced in the flow focusing geometries. Bubbles with a resonance frequency higher (A) and bubbles with a resonance frequency lower (C) than the ultrasound frequency are displaced less than bubbles driven at resonance (B). Figure D shows the measured displacement as a function of the bubble radius (dots) for bubbles displaced in a 185 kHz wave. The solid red line shows the modeled displacement. Figure E shows the measured displacement as a function of bubble radius (dots) for bubbles displaced by a 1 MHz wave. (F) Experimentally obtained displacement of UCA bubbles as a function of the bubble size (dots). The red line shows the modeled displacement of coated bubbles with an initial surface tension of $6 \cdot 10^{-3}$ N/m and the blue line shows the modeled displacement for a initial surface tension of $2 \cdot 10^{-3}$ N/m. Varying the initial surface tension between these two values (gray area) show excellent agreement with the measured displacement.

Results

Figure 2D and 2E show the measured displacement (dots) of bubbles produced in a flow focusing geometry sorted in a 1 MHz and a 2 MHz ultrasound wave, respectively. Figure 2F shows the measured displacement for contrast agent bubbles (BR-14) of different sizes sorted in a 2 MHz traveling ultrasound wave. The solid lines show the displacement modeled by a Rayleigh-Plesset type model [3] coupled to a translation model incorporating the instantaneous radiation force, the drag force and the added mass force.

Conclusions

The modeled displacements are in good agreement with the experimental data for typical shell parameters adapted from literature. The bubbles are sorted by their acoustic property rather than to their size, which can be directly observed from the scatter of data in the figure 2F; two bubbles having the same size can have a different surface phospholipid concentration resulting in a very different acoustical behavior. The proposed sorting strategy is highly efficient for the injection of a smaller dose, yet highly resonant, enriched bubble suspension for preclinical small animal imaging, for targeted molecular imaging using ultrasound, and for drug and gene delivery applications.

References

- [1] T. Segers, M. Versluis, ‘Acoustic bubble sorting for ultrasound contrast agent enrichment’, *Lab Chip*, 2014,14, 1705-1714
- [2] T.G. Leighton, ‘The Acoustic Bubble’, Academic Press, 1994.
- [3] Marmottant *et al.*, ‘A model for large amplitude oscillations of coated bubbles accounting for buckling and rupture’, *JASA*, 2005



Some acoustic properties of cooked spaghetti

Jeremy J Hawkes¹, Jorge A Yescas Hernandez², Sara J Baldock¹, Kenji Yasuda³

¹Manchester Institute of Biotechnology
The University of Manchester
131 Princess Street, Manchester
M1 7DN, United Kingdom
Email: JeremyJHawkes@gmail.com
Email: sara.baldock@manchester.ac.uk

²School of Mechanical, Aerospace and
Civil Engineering
The University of Manchester,
Pariser Building, Sackville Street
Manchester, M13 9PL, United Kingdom
Email: jayescash@hotmail.com

³ Institute of Biomaterials and
Bioengineering
Tokyo Medical and Dental University
2-3-10 Kanda-Surugadai, Chiyoda
Tokyo 101-0062 Japan
Email: yasuda.bmi@tmd.ac.jp

Introduction

This abstract describes some experiments which show that high water content materials such as gels (and pasta): 75-97.5 % water, are suitable for forming resonant chambers and acting as waveguides. The motivation is to show that these chambers can be used for manipulating particles in ultrasound-standing-waves. Compared to traditional chambers for particle manipulation many aqueous gels are low cost, biodegradable, non-toxic and easily formed into microfluidic chambers using casting or laser cutting technologies.

Silent resonance

Some freely suspended materials such as metal, glass and even polystyrene emit sound when they resonate. Emitting sound causes the resonance to die away. Multiple wave modes produce destructive interference which also removes energy from resonances in the form of heat. Liquids must be held in a container and this leads to further destructive interference between reflections at the inner and outer vessel walls. Streaming also attenuates sound in liquids. Sound attenuation in the bulk material is often very low and may have little influence on the time for a resonance to die. For example sonar and whale songs transmit over long distances in water but longitudinal waves attenuation is even less in other materials: Attenuation in water is 10,000 times greater than aluminium and 7 times greater than polystyrene. Both freely suspended, aluminium and polystyrene resonate audibly when tapped. Water remains silent (in the absence of a splash).

Gels; like water, do not emit sound, and their shear modes are minimal. Gels; unlike water, do not need a container and do not support streaming.

Vibration transfer

Vibration energy for a resonant chamber must be transferred to the fluid from a drive source (e.g. from a pzt through a chamber wall). In systems where the wall and fluid materials are different: The impedance difference determines transfer of longitudinal waves; the wave-length difference determines leakage from plate waves.

Gels are similar to water, and so we expect an efficient transfer of longitudinal and plate wave vibrations.

Experiments and results

Materials tested for aqueous gel chambers: 2.5 % Agar, Pasta: boiled for 20 min final cross section 2.5 x 5 mm (not shown, 4 % gelatine and rice noodles boiled for 10 min). (All dyed red with Amaranth to enhance view of the near-white yeast suspension).

Suspension: 0.5 % wt/vol dried yeast suspended in water.

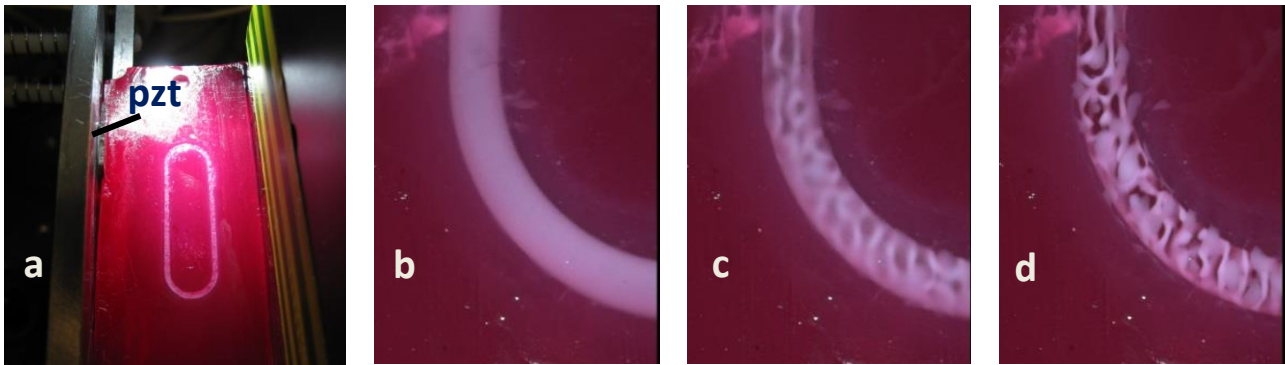


Figure 1. Agar gel block 20 x 70 mm 6 mm thick. Moulded shape: oval 10 x 30 mm, square section 1 x 1 mm. Frequency 1.5 MHz. a) Agar gel block held between pzt (left) and clamping plate(right). b-d) Corner of duct, close up. b) Sound off, c) Sound on 1 s, d) Sound on 10 s. c and d) Two particle collection formations are present, here we consider only the highly concentrated lines, the upper diffuse clouds are related to the upper air interface.

In figure 1 c and d the nodal lines do not follow the curve parallel to the duct walls instead, at the top left and bottom right of the pictures nodal lines indicate that the resonance is along the axis pzt - clamping plate. Elsewhere the curved gel does appear to deform the nodal planes. Conclusion: the resonance is mainly governed by the outer planes of the Agar gel, the interface between the water and duct walls does not interrupt the sound path enough to form a resonance bounded by the walls.

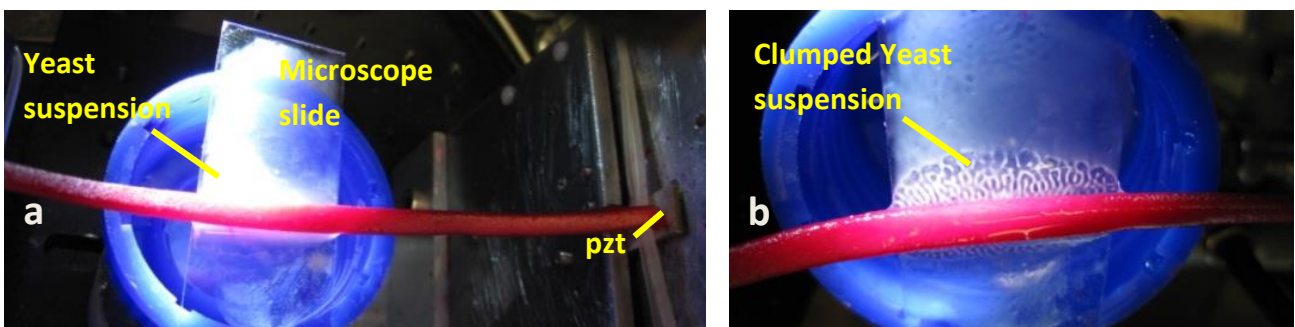


Figure 2. Thread of pasta carrying 1 MHz sound 90 mm from a pzt to yeast suspension on a microscope slide. a) Sound off. b) Close view sound on. Yeast clumps make the nodal lines visible.

In figure 2, pasta is used as a wave guide, sufficient 1 MHz sound passed through pasta thread to form standing-waves in the yeast suspension where a complex pattern of clumps along nodal lines is seen.

Conclusion

These preliminary experiments show that high-water-content materials such as pasta are low-loss sound conductors. Water and gels conduct sound silently; most of the energy appears to be transmitted as a form of plate wave which travel more slowly than compression waves in air, resulting in evanescent waves which do not leak to the air.

In contact with water, gels and pasta form leaky waves transferring their energy to the water: where it can be used for manipulating particles.

	Session 4: Droplets
9.00 - 9.20	On-Chip Biochemistry: Droplet Generation and Merging Adrian Neild, Monash University
9.20 – 9.40	Ultrasonic Atomization of sessile drop in an Acoustic levitator Marina Reissenweber, Gerhard Lindner Coburg University
9.40 – 10.00	Droplet handling with acoustophoresis in bulk acoustic wave devices Peter Reichert, Ivo Leibacher, and Jürg Dual ETH Zurich



On-Chip Biochemistry: Droplet Generation and Merging

Adrian Neild¹, David J. Collins¹, Muhsincan Sesen¹, Tuncay Alan¹

¹Laboratory for Micro Systems
Department of Mechanical & Aerospace
Engineering, Monash University, Clayton, 3800,
Vic, Australia
Email: adrian.neild@monash.edu.au
URL: <http://www.labformicrosystems.com/>

Introduction

Digital microfluidics involves the use of small sample droplets in oil filled channels, offers exciting possibilities in biochemistry. With the ability to form nano or picolitre droplets, there is potential for massive miniaturisation of high throughput screening (HTS) processes, where the full functionality of microtitre plate technology is replicated on a single chip for improved efficiency and substantially reduced costs. To implement such a system, the ability to create reagent mixtures on-chip in multiple permutations is required. We have previously examined the use of surface acoustic wave (SAW) excitation as a method to generate single droplets on-demand, in this work we show control their subsequent behaviour, specifically in the merging of two droplets on-demand, such that a platform for on-chip HTS can be developed.

Results

In order to enable the reaction of one library of chemicals with another, we have demonstrated the ability to produce single droplets, hence control can be obtained in the sequencing of droplets passing along a channel (not all droplets need be the same as occurs in continuous production methods)¹. However, it is also necessary to be able to merge selected droplets in order to initiate the reactions; this capability is now examined, again by use of SAW actuation so that integration of the capabilities into a single chip becomes straightforward.

In the device presented² focused IDTs (FIDTs) of 80 μm wavelength deposited on lithium niobate are also used. The PDMS defined channel consists of enlargement fluid expansion zone at the location of the focal point of the IDTs. It is in this zone that droplets can be held against the flowing oil stream. The channel expansion results in lower local flow velocity for a given volumetric flow rate, yielding a slower moving droplet as well. The application of acoustic radiation forces by excitation of SAW then provide enough acoustic radiation force to retain the droplet from this slowed state. When a subsequent droplet arrives, it will merge with the held droplet; due to the volume increase the drag of the oil will then carry the combined droplet downstream. This process is shown in Figure 1.

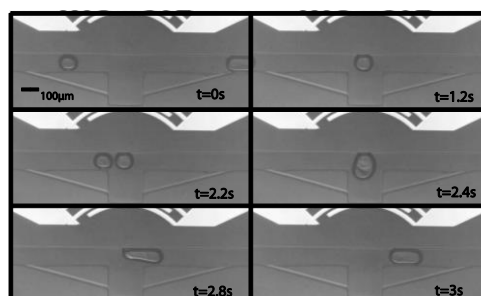


Fig. 1: Droplet merging is shown using a time series of images. The first droplet is held in the expansion chamber, $t = 1.2\text{s}$, which is opposite the focussed IDTs (the last fingers of which are seen at the upper part of the images). When the next droplet arrives, $t = 2.2\text{s}$, they merge, $t = 2.4\text{s}$, at which point the drag caused by the oil flowing around the large volume in such a confined space causes the droplet to flow downstream, $t = 2.8\text{s}$.

Figure 2 shows the power required to capture droplets of different sizes, by use of sufficiently small initial droplets, the number of droplets that can be merged into the same volume is also tunable, with the merger of up to four droplets demonstrated here. Consider the critical volume/power ratio, at which the minimum ARF condition is met to retain a droplet in the focal point of the acoustic beam. When the next incoming droplet arrives this critical ratio is exceeded, resulting in the release of a merged droplet with a volume equal to that of the contributing droplets. If three droplets are to be merged, then the initial droplet volume must be less than half of this critical volume, such that the first merging event renders a volume which can still be held by the acoustic forces, prior to the second merging event causing the departure of the three now-merged droplets. This consideration was used to fix the location of the blue transition line (two to three droplets) with respect to the block dotted line (maximum volume for a single merging event). The blue line is fitted using the drag force relationships based on a stationary sphere confined in a circular pipe as formulated analytically by Haberman and Sayre³. Here, the drag force is related to the acoustic radiation force that can be generated, this being proportional to the power applied. Though it should be noted that Haberman and Sayre's assumptions do not match perfectly with the proposed system, it is nevertheless useful here to understand the obtained results, especially with regard to the non-linear increase in the drag force.

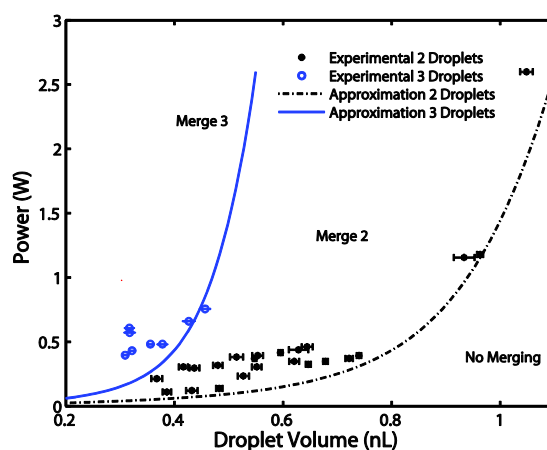


Fig. 2: Data points for the minimum required actuation power to trap droplets are shown². Black data points (asterisks) represent the merging of two droplets of the shown volume, whereas the blue data points (circle) are for merging three consecutive droplets of the shown volume. Droplet volumes are calculated via video analysis for a minimum of three times, standard deviations shown. Curve fits based on Haberman and Sayre's³ analytical drag coefficient for a sphere confined in a circular tube are also plotted as approximating curves for merging of two (dash-dot) and three (solid line) consecutive droplets, thus, regions where merging of none, two or three droplets will occur are predicted.

CONCLUSION

Focussed SAW has been demonstrated here for the on-demand merging of droplets using an acoustic trap. The volume of the trapped droplet and the number of droplets to be merged prior to release dictates the minimum actuation power required. Combined with SAW induced droplet formation, these techniques represent a promising new paradigm for controlled biochemistry reactions on-chip, vital for the testing of chemical libraries for HTS.

Acknowledgments

The devices developed for this work have been fabricated at the Melbourne Centre for Nanofabrication.

References

- [1] D. Collins, T. Alan, K. Helmersen, A. Neild, Surface acoustic waves for on-demand production of picoliter droplets and particle encapsulation, *Lab on a Chip*, 13 (16), 3225 - 3231 (2013).
- [2] M. Sesen, T. Alan, A. Neild, Microfluidic on-demand droplet merging using surface acoustic waves, *Lab on a Chip*, DOI: 10.1039/C4LC00456F
- [3] W. L. Haberman and R. M. Sayre, Motion of Rigid and Fluid Spheres in Stationary and Moving Liquids, David Taylor Model Basin Reports, 1958



Ultrasonic atomization of a sessile drop in an acoustic levitator

Marina Reißenweber and Gerhard Lindner

Institute of Sensor and Actuator Technology
Coburg University of Applied Sciences and Arts
Am Hofbräuhaus 1b
D-96450 Coburg, Germany
Email: m.reissenweber@isat-coburg.de
URL: www.isat-coburg.de

Introduction

An effective atomization of a sessile drop can be accomplished by an acoustic agitation of the substrate, on which the liquid droplet is deposited. [1] The atomization process results in fine spray droplets with a rather narrow size distribution [2] and is accompanied by the formation of capillary waves on the liquid surface [3-5]

Besides, another mechanism has been observed: spray droplets are released near isolated bulges on the sessile drop by oscillation and collapse of cavitation bubbles formed at condensation nuclei by the agitating acoustic wave field [6].

In previous investigations the coagulation of such spray droplets in an acoustic levitator has been studied, in which the spray droplets were trapped in the nodes of a standing wave field [7].

In order to obtain information about the kinetic energies of the spray droplets ejected by the different processes described above, the same acoustic levitator was employed for the trapping of droplets of different water-glycerol mixtures allowing the study of the influence of viscosity on the prevailing atomization mechanism and the resulting energy distribution of the spray droplets.

Experiment

The experimental setup consists of a 24 kHz ultrasonic processor (Hielscher UP200S) and a plane glass reflector forming together an acoustic levitator in air [7]. The ultrasonic horn reaches the maximal oscillation amplitude of 12 μm and can be regulated continuously by the input power. The oscillation itself is monitored by piezoelectric sensors attached to the horn and the reflector, respectively.

A droplet with a volume of 20 μl was deposited in the centre of the ultrasonic horn before switching on the processor. The acoustic power was gradually increased and the sessile droplet atomized continuously and completely due to its vibrations. In order to investigate the influence of the viscosity on the atomization process droplets from water-glycerol-solutions with different glycerol concentrations were used. The processes were recorded by a high-speed microscope (Keyence VW-9000) and subsequently analysed.

Results

Two different coexisting mechanisms were observed in the atomization process attributed to the glycerol concentration and thereby to the viscosity of the droplet: at low glycerol concentrations, the pinch-off of the spray droplets predominantly seems to be caused by capillary waves on the surface of the sessile drop (fig. 1a). They were trapped in the pressure nodes of the standing wave field of the levitator (fig. 2). At high glycerol concentrations spray droplets were predominantly erupted from isolated bulges resulting from the generation, oscillation and collapse of cavitation bubbles (fig 1b). These spray droplets were less homogeneous in their velocity and size distribution and they were less effectively trapped in the levitator indicating higher kinetic energies.

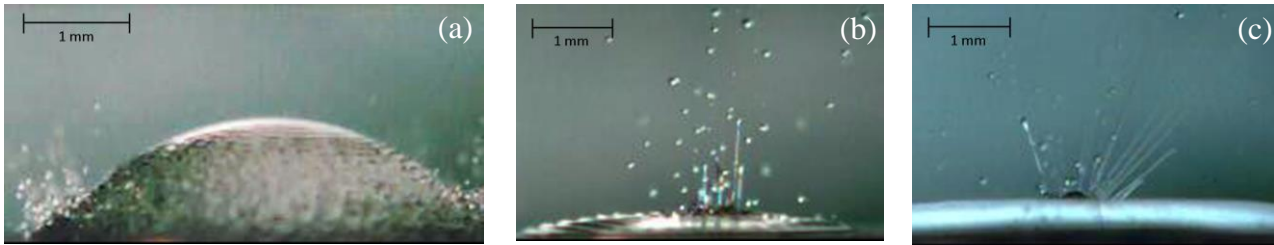


Fig. 1. (a) Vibration induced atomization of a sessile droplet of water by generation of capillary waves on its surface (switch-on-impulse) (b) Atomization of a sessile drop of 98% glycerol. Different atomization mechanisms – capillary waves and the oscillation of a cavitation void – can be observed. (c) Atomization of 98% glycerol caused by the collapse of a cavitation bubble.

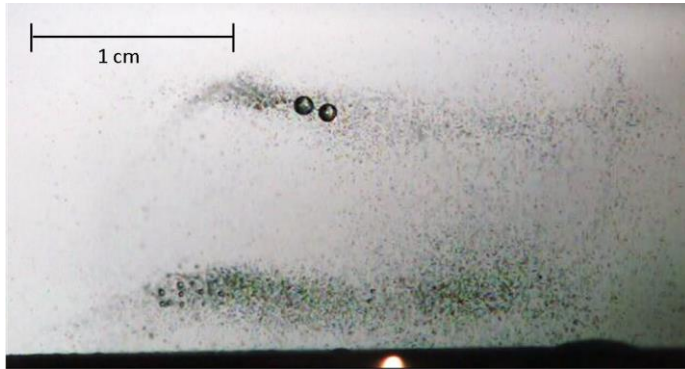


Fig. 2. Recoagulation of spray droplets in an acoustic levitator after vibration induced atomization. According to their kinetic energy the droplets are trapped in the concerning pressure nodes of the standing wave field.

Conclusion

The spray droplets resulting from cavitation bubble atomization seems to possess higher kinetic energy than those from capillary wave pinch off, since they were less effectively trapped in the levitator. This allows a simple and fast fractionation of the spray droplets according to their kinetic energy. In that respect, the levitator acts as an energy analyser, in which gravitational and acoustic forces balances the momentum of the spray droplet in the corresponding level. This approach promises to provide further information about the energy transfer from a vibrating plate to the sessile drop and to the released spray droplets.

Acknowledgement

This work is part of the program “Aufbruch Bayern”, the project “Technologie Allianz Oberfranken”, both supported by the government of the state of Bavaria, and the EFRE project “Actuations” supported by the European Union.

References

- [1] James, A., Vukasinovic, B., Smith, M., et al., *Vibration-induced drop atomization and bursting*, J. Fluid Mech. 476, pp. 1–28 (2003).
- [2] Vukasinovic, B., Smith, M., and Glezer, A., *Spray characterization during vibration-induced drop atomization*, Phys. Fluids 16(2), pp. 306–316 (2004).
- [3] Mir, J., *Cavitation-induced capillary waves in ultrasonic atomization*, J. Acoust. Soc. Am. 67(1), pp. 201–205 (1980).
- [4] Yule, A. and Al - Suleimani, Y., *On droplet formation from capillary waves on a vibrating surface*, Proc. R. Soc. Lond. A 456(1997), pp. 1069–1085 (2000).
- [5] Qi, A., Yeo, L., and Friend, J., *Interfacial destabilization and atomization driven by surface acoustic waves*, Phys. Fluids 20(7), 74103 (2008).
- [6] Brennen, C., *Cavitation and bubble dynamics*, Oxford University Press, (New York, 1995).
- [7] Reißerweber, M., Krempel, S., and Lindner, G., *High-speed camera observation of multi-component droplet coagulation in an ultrasonic standing wave field*, Proc. SPIE 8923, Micro/Nano Materials, Devices, and Systems, 89234K (2013).

Droplet handling with acoustophoresis in bulk acoustic wave devices

Peter Reichert and Ivo Leibacher, Jürg Dual

Institute of Mechanical Systems
 Swiss Federal Institute of Technology Zurich
 ETH Zurich, Tannenstr. 3
 CH-8092 Zurich
 Email: repeter@ethz.ch
 URL: www.zfm.ethz.ch/e/exp-dyn

Introduction

In the field of “droplet microfluidics” biological-chemical laboratory procedures have been miniaturized over the last years. Droplet-based applications require unit operations such as droplet fusion, sorting and storage [1]. In the following, we present a new method to handle these unit operations. We show that with acoustophoresis in bulk acoustic wave (BAW) devices [2] water droplets that are dispersed into silicone oil can be manipulated.

Experiment

As illustrated in Fig. 1(a), the experimental setup consists of a silicon/glass chip with microfluidic channels for both droplet generation and subsequent acoustophoretic manipulations. Up to 5 syringe pumps were connected to generate water-in-oil droplets (silicone oil, Dow Corning 200) with diameters ranging from 50 μm to 250 μm with T-junction and flow focusing geometries. A laminar oil flow was set in the main channel with oil flow rates between 15 to 40 $\mu\text{l}/\text{min}$. For acoustophoresis, a piezoelectric transducer for the excitation of harmonic bulk acoustic waves was glued on the back side of the device. The transducer was excited by a function generator and amplifier at a channel resonance frequency of 470 kHz with 35 V_{rms} amplitude. For experiments with fluorescent droplets and particles the setup in Fig. 1(b) was used. The experiments were monitored by a high speed camera.

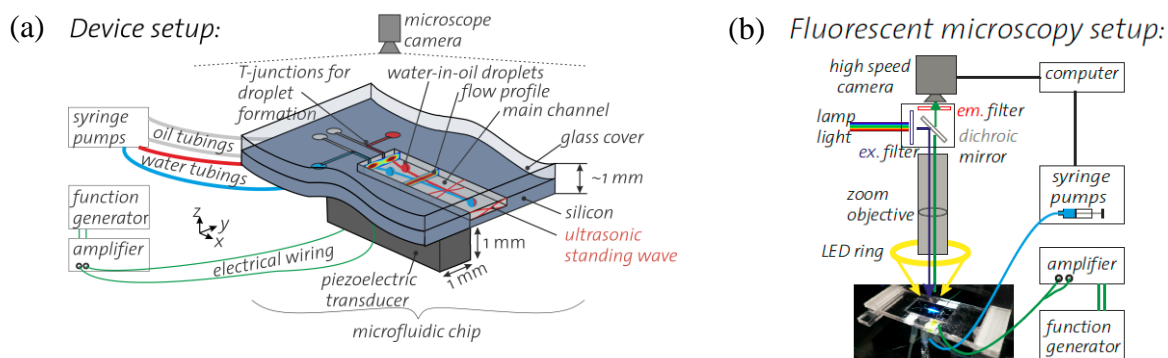


Fig. 1. (a) Silicon/glass chip contains a main channel of length $l > 8$ mm, width $w = 1$ mm, and height $h \sim 200$ μm . The formation and main channels are etched down into the silicon chip of thickness $h_{\text{si}} = 425$ μm and are covered by a glass lid of thickness $h_{\text{glass}} = 500$ μm . The devices have a dimension of typically 8 mm x 24 mm. A piezoelectric transducer Pz26 (Ferroperm) of typically 8 mm x 1 mm x 1 mm is mounted on the device. (b) An illustration of the experimental fluorescent microscopy setup with an excitation (470 \pm 20 nm) and emission filter (525 \pm 25 nm) is shown.

Results

Two droplets with different sizes are generated temporally synchronized in two parallel T-junctions in Fig. 2(a). The one-to-one **fusion** of droplets in a continuous flow is induced by focusing them on the channel centerline with acoustophoresis and a spatial self Synchronization due to different droplet flow velocities. A resonance mode with a standing pressure wave of $\lambda/2$ across the channel width is tuned. In Fig. 2(b) the mixing of a dark water and a white fluorescein droplet in a laminar oil flow is shown. The white fluorescein is diffused homogeneously inside the water droplet after ~ 1 s due to vortices inside the merged droplet. The shown active droplet fusion method allows fluid

sample handling operations such as reaction initiation, droplet dilution and reagent dosing. Moreover, the fusion of a white fluorescent droplet and a dark water droplet with a fluorescent particle inside is presented in Fig. 2(c). The experiment with the cell-surrogating fluorescent particle shows the possibility of the acoustophoretic fusion method to perform biological analyses.

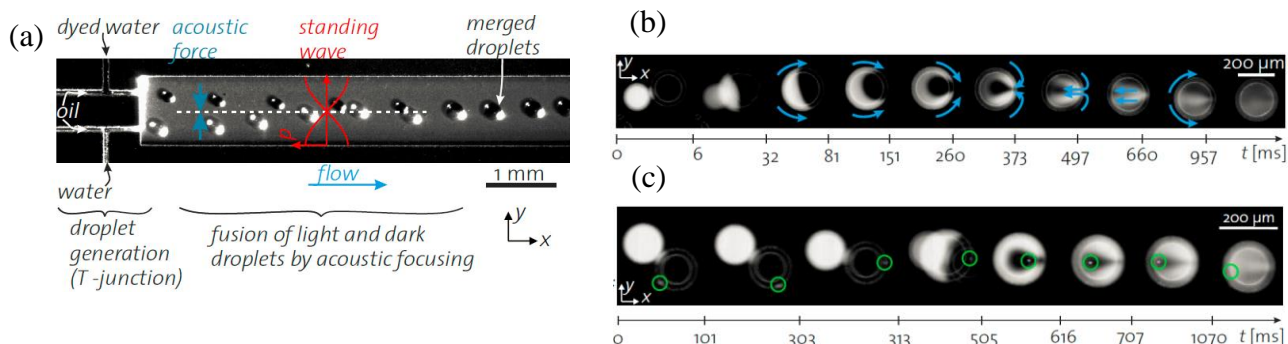


Fig. 2. (a) Fusion of synchronized droplet pairs by acoustic focusing to the channel middle. (b) Mixing of a dark water and a white fluorescein droplet. (c) Fusion of a fluorescein droplet and a water droplet containing a cell-surrogating fluorescent particle.

Droplets can be **sorted** and simultaneously the suspending **continuous phase** can be **changed**. In Fig. 3, droplets experience an exchange of their suspending continuous phase from the dyed oil (center) to the oil in the lower third of the channel. This is feasible because the acoustic radiation force acts selectively on the dispersed water due to its spherical shape and its acoustically contrasting fluid. At the same time, droplets can be guided into different channel outlets by turning the acoustophoretic transducer on/off or by frequency switching. In Fig. 3(b) droplets are forced to the pressure nodal line of the λ resonance mode. Combined with e.g. an upstream optical droplet sensor, this technique enables droplet sorting tasks.

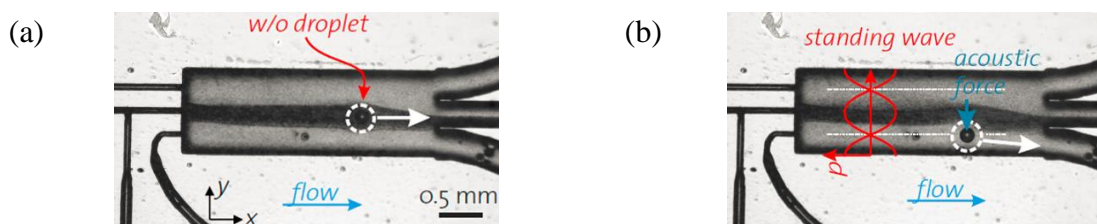


Fig. 3. (a) A water droplet in dyed oil (centre) leaves the centre outlet as the piezoelectric transducer is switched off. (b) Droplets change their surrounding medium and are guided to the bottom outlet.

These and further methods, like storage of droplets, were analysed experimentally, numerically and analytically.

Conclusion

The presented acoustophoretic droplet handling in BAW devices enables a range of unit operations for droplet microfluidics, such as droplet fusion, sorting and the exchange of the continuous phase. Compared to the alternative surface acoustic wave (SAW) method, the BAW method has a simpler setup and its lower operation frequency allows the handling of larger droplets up to $\sim 500 \mu\text{m}$ size [3]. Therefore, the method is ideally suited for droplet handling tasks in portable lab-on-a-chip systems. The shown contactless fluid sample handling by sound offers significant benefits for applications e.g. in laboratory diagnostics/analytcs and biochemical research.

References

- [1] X., Casadevall i Solvas and A. de Mello, *Droplet microfluidics: recent developments and future applications*. Chemical communications, **47**(7), p. 1936–42 (2011).
- [2] H. Bruus, et al. *Forthcoming Lab on a Chip tutorial series on acoustofluidics: Acoustofluidics—exploiting ultrasonic standing wave forces and acoustic streaming in microfluidic systems for cell and particle manipulation*. Lab on a Chip **11**(21), p. 3579–3580 (2011).
- [3] S. Li, et al. *An on-chip, multichannel droplet sorter using standing surface acoustic waves*. Analytical chemistry **85**(11), p. 5468–5474 (2012).

10.30 – 11.10	<p>Keynote Lecture – James Friend Beyond SAW in Acoustic Microfluidics RMIT University</p>
	Session 5: SAW Technologies
11.10 - 11.30	<p>Towards high efficient SAW-based microfluidic actuators Raimund Brünig, Andreas Winkler, Florian Kiebert, and Hagen Schmidt IFW Dresden</p>
11.30 - 11.50	<p>Interaction-free phononic crystal droplet sensing for portable surface acoustic-wave driven microfluidic devices M. Agostini, M. Travagliati, G. De Simoni, R. J. Shilton, V. Piazza, M. Cecchini Scuola Normale Superiore and Istituto, Istituto Italiano di Tecnologia</p>
11.50 - 12.10	<p>SAW-based fluid atomization using mass-producible chip devices Andreas Winkler, Stefan Harazim, and David J. Collins IFW Dresden, Monash University</p>

Beyond SAW in Acoustic Microfluidics

James Friend¹

¹ School of Electrical and Computer Engineering
RMIT University
Melbourne
Victoria 3001
Australia
Email: james.friend@rmit.edu.au

In the past decade, surface acoustic wave (SAW) devices have found a new life as a means to drive a diversity of microfluidics phenomena, from particle manipulation to digital microfluidics, microcentrifugation, jetting for rheology, and drug delivery. It has long been known that there are other methods for generating and transmitting waves in solid media, yet the assumption has long been that SAW would prove to be the most efficient and useful means of providing acoustic energy to do work in microfluidics, particularly at the high MHz-order frequencies demanded at these small dimensions.

In fact, bulk Lamb waves are proving to be a far superior choice in accomplishing all the same aims of SAW microfluidics, with a simplicity in construction, integration, and operation that belies the efficiency and precision possible with such waves at up to 100 MHz order resonances. However, the choice of Lamb waves introduces a collection of new problems to be aware of, particularly the necessity to form traveling waves by providing a energy sink that is as important as the energy source. This is illustrated through a unique flow phenomena—poloidal flow—present only due to the rapid attenuation of the Lamb wave. We close with some ideas for the future in non-SAW acoustic microfluidics.

Biography:

James Friend is a Professor and Vice-Chancellor's Senior Research Fellow at RMIT University in Melbourne, Australia. His current roles include the directorship of the forthcoming \$35 million MicroNano Research Facility at RMIT University, comprising a 1200 sqm cleanroom and biolab facility in downtown Melbourne, five technical staff, and over 50 major nanofabrication and metrology tools; the Vice-Chancellor's Senior Research Fellowship 2012-5, RMIT University; and co-directorship of the MicroNanophysics Research Laboratory, with four academics, three post-doctorates and nine PhD students in a burgeoning group at RMIT. With over 130 peer-reviewed research publications and 25 patents in process or granted, he received excellence in teaching, early career research, and research awards from the Monash Faculty of Engineering in 2006, 2008, and 2011, respectively, a Future Leader award from the Davos Future Summit in 2008, was awarded as a Top 10 emerging scientific leader of Australia by Microsoft and The Australian newspaper in 2009, and is an associate editor of *Biomicrofluidics* and a senior member of the IEEE.

Towards high efficient SAW-based microfluidic actuators

Raimund Brüni^{*}, Andreas Winkler, Florian Kiebert, and Hagen Schmidt

IFW Dresden, SAWLab Saxony
 PF 270116, 01171 Dresden, Germany
^{*} Email: r.bruenig@ifw-dresden.de

Introduction

Surface acoustic wave (SAW) devices provide a promising way for liquid actuation inside microfluidic devices or vessels. However, as SAW devices are mainly used in high frequency telecommunication, they are only marginally optimized for microfluidic actuators, where high input power, local fluid contact and functional top layers are obligatory. Here, the main difficulties are electric and acoustic losses resulting in a relatively large self-heating as well as an efficient acoustical coupling of the transducers to the microfluidic part. In order to extend the applicability and performance, we present several approaches for optimizing the power efficiency of SAW fluid actuators, especially considering an ongoing miniaturization towards mobile usage.

Considerations towards higher efficiency

We investigated and optimized several components which are of importance for SAW-based agitation of liquids. For improving the energy efficiency we propose five approaches:

(1) A task specific selection of the SAW wavelength to concentrate as much energy into the fluid as possible. In case of agitating liquids inside a microfluidic channel, the acoustic wave is usually generated outside and must pass the channel material which leads to some energy losses (Fig. 1). The energy efficiency then depends on the ratio of the acoustic waves coupled into the fluid (c) and coupled into the channel material (b, d, e).

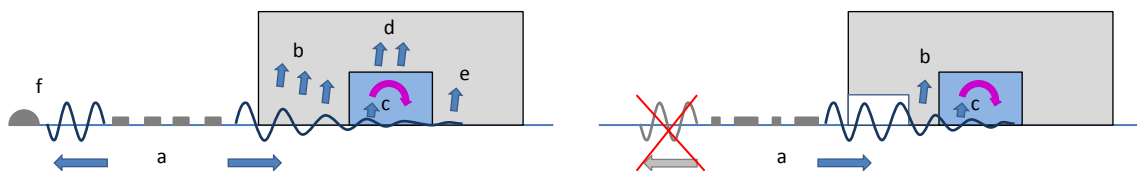


Fig. 1: (Left) Cross section of SAW-based acoustic coupling in a microfluidic channel. Energy losses of a bi-directional SAW-transducer occur at the channel material (b,d,e) and through the second wave (f) which travels away from the channel position. (Right) Unidirectional SAW excitation towards the channel position using TF-SPUDTs (a) and reduced energy losses in the acoustic path by providing an air gap above the IDT and parts of the channel material (b).

(2) Optimizing the acoustic coupling into the microfluidic flow by designing the channel geometry to provide an air gap in the acoustic path to reduce energy losses, while still maintaining enough mechanical stability and tightness against leakage.

(3) Special unidirectional transducer designs (TF-SPUDT, Fig. 1 (Right image)) [2], with preferred SAW towards the channel position.

High frequency devices should be matched electrically to the system impedance of 50Ω to achieve good energy conversion from the electric signal into the mechanical vibration. Considering the ongoing miniaturization towards mobile usage electrically matched devices also allow more cost efficient electronics for generating the required power in actuator applications. Therefore we present two further approaches:

(4) Electrical optimization by design of SAW-exciting interdigital transducers (IDT) including SiO_2 top layer to work in air as well as for direct contact with water.

In cases where impedance-matched transducers design for liquid loading is not reasonable, we demonstrate

(5) Miniaturized wavelength- and device-specific matching circuits (Fig. 2.1).

Experiment

For evaluation of matching circuits, SAW-devices with a SiO_2 top layer were glued to a small PC-board and electrically connected with wire-bonds, whereby the bondpads were encapsulated in epoxy resin. This setup was immersed in deionized water and streaming velocities were measured using particle image velocimetry (PIV). High-frequency input signals were provided by a PowerSAW Signal Generator (BelektronikG, Germany) SAW driving unit [1]. Measurements of $|S_{11}|$ for electrical device characterization were performed using an E5071C network analyzer (Agilent).

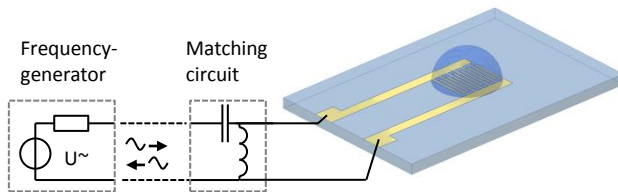


Fig. 2.1: Usage of a matching circuit to reduce electric reflection of the IDT when immersed in water.

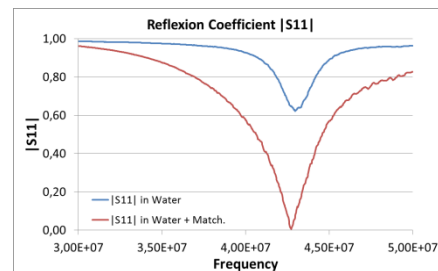


Fig. 2.2: Reflection coefficient $|S_{11}|$ of a $90\mu\text{m}$ (43MHz) SAW-transducer immersed in water. The minima represent the optimal excitation frequencies. The reflected power is reduced from 41.7% (blue curve $|S_{11}|=0.646$) to almost zero (0.06% corr. to $|S_{11}|=0.0245$ red curve).

The properties of optimized SAW-transducers and the effect of matching circuits were analyzed in terms of the reflection coefficient $|S_{11}|$ (Fig. 2.2) as well as by particle image velocity (PIV, Fig. 3). An increase in power efficiency of up to 40% was observed.

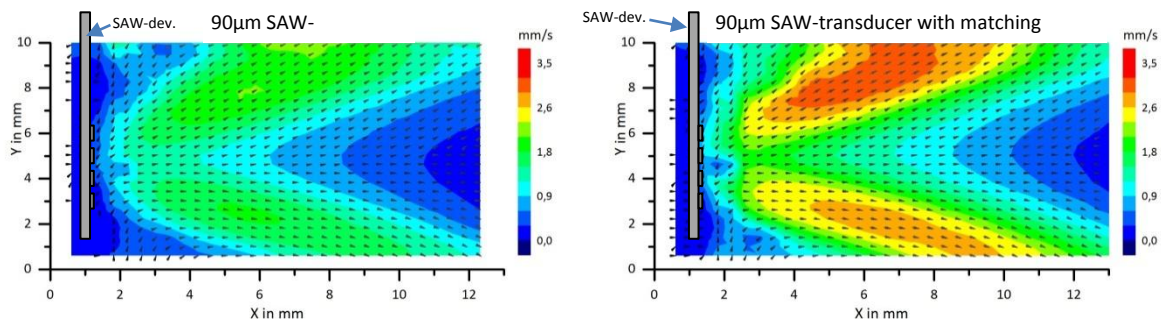


Fig. 3: Particle image velocimetry (PIV) of an immersed $90\mu\text{m}$ (43MHz) SAW-transducer without (left) and with matching circuit (right) at the same excitation power. The two lobes at top and bottom result from the two excited acoustic beams of a bi-directional transducer. The right image shows an increase in streaming velocity due to the matching circuit which matches the expectations from the measurement in Fig. 2.2.

Conclusion

We present several approaches for improving the energy efficiency of SAW-based acoustic actuators which help to overcome current limitations in their usage for microfluidic devices. Achieved improvements in energy efficiency compared to standard bi-directional transducers are about 30% through the usage of SPUDTs and up to 40% through matching circuits. Of course, depending on the type of setup, several of our presented approaches can be combined to further optimize energy efficiency.

References

- [1] R. Bruenig, A. Winkler, G. Guhr, H. Schmidt: *Active mixing in microfluidic systems using surface acoustic waves*, 2011 IEEE International Ultrasonics Symposium (IUS) Proceedings, 794-796 (2011)
- [2] G. Martin, S.V. Biryukov, H. Schmidt, B. Steiner, B. Wall: *Two-finger (TF) SPUDT cells*, IEEE Transactions on Ultrasonics, Ferroelectrics, and Frequency Control 58 (2011) Nr. 3, S. 658-661

Financial support by German BMBF (InnoProfile-Transfer grant 03IPT610A) is gratefully acknowledged. The Authors further like to thank Ms. Kerstin Eckert (TU-Dresden) for support using PIV.

Interaction-free phononic crystal droplet sensing for portable surface-acoustic-wave driven microfluidic devices

M. Agostini^{1,2}, M. Travagliati^{1,2}, G. De Simoni², R. J. Shilton², V. Piazza², M. Cecchini¹

¹NEST, Scuola Normale Superiore and Istituto Nanoscienze-CNR
Piazza San Silvestro 12, I-56127, Pisa, Italy
Email: matteo.agostini@sns.it

²Center for Nanotechnology Innovation @NEST, Istituto Italiano di Tecnologia
Piazza San Silvestro 12, I-56127, Pisa, Italy

Introduction

Over the last two decades the microfluidic community has devoted efforts towards the development of portable micro total analysis systems. Surface acoustic wave (SAW) microfluidics represents one of the most attractive fluid actuation methods for this aim, driving a variety of functional operations such as droplet translation and atomization, particle concentration and separation, and fluid pumping in microchannels, to mention a few [1]. In view of portable applications, blind automation of these processes is of paramount importance. Here we show the first scheme allowing automated on-chip SAW droplet routing without any additional external controllers [2,3]. This relies on the SAW interaction-free sensing of fluid based on the resonant coupling between travelling SAWs—actuating the fluids—and the eigenmodes of a SAW phononic crystal—addressing the target position. Exploiting this principle, we demonstrated in the realm of SAW digital microfluidics the automatic, feedback-free, blind positioning of fluids. Application in routing of fluids in microchannels, integrated logic gates, sequencers and SAW phononic crystal biosensors in completely portable lab-on-a-chip devices are discussed.

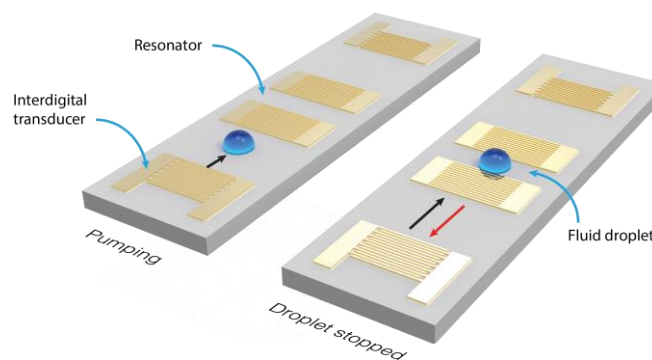


Fig. 1. Schematic of the device working principle. The device consists of a 128° XY lithium niobate substrate with two 15-finger pair, single-electrode IDTs for SAW excitation and detection, and a PnC comprising two 80-fingers shorted-reflectors separated by 475 μm . Acoustic aperture is 750 μm . The device metal deposition comprises 15 nm of Ti adhesion layer and 100 nm of gold.

Experiment

Devices geometry (Figure 1) has been simulated by finite element methods to tune a single mode phononic crystal (PnC) cavity with the single-electrode-interdigital transducers (IDTs) centered at 160 MHz. Within the phononic crystal bandwidth, when a travelling SAW impinges on the cavity there are two possibilities: 1) its frequency matches an eigenfrequency of the PnC, it couples to an eigenmode and is fully transmitted (*resonant condition*), or, 2) its frequency doesn't match the eigenfrequency, it doesn't penetrate in the PnC and is fully reflected (*non-resonant condition*). If

the device is designed such that the SAW exiting the actuating IDT and the cavity along the SAW propagation direction are resonantly coupled: 1) if a droplet is between the actuator and the PnC, it is moved toward the cavity due to droplet-SAW interactions 2) if a droplet is in between the cavity reflectors, the droplet itself changes the PnC eigenmode's spectrum, therefore the actuator and cavity will be in the non-resonant condition. In this case the droplet-SAW interaction will be suppressed and the droplet remains in the PnC even if the actuator is turned on. The SAW will be reflected back to the actuating IDT enabling interaction-free detection of the droplet position. This behaviour has been tested on devices fabricated with standard lithography techniques. Acoustic transmission properties have been characterized both with network analyzer and laser Doppler vibrometer. Automatic routing capabilities have been tested using 1 μ L drops of deionized water.

Results

Figure 2a reports the transmission spectrum of a representative device: the spectral region with a reduced transmitted power corresponds to the PnC bandwidth (light blue area). The peak at $f_c = 159.17$ MHz corresponds to a PnC eigenmode. In Fig. 2b, a laser Doppler vibrometer (LDV) scan of the surface displacement amplitude is depicted at f_c . As expected, the majority of the wave energy at the resonant frequency is confined in the PnC eigenmode. Figures 2c and 2d report a sequence of frames of a representative droplet actuation experiment, recorded at 100 fps. A continuous-wave RF signal at the resonance frequency f_c was applied to the left IDT (Fig. 2c). Once the droplet entered into the cavity, it remained there as the PnC became detuned. Fig. 2d reports a sequence of frames for a representative droplet actuation experiment at $f_o = 157.55$ MHz, out of the PnC bandwidth. In this condition we observe that the droplet crosses the cavity without any velocity reduction in between the reflectors. Therefore we conclude that the droplet positioning at the resonant frequency is due to the interaction-free principle.

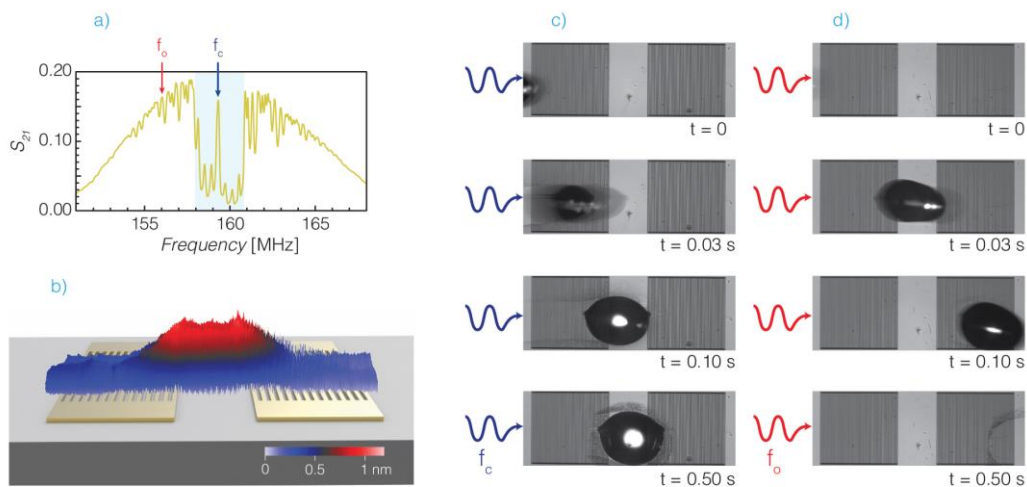


Fig. 2. (a) Free delay line transmission spectrum. (b) LDV measurement of the resonant cavity mode at $f_c = 159.17$ MHz, (c) and (d) Recorded frames of droplet trapping at resonant frequency and droplet crossing at $f_o = 157.55$ MHz (out of resonance), respectively.

Conclusion

We demonstrated the first scheme for high-precision, automatic, feedback-free fluid positioning based on interaction-free principle in SAW microfluidic platforms. This is based on the resonant coupling between a traveling wave and the stationary modes of a PnC that are altered when a droplet is placed within the cavity. We believe this result is a useful building block for integrated logic gates based on instantaneous fluid distribution on-chip, either in the form of droplets, or fluid-filled channels by applying its working principle to SAW counterflow pumping[4].

References

- [1] Friend et al., "Microscale acoustofluidics: Microfluidics driven via acoustics and ultrasonics", *Rev Mod Phys*, 83, 647 (2011).
- [2] Travaglini et al., "Interaction-free, automatic, on-chip fluid routing by surface acoustic waves", *Lab Chip*, 12, 2621 (2012).
- [3] Patent WO/2013/054265 A1.
- [4] Cecchini et al., "Acoustic-counterflow microfluidics by surface acoustic waves", *Appl Phys Lett*, 92, 104103, (2008).



SAW-based fluid atomization using mass-producible chip devices

Andreas Winkler*, Stefan Harazim*, and David John Collins**

*IFW Dresden, SAWLab Saxony
PF 270116, 01171 Dresden, Germany
Email: A.Winkler@ifw-dresden.de

**Mechanical and Aerospace Engineering, Monash University
Faculty of Engineering
Building 72, Clayton campus
Monash University, VIC 3800, Australia

Introduction

Surface Acoustic Wave (SAW) fluid atomizers generate droplets between 1 and 30 μm diameter without the need for moving parts or nozzles, which makes them interesting for medical inhalators [1], devices for particle synthesis [2], as well as for thin film and particle deposition via aerosol condensation [3]. The interaction between SAW and a fluid meniscus placed in the acoustic propagation path leads to the development and stabilization of a fluid film with several 10 μm thickness [4,5]. At increased SAW amplitude, droplets are ejected out of this thin fluid film forming an aerosol mist. The fluid supply technique plays a crucial role in the aerosol formation process and influences the droplet size distribution. Conventionally, droplets [6] or wetted fabrics [4,7] are placed on the chip surface in the center of the acoustic path. However, these techniques are limited in their practical application, especially with regard to the variability in droplet size distribution due to the acoustic excitation of a meniscus and subsequent secondary effects including mixing, capillary wave excitation and Rayleigh-Taylor instabilities (“Jetting”). Here we show a fluid supply at the boundary of the acoustic beam which (I) narrows the droplet size distribution, (II) leads to more defined aerosol streams and (III) permits use of microfluidic channels for fluid supply. Furthermore, we demonstrate a simple, reliable and highly accurate method of producing appropriate microchannels suitable for wafer-scale manufacturing.

Experiment

Common procedure: Interdigital transducers (65 MHz, 1 mm aperture, impedance matched) were prepared via electron-beam evaporation of Ti and Al on a photoresist mask on 128°YX-LiNbO₃ substrate and subsequent lift-off patterning. Then, a 1000 nm thick SiO₂ layer was sputter-deposited on the chip surface. High frequency signals were supplied via SMA cables from a PowerSAW3 signal source (BelektroniG GbR) to spring pin contact plates contacting the SAW chip. **Analysis of fluid supply position:** Deionized water was delivered via a glass capillary with attached tissue in the middle between the IDTs, either directly onto the center line (sketch in Fig. 1a) or at the outer boundary of the SAW beam (sketch in Fig. 1b). High-speed micrographs were taken of the atomization zone. **Microchannel fabrication:** For channel preparation, layers of Ti (50 nm) and SU8 photoresist (100 μm) were deposited and structured, forming triangular blocks (side length 3 to 4 mm) with integrated microchannels of (200x80) μm^2 cross section area (Fig. 2c). To connect the fluid source, two PMMA tubes were glued on top of the SU8 using Vitralit 7041 resin (Panacol-Elosol GmbH). Fluid (DI-H₂O) supply was carried out by a Nemesys syringe pump (Cetoni GmbH) with a flowrate of 5 $\mu\text{l}/\text{min}$.

Results

Analysis of fluid supply position: When a fluid is supplied on a chip surface via paper or as a droplet, it forms a meniscus of several pl to μl volume, according to the local wetting and fluid supply conditions. The interaction of SAW with a fluid meniscus in the acoustic path causes longitudinal pressure wave excitation in the meniscus and leads to effects like mixing, jetting, capillary wave excitation and atomization (see video image in Fig. 1a). The latter occurs solely at regions, where a thin fluid film is stabilized by the SAW [4], while the other effects occur inside the meniscus volume. In contrast to previously demonstrated techniques, we supplied fluid at the boundary of the SAW path – i.e. at the side regions, where the wavefield is dominated by diffraction effects, causing an amplitude gradient towards the beam center line (see sketch in Fig. 1b). When a fluid is placed into this region, a lateral separation of meniscus position, fluid thin film elongation and fluid atomization zone can be achieved. As only a thin fluid film is present in the “atomization zone”, no jetting occurs and, thus, no large droplets (>30 μm) are observed in the aerosol (compare video images in Fig. 1) and the aerosol stream is more consistent. **Microchannel fluid supply:** In order to make use of this effect for

reliable and cheap production of devices with integrated fluid supply, we created triangular SU8-blocks with microchannels on the substrate surface (Fig. 2a). The channels have a rectangular cross-section with SU8 walls/ceiling and SiO₂ bottom. They possess an opening directed towards the center of the acoustic beam. The interaction of the SAW with the fluid meniscus at the channel outlet generates and stabilizes a thin fluid film, which is laterally spreading into the aperture center due to the amplitude gradient, where atomization takes place due to higher SAW amplitude. This unique approach makes SAW fluid atomization continuous and highly reproducible.

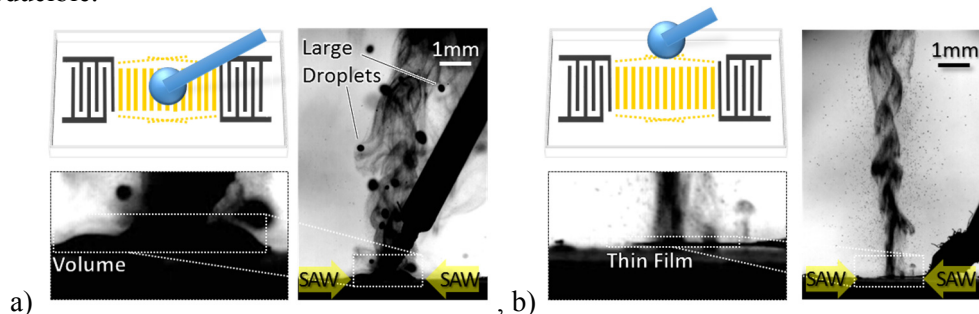


Fig. 1. Aerosol generation for different fluid supply positions (standing SAW, 60 μ m wavelength): Fluid supplied via glass capillary, (a) in the center and (b) at the outer boundary of the acoustic beam; **top left:** Sketch of fluid supply position with indicated acoustic path (orange), **right:** Image of aerosol formation zone from recorded high-speed video of SAW-based atomization, **bottom left:** Detail of video image showing the glass capillary, the produced aerosol and either (a) the developed fluid meniscus or (b) the thin fluid film

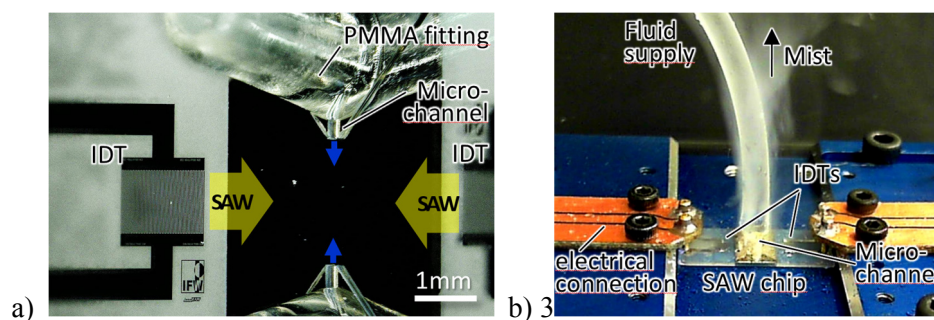


Fig. 2. The SAW atomization chip with two IDTs (1 mm aperture, 65 MHz) and SU8-structures with integrated microchannels (200 μ m wide x 80 μ m high) for fluid supply towards the acoustic propagation path (indicated by arrows; outlets located 500 μ m from aperture boundary). For lab testing, the SU8-structures were connected to the fluid supply via PMMA fittings; (b) Experimental setup with the SAW atomization chip, two high frequency signal spring pin-connectors (orange) and a fluid supply tube on a custom chip holder (blue) (Atomization at approx. 2x 2 W SAW power, 1 μ l/s water flowrate)

Conclusion

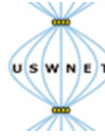
In SAW-based fluid atomization, the method of fluid supply is of crucial importance for the aerosol formation process, the aerosol properties and, finally, the usability of the chip devices. We combined two new techniques to improve the SAW atomization devices: On the one hand, a fluid supply at the boundary of the acoustic propagation path improves the droplet size distribution, the aerosol stream stability and the reproducibility of experiments. On the other hand, integrated SU8 microchannels enable a precise wafer-scale production of SAW atomization devices and a continuous fluid supply. We also demonstrate the lateral separation of fluid delivery, fluid thin film elongation and atomization, which suppresses secondary fluid actuation effects like jetting and mixing. Using the demonstrated technique, SAW fluid atomizers for integrated therapeutic and industrial applications come into reach.

(Financial support by German Research Council (Grant No. WI 4140/2-1) is gratefully acknowledged.)

References

- [1] L. Y. Yeo, J. R. Friend, M. P. McIntosh, E. N. T. Meeusen, and D. A. V. Morton, *Ultrasonic nebulization platforms for pulmonary drug delivery*, *Expert Opinion on Drug Delivery* **7**, 663 (2010).
- [2] K. C. Ng, A. S. Qi, L. Y. Yeo, J. Friend, and W. L. Cheng, *Evaporative Self-Assembly of Gold Nanorings via a Surface Acoustic Wave Atomization*, *Smart Nano-Micro Materials and Devices*, Spie-Int Soc Optical Engineering (Bellingham, 2011)
- [3] N. Murochi, M. Sugimoto, Y. Matsui, and J. Kondoh, *Deposition of thin film using a surface acoustic wave device*, *Japanese Journal of Applied Physics Part 1-Regular Papers Brief Communications & Review Papers* **46**, 4754 (2007).
- [4] D. J. Collins, O. Manor, A. Winkler, H. Schmidt, J. R. Friend, and L. Y. Yeo, *Atomization of thin water films generated by high-frequency substrate wave vibrations*, *Physical Review E* **86**, 1 (2012).
- [5] A. R. Rezk, O. Manor, J. R. Friend, and L. Y. Yeo, *Unique fingering instabilities and soliton-like wave propagation in thin acoustowetting films*, *Nat Commun* **3** (2012).
- [6] J. Ju, Y. Yamagata, H. Ohmori, and T. Higuchi, *Standing wave type surface acoustic wave atomizer*, *Sensors and Actuators A-Physical* **147**, 570 (2008).
- [7] A. Qi, L. Yeo, J. Friend, and J. Ho, *The extraction of liquid, protein molecules and yeast cells from paper through surface acoustic wave atomization*, *Lab on a Chip* **10**, 470 (2010).

Session 6: SAW Devices	
12.55 – 13.20	Invited Lecture – Richie Shilton Ultra high frequency surface acoustic wave driven microfluidics Istituto Italiano di Tecnologia
13.20 – 13.40	Acoustic and dielectrophoretic particle sorting using virtual deterministic lateral displacement (vDLD) David J Collins, Tuncay Alan and Adrian Neild Monash University
13.40 - 14.00	Combined acoustic torques and forces on spherical particles obtained by the leakage of two standing orthogonal surface acoustic waves Ianis Bernard, Philippe Marmottant, David Rabaud, Cédric Poulain, and Pierre Thibault Univ. Grenoble Alpes
14.20 - 14.40	Cell and droplet sorting with surface acoustic waves Thomas Franke University of Glasgow



Ultra high frequency surface acoustic wave driven microfluidics

Richie Shilton¹, Marco Travaglini^{1,2}, Fabio Beltram^{1,2}, and Marco Cecchini²

¹Center for Nanotechnology Innovation@NEST,
Istituto Italiano di Tecnologia,
Piazza San Silvestro, 12
Pisa, 56127, PI, Italy
Email: richard.shilton@iit.it

²NEST, Scuola Normale Superiore and Istituto Nanoscienze-CNR,
Piazza San Silvestro, 12
Pisa, 56127, PI, Italy
Email: marco.cecchini@nano.cnr.it

Introduction

Portable lab-on-a-chip devices require fine control over internal fluid flows for processes such as fluid mixing and particle manipulations in miniaturized bioreactors and biosensors. There is in general a lower limit—on the order of microliters—to which interesting and controllable internal flows have been demonstrated within digital microfluidics. Surface acoustic waves (SAWs) have been shown to be a fast, efficient, and truly portable method for generating these flows and patterns [1-3]. Within SAW microfluidics, the lower size limitation is in part due to the typical frequencies of operation being on the order of 250 MHz or below. Here we demonstrate for the use of ultra high frequency (UHF) SAW—up to over 1 GHz—allowing further miniaturized device design and microfluidic capabilities [4].

Experiment

We fabricated SAW devices at a range of frequencies to investigate frequency effects on droplet patterning, acoustic streaming, heating, and channel pumping via acoustic counterflow. Each SAW device (Fig. 1a) consisted of a 128° Y-cut, X-propagating lithium niobate (LN) substrate, patterned with a 100 nm gold IDT and a 10 nm titanium adhesion layer. The nominally 50, 100, 200, and 400 MHz transducers were patterned via standard optical lithography, with designed finger widths of 20, 10, 5, and 2.5 μm respectively. The 833 MHz and 1.25 GHz transducers were patterned via electron beam lithography (EBL), owing to the reduced finger widths of 1.2 μm and 0.8 μm . Each IDT had an aperture of 700 μm , and was aligned such that a Rayleigh wave was induced along the substrate surface. After metallization and patterning, each chip was silanized according to the experimental requirements, eg, for the droplet experiments hydrophobic wells were patterned to restrain the droplets. Each device was connected to an RF signal generator and amplifier and operated at its resonant frequency, and SAW amplitudes were calibrated against input powers using a laser Doppler vibrometer (LDV; UHF-120 Ultra High Frequency Vibrometer, Polytec, Germany). Droplet patterning, streaming, and mixing were recorded with a high speed camera mounted on an inverted microscope, and thermal measurements were made with a thermal camera.

Results

Figure 1b demonstrates acoustic patterning and streaming in nanoliter order droplets, controlled by the choice of operational frequency. When operated at typical SAW-microfluidic frequencies and constant amplitude—here ~ 50 MHz—we see particle patterning in concentric circles within the droplet. Conversely, as the frequency is increased significantly—here to ~ 1.1 GHz—we see acoustic streaming occurring in the miniaturised droplets, useful for microfluidic mixing. We can describe the two schemes in terms of the *SAW damping length*, $x_s = 0.45 \lambda_s (\rho_s c_s) / (\rho_f c_f)$ where λ_s is the SAW wavelength, ρ_i and c_i are the densities and speeds of the wave, and subscripts s and f represent the substrate and fluid respectively. We see in our experiments that acoustic streaming was generated when $d/x_s \gg 1$, (where d is the droplet diameter) while particle accumulation

patterning occurred when $d/x_s \ll 1$. We applied the GHz order SAW to nanoliter droplet sized fluid mixing, and showed a dramatic reduction of mixing time as compared to mixing driven by diffusion alone [4]. We also characterized for the first time frequency effects on microfluidic droplet heating, and discuss the relevant length scales for thermal control and application for bio-systems. In addition to the digital microfluidic studies, we investigated the use of increasing the SAW frequency to the UHF range with the acoustic counterflow pumping device, and demonstrated further miniaturization of the channels, the fluid flows, and the completed devices themselves.

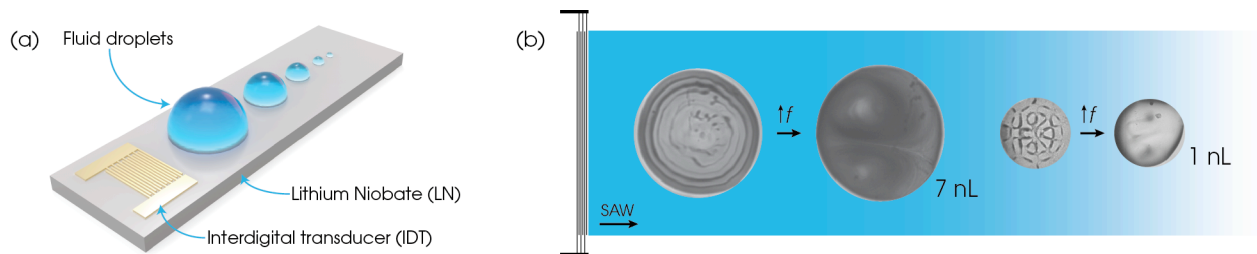


Fig. 1. (a) Schematic of a typical device (multiple droplet sizes shown). (b) Acoustic patterning and streaming in nanoliter-order free-droplets can be controlled by increasing the frequency of operation of the SAW device to the ultra high frequency regime. Here the droplets show comparison between ~ 50 MHz (left) and ~ 1.1 GHz devices (right).

Conclusion

Depending on the frequency of operation, we show nanoparticle patterning and mixing type flows in a range of droplet sizes (nano- to micro-liter), and demonstrate the principles used to tailor these internal flows. We also discuss frequency impact on microfluidic heating and microchannel channel flows. This new class of ultra high frequency SAW microfluidic device is suited to integration in portable lab-on-a-chip biosensor and bioreactor systems owing to the reduced size and increased flexibility of fluid manipulations.

References

- [1] J. Friend and L. Y. Yeo, *Microscale acoustofluidics: Microfluidics driven via acoustics and ultrasonics*, Rev Mod Phys, **83**, 647 (2011)
- [2] M. Cecchini, S. Girardo, D. Pisignano, R. Cingolani, and F. Beltram, *Acoustic-counterflow microfluidics by surface acoustic waves*, Appl Phys Lett, **92**, 104103 (2008)
- [3] R. Shilton, M. K. Tan, L. Y. Yeo, and J. R. Friend, *Particle concentration and mixing in microdrops driven by focused surface acoustic waves*, J Appl Phys, **104**, 014901 (2008)
- [4] R. J. Shilton, M. Travagliati, F. Beltram, and M. Cecchini, *Nanoliter-Droplet Acoustic Streaming via Ultra High Frequency Surface Acoustic Waves*, Adv Mater, DOI: [10.1002/adma.201400091](https://doi.org/10.1002/adma.201400091) (2014)

Acoustic and dielectrophoretic particle sorting using virtual deterministic lateral displacement (vDLD)

David J Collins¹, Tuncay Alan¹ and Adrian Neild¹

¹Department of Mechanical and Aerospace Engineering
 Monash University
 Room 204, Building 82
 Wellington Rd, Clayton VIC 3800, Australia
 Email: davidjohn.collins@monash.edu
 URL: www.davidcollins.webs.com

Introduction

The separation of cells and particles based on their physical properties is a necessary pre-conditioning step in a variety of microfluidic applications, increasing detection efficiency or for on-chip cell culturing. To address this need, a number of methods have been developed that make use of passive or active force gradients, generated by hydrodynamic, acoustic, dielectrophoretic (DEP), magnetic or optical means. The most significant drawback of methods demonstrated to date, however, has been the relatively poor sensitivity by which these separations can be performed in microfluidic systems, the exception here being hydrodynamic deterministic lateral displacement (DLD), whereby particles in angle pillar array take discrete paths as a function of their size relative to a critical dimension threshold [1]. Size sensitivity is important for applications such as detection of circulating tumour cells, which may vary in size from other circulating blood cells by only a few microns [2]. The widespread use of even this method, however, is limited by the potential for clogging, the small angle of separation (and therefore relatively long path lengths required) and the range of particle sizes that can be separated. Here we present a system design for the deterministic separation of particles in a microfluidic system, where either acoustic and DEP forces can be used. This method is termed virtual deterministic lateral displacement (vDLD), a reference to both the deterministic way in which particles can be separated and the means by which the critical diameter is determined, where a force field acts through a fluid media, as opposed to the physical pillars in a DLD array.

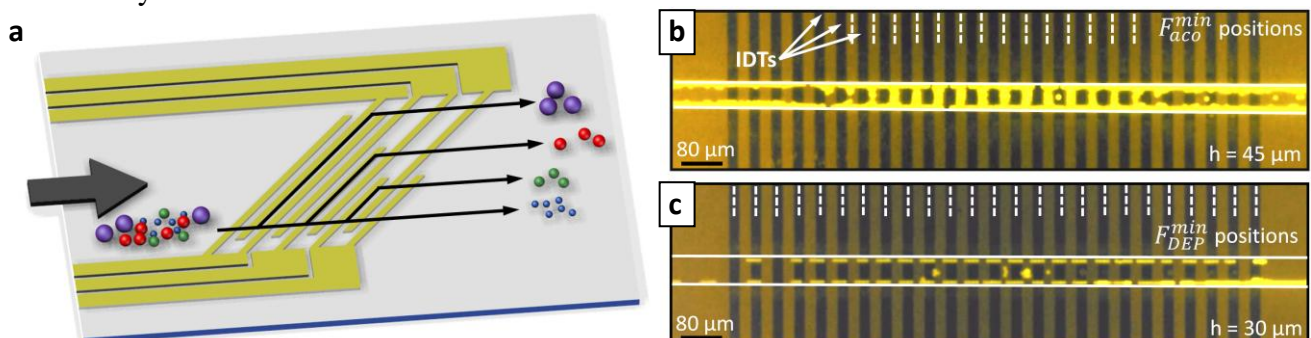


Fig. 1. (a) Diagram of the vDLD concept: particles larger than some critical diameter follow the force field (either acoustic or DEP) minima created by a series of IDT finger-pairs arrayed on a LN substrate. A multichannel version of the concept is shown here. The dominance of the acoustic or DEP force is a function of height above the substrate, where (b) the acoustic force is dominant in the far field, with particle alignment in the acoustic nodes in between finger-pairs and (c) the DEP force is dominant closer to the substrate, with alignment in the DEP nodes on top of the electrodes.

Concept

The vDLD system can make use of potentially any patternable force field where the axis of this field is oriented at an angle to the fluid flow. Here, we demonstrate the concept using both acoustic and DEP forces. To make use of both forces in the same device, a series of interdigital transducers (IDTs) are arrayed on a lithium niobate (LN) substrate. The IDTs produce an electric field in a fluid media in their immediate vicinity, while LN is used for its piezoelectric properties; when an electric potential is applied across the IDTs at a frequency such that the mechanical displacements

emanating from a set of IDT finger-pairs is reinforced by the adjoining set, a surface acoustic wave (SAW) is produced on the substrate [3]. Particles are separated deterministically based on their dimensions by virtue of the fact that larger particles will experience greater 'virtual' forces acting in opposition to drag forces. When the acoustic/DEP force (where $F_{aco/DEP} \sim R^3$) is greater than the induced drag force (with $F_D \sim R$), particles follow the force field lines; otherwise, particles will continue in the direction of the fluid flow. A multichannel version of the vDLD system concept is shown in Fig. 1(a), where multiple particle sizes can be deterministically sorted by increasing the field strength in the direction of fluid flow.

Because the decay constant is significantly greater for DEP than the acoustic field assessed vertically from the substrate, DEP is dominant in the vicinity of the IDTs, where the acoustic force is dominant in the far field. In the system demonstrated, where both forces act (repulsively) on the particles, the chamber height determines the dominant force and therefore the position of particles when trapped in a force field node (at the minimum F_{DEP}, F_{aco}), above the IDTs in the case of DEP and between them in the case of acoustic forces, as shown in Fig. 1(b,c).

Experiment

The vDLD device demonstrated consists of a series of 18 finger-pair 5/250 nm chrome/aluminium IDTs arrayed on a 0.5 mm thick, double side polished 128° Y-cut, X-propagating LN substrate operated at 49 MHz. A polydimethylsiloxane (PDMS) chamber was bonded on top of the substrate such that the flow is angled at $\sim 45^\circ$ to the long axis of the IDTs. DEP-dominant particle separation is demonstrated in a chamber 15 μm high, while acoustic particle separation is demonstrated in a chamber 45 μm in height.

Results

Fig 2. shows the experimental particle trajectories for a mixture of 5.0 μm and 6.6 μm particles in the case of a 15 μm high DEP-dominant (Fig. 2[a]) and a 45 μm high acoustic-dominant chamber (Fig. 2[b]). While the dominant force differs, the results are qualitatively similar, with ≥ 98 separation efficiency.

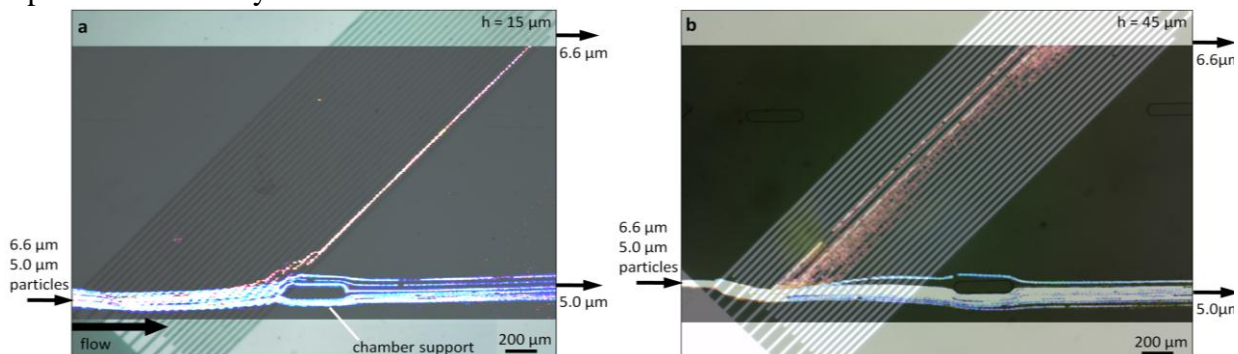


Fig. 2. Particle trajectories of a mixture of 5.0 μm (blue) and 6.6 μm (red) particles in the vDLD system, here in the (a) DEP dominant (chamber height = 15 μm) and (b) acoustic dominant (height = 45 μm) cases.

Conclusion

We have demonstrated the deterministic separation of particles in a microfluidic system by size, where the critical particle volume can be determined by acoustic or DEP forces. The ability to deterministically separate particle and cell populations in a tunable, pillar-free system will increase both the number of applications to which microfluidic processes can be applied and the efficiency by which they are performed.

References

- [1] L. R. Huang, E. C. Cox, R. H. Austin, and J. C. Sturm, *Continuous particle separation through deterministic lateral displacement*. Science 304, 987 (2004).
- [2] Sunitha Negrath, Lecia V Sequist, Shyamala Maheswaran, Daphne W Bell, Daniel Irimia, Lindsey Ulkus, Matthew R Smith, Eunice L Kwak, Subba Digumarthy, Alona Muzikansky, et al. Isolation of rare circulating tumour cells in cancer patients by microchip technology. Nature, 450(7173):1235–1239, 2007.
- [3] David J Collins, Tuncay Alan, and Adrian Neild. Particle separation using virtual deterministic lateral displacement (vDLD). Lab on a Chip, 14(9):1595–1603, 2014.

Combined acoustic torques and forces on spherical particles obtained by the leakage of two standing orthogonal surface acoustic waves

Ianis Bernard¹, Philippe Marmottant¹, David Rabaud², Cédric Poulain², and Pierre Thibault¹

¹Univ. Grenoble Alpes
LIPHY UMR CNRS 5588
F-3800 Grenoble, France
Email: pierre.thibault@ujf-grenoble.fr
URL: <http://www-liphy.ujf-grenoble.fr>

²Univ. Grenoble Alpes
CEA, LETI MINATEC Campus
F-38054 Grenoble, France
Email: cedric.poulain@cea.fr

Introduction

We study the rotation of axisymmetric particles obtained by two phase-shifted orthogonal standing waves, due to a viscous effect in the external fluid. Depending on the particle density and compressibility relative to the ambient fluid, we predict different acoustic torques [1] in the acoustic potential wells in which the particles are trapped. We observe that the viscous torque is “degenerated”, either clockwise or anti clockwise. A preferred sense of rotation exists with a spatial period that is not that of the standing wave ($\lambda/2$) but λ instead. The benefits for the control of both the position and the orientation of particles are illustrated by single biological cell manipulation.

Predictions and experiment

The Gor'kov radiation force potential [2] we expect for a spherical particle is represented on Fig. 1(a), together with the viscous torque obtained from the approach by Busse et al.[1]. Fig. 1 (a) has been plotted assuming small elastic particles denser and less compressible than the surrounding fluid. It appears that potential wells, in which particles are trapped, coincide with the maximum absolute torque, but with a sense of rotation alternating from a well to the other. The absolute torque is proportional to $\sin(\varphi)$ where φ is the time phase shift between the two standing waves. The experimental setup is based on the acoustic platform described in Ref. [3] and depicted on Fig. 1(b). Four interdigitated transducers (IDTs) generate two orthogonal phase shifted waves, leaking in a $1\text{mm} \times 1\text{mm} \times 160\mu\text{m}$ silicone (PDMS) square microcavity. The overall excitation frequency corresponding to the electrodes pitch ($\lambda=100\mu\text{m}$) is set to 36.3 MHz.

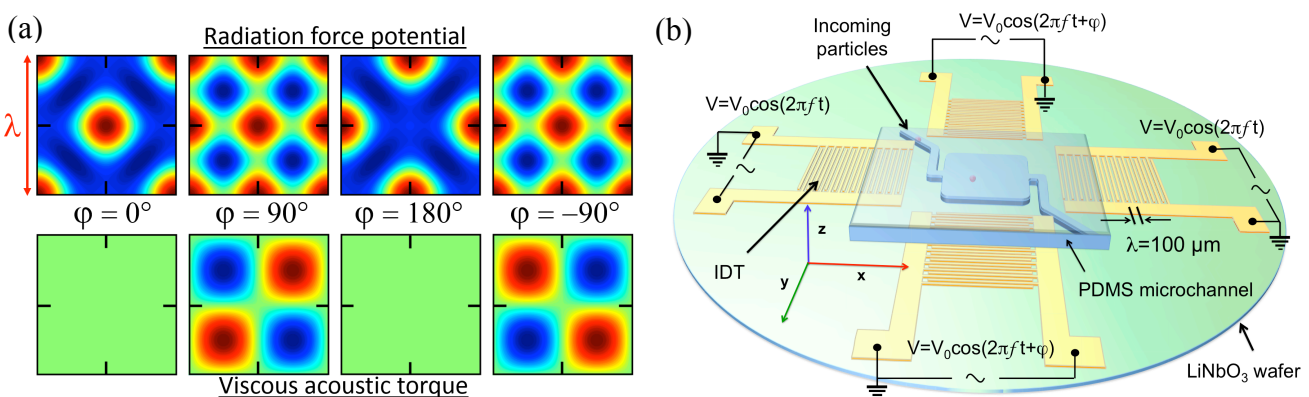


Fig. 1. (a) 2D simulation of the acoustic potentials in a $\lambda \times \lambda$ region (top, red barriers and blue wells) and of the acoustic torques (bottom, red clockwise and blue counter clockwise) exerted on a small spherical particle (radius $a \ll \lambda$) in the acoustic cavity submitted to two orthogonal phase shifted standing waves. From left to right, the phase differences are respectively $\varphi = 0^\circ, 90^\circ, 180^\circ$ and 270° . (b) Scheme of the acoustic device for particle manipulation, after the assembly of a transparent PDMS microfluidic device and a LiNbO₃ piezoelectric substrate.

Results

Measurements are performed on $\text{Ø}10\ \mu\text{m}$ Janus latex beads (half-metallized particles). As predicted by theory, Fig. 2 (a) shows that the beads are spaced with $\lambda/2$ in terms of equilibrium positions and are rotating in opposite directions. Moreover, we observed that cells such as white blood cells, slightly less compressible than water, were also rotating, as shown on Fig. 2 (b). In addition, micron-sized latex particles agglomerated in potential wells, forming roughly $10\ \mu\text{m}$ clusters. Those clusters, pictured on Fig. 3 (a) were seen to be trapped in a nearly $\lambda/2$ step width square lattice, coinciding with the maximum absolute torque, which sign is alternating from a well to the other, in good agreement with the theory pictured on Fig. 1(a). However, for droplets that are less dense and more compressible than the surrounding fluid the potential map is inverted, and they are generally trapped in a diamond pattern but experience no torque.

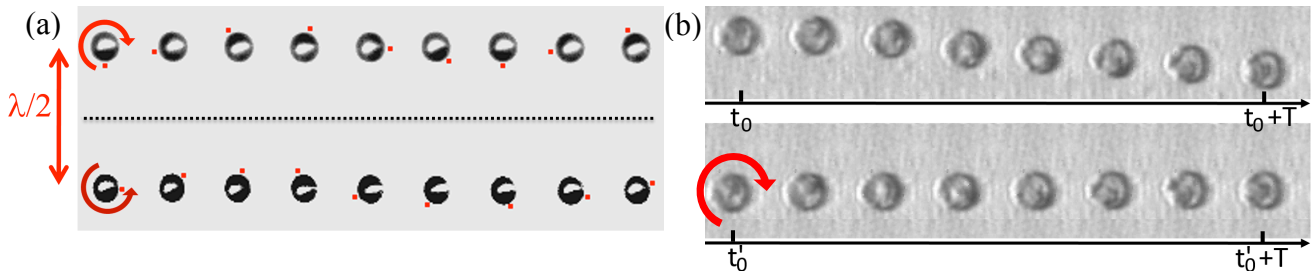


Fig. 2. (a) Top: Successive orientations of a $10\ \mu\text{m}$ Janus bead recorded at 15 fps and for 2 adjacent positions (period $\sim 0.5\ \text{s}$) (b) Snapshots (1 fps) showing the controlled slow rotation of a leukocyte ($\text{Ø}\ 12\ \mu\text{m}$) with the device of Fig. 1a). The 2 lines correspond to 2 successive full rotations of the cell (period = 8s)

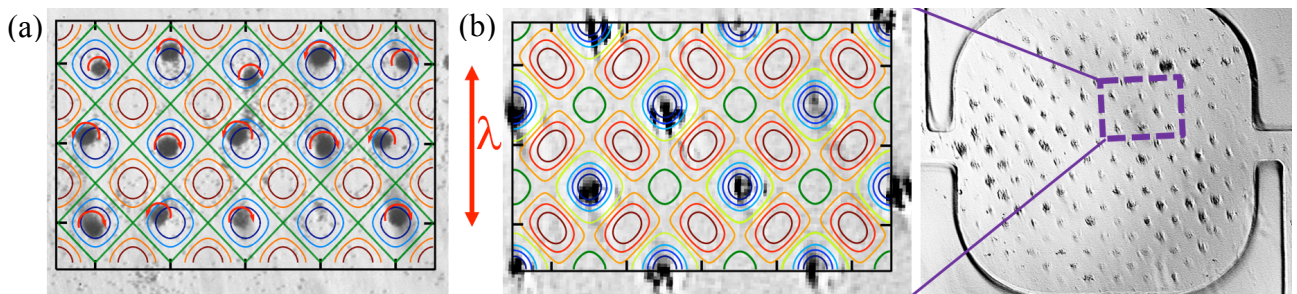


Fig. 3. Zoom on the lattice. (a) Image of the square lattice of $1\ \mu\text{m}$ diameter latex beads forming rotating clusters superimposed with colored lines obtained by simulation for an imposed time phase shift assumed to be $\varphi = 90^\circ$. Latex beads are denser and less compressible than water (ambient fluid). In red, the observed sense of rotation. (b) Droplets diamond lattice, obtained by mixing a concentrated solution of potassium iodide (KI) with soap, superimposed with simulation results obtained for assumed $\varphi = 70^\circ$. Droplets are less dense and assumed to be more compressible than almost saturated salted water (ambient fluid). No rotation was observed.

Conclusion

We found that dense particles could be rotated using surface acoustic waves. In perspective, these results can lead to a new tool for cell handling.

References

- [1] F.H. Busse and T.G. Wang, *Torque generated by orthogonal acoustic waves—theory*, JASA **69**, 1634–1638 (1981)
- [2] L.P. Gorkov, *on the forces acting on a small particle in an acoustical field in an ideal fluid*, Soviet Physiks - Doklady, **6**, 773-775 (1962).
- [3] S.B.Q. Tran, P. Marmottant, and P. Thibault, *Fast acoustic tweezers for the two-dimensional manipulation of individual particles in microfluidic channels*, App. Phys. Lett. **101**, 114103 (2012)



Cell and droplet sorting with surface acoustic waves

Lothar Schmid^{a,b} and Thomas Franke^{a,b}

^a Lehrstuhl für Experimentalphysik I, Soft Matter Group, Universität Augsburg, Universitätsstr. 1, 86159 Augsburg, Germany

^b Chair of Biomedical Engineering, School of Engineering, College of Science & Engineering, Glasgow University, Rankine Bldg., Oakfield Av. R522, Glasgow, UK

Email: Thomas.Franke@glasgow.ac.uk

Introduction

Fast sorting of single cells is an important technique for applications such as drug screening, diagnostics, rare cell detection and stem cell isolation. The most common approach is to use fluorescence-activated cell sorting (FACS), which identifies the target cells by fluorescence-based flow cytometry and breaks up the sample fluid into aerosol droplets, which are sorted by applying an electric field. [1], [2]

Microfluidic devices offer an alternative approach to cell sorting that allows for cheaper, small scale sorters, however existing actuation mechanisms require labeling the cells with microbeads [3], [4] or prior encapsulation into microemulsion droplets [5–7].

Recently, acoustic radiation forces in a gradient of a standing acoustic wave field have been used to deflect cells [8–11], but all of these actuation mechanisms critically depend on the volume and acoustic contrast of the sorted objects; This makes especially small objects difficult to sort.

We demonstrate a sorter that employs acoustic streaming induced by a travelling acoustic wave for actuation. This allows for sorting cells and other objects independent of their size and contrast directly from the bulk solution. The response times of the acoustic actuation are extremely short and enable extremely high sorting rates.

Experiment

We use a hybrid microfluidic device consisting of a transparent piezoelectric substrate (polished 128° rot Y-cut LiNbO₃) featuring a tapered interdigital transducer (T-IDT) generating the surface acoustic wave.

On top, we place a two-layered PDMS design. The top layer contains the actual microchannel, which contains a sample inlet and a sheath flow for hydrodynamic focusing the sample prior sorting into two or more outlets. The sheath flow is calibrated to align the sample trajectory and guide it into the waste channel in the absence of acoustic actuation. The bottom layer consists of a thin film sealing the channel, with a post (or two posts for triple sorting) protruding from the bottom, which couples the acoustic wave into the fluid inside the microchannel near the outlet junction. The acoustic wave is strongly attenuated in the fluid, transferring its momentum to the fluid and generating a vortex which pushes the sample to the collect channel.

Sample detection is performed by a fluorescence setup. If the intensity of the signal exceeds a preset threshold, a SAW pulse is generated, initiating sorting.

Results

We sort microemulsion droplets at rates of up to 3000/s at moderate SAW powers of 15dBm, with perfect purity and efficiency. We also extend the sorter to sort droplets into three different outlets. B16F10 mouse melanoma cells were sorted directly from the bulk solution without encapsulation, with high cell viability after sorting. Since cells cannot be aligned, a constant cell distance cannot be achieved. This leads to a trade-off between sorting rate, purity and efficiency, similar to conventional FACS machines.

Conclusion

We have introduced a versatile SAW-actuated microfluidic sorter for sorting cells and microemulsion droplets at high rates. As the actuation mechanism works directly on the fluid, sorting is independent of particle properties and does not require labelling.

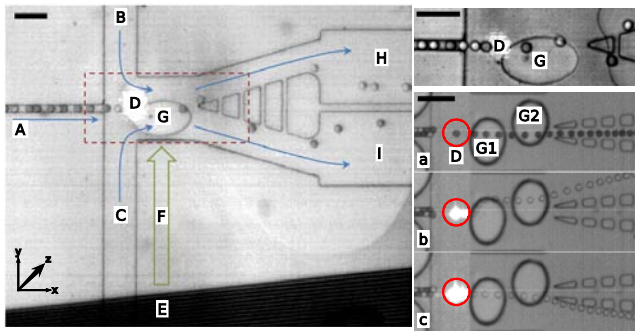


Fig. 1: (left) Top view of the droplet sorter setup. The droplets enter the sorting device through the inlet channel A. The top and bottom focusing channels B, C focus the droplets towards the middle of the channel to direct the droplets into the lower default outlet I. If a droplet passing the interrogation region D emits a fluorescent signal, a Surface Acoustic Wave (SAW) is generated by the interdigital transducer E, travelling along a narrow path F towards the contact post G, where the resulting sound field directs the droplet upwards into the upper outlet H. (top right) Zoom view of the two-way droplet sorter. (bottom right) Top view of a triple sorter setup. An additional middle outlet was added to the setup, and the contact post was split into two staggered posts G1, G2. Depending on fluorescence intensity detected at the laser spot D, either the SAW is not activated at all (no fluorescence, a), or is directed towards post 1 or 2 (low or high fluorescence, b & c, respectively). In the first case, the droplets move towards the middle default outlet. If one of the post is activated, the droplets are pushed away from the center of the post, either upwards (G1) or downwards (G2) and into the respective sorting outlets. Images (a,b,c) are montages, each showing a single droplet moving through the sorting channel. The length of the scalebars is 100 μm .

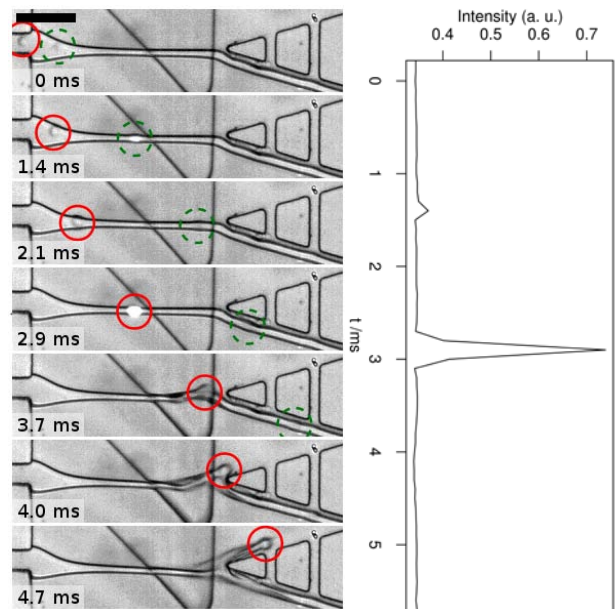


Fig. 2: (left) Top view of a cell sorting experiment. Mouse melanoma cells (B16F10) are treated with a stain sensitive to metabolic activity (Calcein-AM). The cells travel along the channel centre and their fluorescence is measured in the laser spot. The first cell (green dashed circle) has a low fluorescence and is therefore not deflected, flowing into the waste channel. The second cell (red circle) has a high fluorescence which triggers the sorter, deflecting the cell into the collect channel. The scale bar represents 100 μm . (right) Plot of the fluorescence intensity at the laser spot showing the fluorescence peaks of the two cells at $t=1.4$ ms and $t=2.9$ ms respectively.

In contrast to FACS, the sorter is self-contained and does not produce dangerous aerosols. Since the microchannel itself is a low-cost PDMS device, it can be produced as a disposable device, which eliminated cross-contamination problems when sorting different samples. Furthermore, since the sorter works by fluid switching, it is not limited to cell or droplet sorting, but can sort any detectable particle suspended in a fluid, independent of size. We envision sorting of nanoparticles, viruses and bacteria.

Acknowledgement

We acknowledge support (TF) by the German Excellence Initiative via NIM, the German Science Foundation (DFG) and the German Academic Exchange Service (DAAD). This work (DAW) was supported by the NSF (DMR-1006546), the Harvard MRSEC (DMR-0820484), the Mass Life Sciences Center and the NIH (P01GM096971).

References

- [1] H. M. Shapiro, *Practical Flow Cytometry*, vol. 4. Wiley-Liss, 2003, p. 542.
- [2] M. Eisenstein, "Cell sorting: divide and conquer.," *Nature*, vol. 441, no. 7097, pp. 1179–1185, 2006.
- [3] X. Hu, P. H. Bessette, J. Qian, C. D. Meinert, P. S. Daugherty, and H. T. Soh, "Marker-specific sorting of rare cells using dielectrophoresis," *Proceedings of the National Academy of Sciences of the United States of America*, vol. 102, no. 44, pp. 15757–15761, 2005.
- [4] U. Kim and H. T. Soh, "Simultaneous sorting of multiple bacterial targets using integrated dielectrophoretic-magnetic activated cell sorter.," *Lab on a Chip*, vol. 9, no. 16, pp. 2313–2318, 2009.
- [5] J. F. Edd, D. Di Carlo, K. J. Humphry, S. Köster, D. Irimia, D. A. Weitz, and M. Toner, "Controlled encapsulation of single-cells into monodisperse picolitre drops.," *Lab on a Chip*, vol. 8, no. 8, pp. 1262–1264, 2008.
- [6] S. Köster, F. E. Angilè, H. Duan, J. J. Agresti, A. Wintner, C. Schmitz, A. C. Rowat, C. A. Merten, D. Pisignano, A. D. Griffiths, and D. A. Weitz, "Drop-based microfluidic devices for encapsulation of single cells.," *Lab on a chip*, vol. 8, no. 7, pp. 1110–5, Jul. 2008.
- [7] J. J. Agresti, E. Antipov, A. R. Abate, K. Ahn, A. C. Rowat, J.-C. Baret, M. Marquez, A. M. Klibanov, A. D. Griffiths, and D. A. Weitz, "Ultra-high-throughput screening in drop-based microfluidics for directed evolution.," *Proc. Natl. Acad. Sci. USA*, vol. 107, no. 9, pp. 4004–9, Mar. 2010.
- [8] P. Augustsson, C. Magnusson, M. Nordin, H. Lilja, and T. Laurell, "Microfluidic, label-free enrichment of prostate cancer cells in blood based on acoustophoresis.," *Analytical chemistry*, vol. 84, no. 18, pp. 7954–62, Sep. 2012.
- [9] J. Shi, X. Mao, D. Ahmed, A. Colletti, and T. J. Huang, "Focusing microparticles in a microfluidic channel with standing surface acoustic waves (SSAW).," *Lab on a Chip*, vol. 8, no. 2, pp. 221–223, 2008.
- [10] M. Wiklund and H. M. Hertz, "Ultrasonic enhancement of bead-based bioaffinity assays.," *Lab on a Chip*, vol. 6, no. 10, pp. 1279–1292, 2006.
- [11] O. J. E. Jakobsson, C. Grenvall, M. Nordin, M. Evander, and T. Laurell, "Acoustic Actuated Fluorescence Activated Sorting of Microparticles," *Lab on a Chip*, 2014.

Session 7: Particle Manipulation	
15.10 - 15.30	<p>Cell trapping on acoustofluidic edge structures</p> <p>Ivo Leibacher and Jürg Dual ETH Zurich</p>
15.30 - 15.50	<p>Engineering single-vortex acoustic streaming for sub-micrometer particle handling</p> <p>P. B. Muller, M. Antfolk, P. Augustsson, T. Laurell, and H. Bruus Technical University of Denmark, Lund University</p>
15.50 - 16.10	<p>Efficiency Assessment of Acoustic Solid-Particle Separation in Gases</p> <p>Ramin J. Imani, Etienne Robert Royal Institute of Technology (KTH), Polytechnique Montréal</p>
16.10 – 16.30	<p>A novel combination of an optical trap with an acoustofluidic device to provide direct acoustic force measurements</p> <p>Andreas Lamprecht, Stefan Lakämper, Iwan Schaap, and Jurg Dual ETH Zurich, Georg-August Universität</p>
16.30 – 16.50	<p>Acoustic trapping for sepsis diagnosis using MALDI-MS</p> <p>B. Hammarström, B. Nilson, T. Laurell, J. Nilsson and S. Ekström Lund University, Dongguk University</p>
16.50 – 17.10	<p>SAW induced particle deflection in a microchannel using PDMS posts</p> <p>Richard Rambach and Thomas Franke University of Glasgow, Augsburg University</p>

Cell trapping on acoustofluidic edge structures

Ivo Leibacher and Jürg Dual

Institute of Mechanical Systems
 Department of Mechanical and Process Engineering
 Swiss Federal Institute of Technology ETH Zurich
 CH-8092 Zurich, Switzerland
 Email: leibacher@imes.mavt.ethz.ch
 URL: www.zfm.ethz.ch/e/exp-dyn/

Introduction

Cell and particle trapping on distinct locations in a microfluidic channel is an important operation for cell-biological lab-on-a-chip systems [1]. Such trapping provides a well definable, controlled chemical-thermal microenvironment for cell enrichment and screening, cell response studies and perfused cell culturing [2]. Other than the well-known particle trapping in acoustofluidic square or oval chambers with ultrasonic standing waves [3,4], here we present a physically novel cell trapping method. The method is based on the acoustic fields around vibrating edge structures, which protrude into a microfluidic channel.

Experiment

Edge structures (125-250 μm length, 10-80 μm width) were fabricated on a silicon wafer in a 30 μm deep and 1 mm wide microfluidic channel, Fig. 1(a). Excitation of the whole silicon structure was achieved by a piezoelectric transducer, driven at about 1 MHz by a sinusoidal voltage of $\sim 10 \text{ V}_{\text{rms}}$. Yeast cells/particles of 5-10 μm size were suspended in water and injected into the microfluidic channel. The dynamics of those particles was observed with up to 400 frames per second by a high speed camera (Fastec Imaging HiSpec 1) on a microscopic system with illumination by coaxial reflected light.

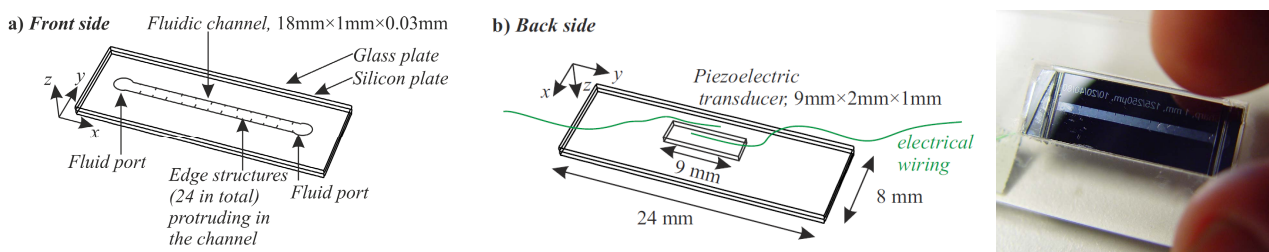


Fig. 1. (a,b) Sketch of the microfluidic device. (c) Photograph of the micromachined device in a laser-cut Plexiglas chip clamping.

Results

Upon ultrasonic excitation, the edge structures were found to attract yeast cells (and particles with contrast factor $\Phi > 0$) strongly and reliably, as observed in the time series of Fig. 2(a-c). This effect was analysed and understood by a numerical model of the radiation forces in the acoustic field around the vibrating edge structure. 3D frequency domain simulations (Comsol Multiphysics) outlined the validity of Gor'kov's theory for the given acoustic system. A simulated Gor'kov potential result is shown in Fig. 2(e), where the edge vibration was modelled as a harmonic rigid body motion in x -direction. This proposed modelling was then evaluated experimentally: The streamlines of the force field in Fig. 2(e) correspond well to the particle paths in Fig. 2(d) which were tracked with a video analysis software (ProAnalyst).

The physical trapping effect was further characterized with hollow particles of negative acoustic contrast $\Phi < 0$. These particles were repelled from the vibrating edge as predicted by the numerical model.

Furthermore, in Fig. 2(f,g) a PIV analysis of the acoustic streaming around the edge structures confirmed the results of Huang et al. [5]. As discussed by Rogers et al. [6], the dynamics of cells in the acoustic field was found to depend on the interplay between the described acoustic radiation forces and drag forces from the acoustic streaming.

Finally, the transfer function between the applied voltage on the piezoelectric element and the device surface velocity was measured by means of laser vibrometry. The described acoustofluidic trapping effect was found to work best at frequencies where a maximal velocity amplitude was measured. The trapping performance is therefore mainly dependent on transducer characteristics.

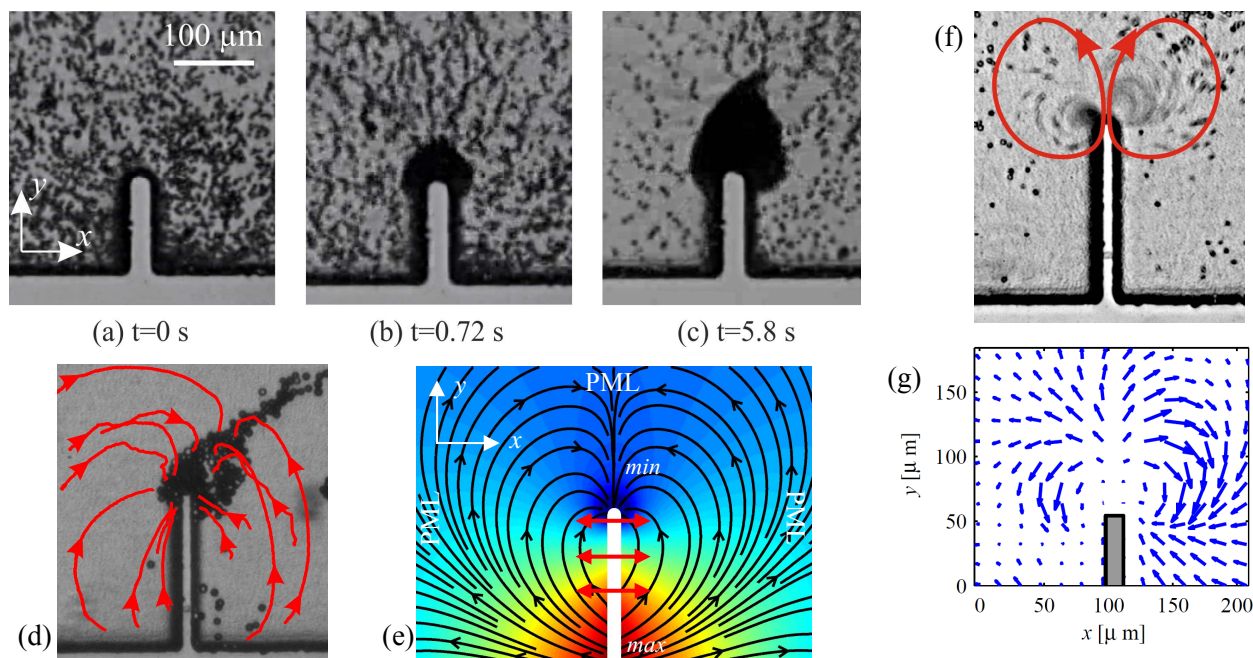


Fig. 2. (a-c) Time series of yeast cell trapping. Yeast cells (seen as dark dots) are suspended in a microfluidic channel. Upon mechanical excitation of 924 kHz at time $t > 0$, the yeast cells are attracted to the edge of size $125 \mu\text{m} \times 20 \mu\text{m}$. (d) Trapping of $11 \mu\text{m}$ co-polymer particles on an edge structure of $250 \mu\text{m} \times 10 \mu\text{m}$. Red lines mark the tracked particle paths which correspond well to the streamlines in (e). (e) shows the simulated Gor'kov potential around the vibrating edge structure for $\Phi > 0$ ($f_1 = 0.76$, $f_2 = 0.034$) with surrounding perfectly matched layer (PML) boundaries. The modelled harmonic edge vibration is illustrated by three red arrows. Particles are attracted to the blue minima of the Gor'kov potential, as denoted by the plotted streamlines of the radiation force field. (f) Acoustic streaming at the edge. Yeast cells are moved by circular counter rotating fluid flows. (g) PIV analysis result of the acoustic streaming field from the same experiment as in (f).

Conclusion

The shown acoustofluidic method allows to trap cells on a edge at an arbitrary position in a microfluidic channel. Stable and robust trapping was observed because the trapping method does not require a precise tuning of the excitation frequency. These features are advantageous compared to known acoustophoretic trapping methods with standing waves, where (1) the trapping of cells was only possible on pressure nodal lines between wave-reflecting system boundaries (spatial restriction) and (2) the excitation frequency had to be precisely tuned to match the temperature-sensitive fluid resonance frequency.

With these advantages and its relatively simple setup, the discussed device is believed to be suitable for a wide range of cell analysis applications such as clinical diagnostics, drug discovery and screening as well as single/cancer/stem cell research.

References

- [1] J. Nilsson, M. Evander, B. Hammarström and T. Laurell, *Review of cell and particle trapping in microfluidic systems*, *Analytica chimica acta* **649**, 141-157 (2009).
- [2] M. Evander and J. Nilsson, *Acoustofluidics 20: Applications in acoustic trapping*, *Lab Chip* **12**, 4667-4676 (2012).
- [3] O. Manneberg, B. Vanherberghen, J. Svennebring, H. M. Hertz, B. Önfelt and M. Wiklund, *A three-dimensional ultrasonic cage for characterization of individual cells*, *Applied Physics Letters* **93**, 63901 (2008).
- [4] J. Dual, P. Hahn, I. Leibacher, D. Möller, T. Schwarz and J. Wang, *Acoustofluidics 19: Ultrasonic microrobotics in cavities: devices and numerical simulation*, *Lab Chip* **12**, 4010-4021 (2012).
- [5] P. Huang, Y. Xie, D. Ahmed, J. Rufo, N. Nama, Y. Chen, C. Y. Chan and T. J. Huang, *An acoustofluidic micromixer based on oscillating sidewall sharp-edges*, *Lab Chip* **13**, 3847-3852 (2013).
- [6] P. Rogers and A. Neild, *Selective particle trapping using an oscillating microbubble*, *Lab Chip* **11**, 3710-3715 (2011).



Engineering single-vortex acoustic streaming for sub-micrometer particle handling

P. B. Muller¹, M. Antfolk², P. Augustsson², T. Laurell², and H. Bruus¹

¹Department of Physics
Technical University of Denmark
DTU Physics, building 309
DK-2800 Kongens Lyngby, Denmark
URL: www.staff.dtu.dk/~bruus/researchgroup

²Department of Biomedical Engineering
Lund University
Box 118
SE-221 00 Lund, Sweden

Introduction

Handling of sub-micrometer bioparticles such as bacteria is becoming increasingly important in the biomedical field and in environmental and food analysis. The usual quadrupolar vortex streaming flow of half-wavelength bulk acoustic wave devices of rectangular cross section does not allow for focusing of sub-micrometer particles, since the streaming induced drag counteracts the radiation force [1]. With surface acoustic waves at high frequencies it is possible to focus sub-micrometer particles, however at significantly lower flowrates [2]. In this combined numerical and experimental study we identify and optimize a single-vortex bulk streaming flow that allows for focusing of sub-micrometer particles by the primary radiation force. The single-vortex streaming flow is obtained by single-frequency simultaneous excitation of close-lying resonances of a nearly-square microchannel cross section.

Numerical model

The numerical analysis follows the scheme developed by Muller *et al.*[1] for calculation of the steady streaming flow and particle trajectories in the cross-sectional plane of a long straight microchannel. The numerical scheme is applied to a nearly-square channel 230.5 μm wide and 229.5 μm high. The oscillating first-order velocity boundary conditions applied to the walls was $u_{bc} = u_0 \cos(\omega t) \mathbf{e}_y$ on the left and right walls and $u_{bc} = u_0 \cos(\omega t + \phi) \mathbf{e}_z$ on the top and bottom walls, where u_0 is the amplitude, $\omega = 2\pi f$ is the angular frequency of the transducer, ϕ is a constant phase shift, and \mathbf{e}_y and \mathbf{e}_z are the unit vectors in the transverse horizontal and vertical directions, respectively.

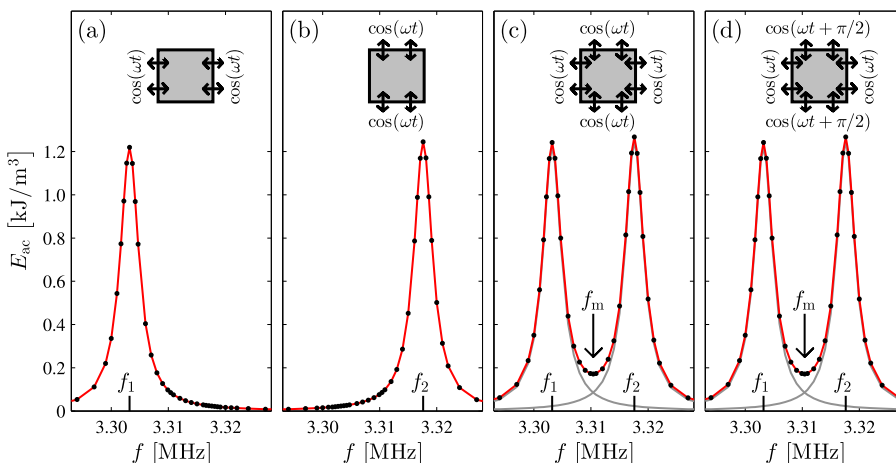


Figure 1: Resonance curves, obtained by plotting the average acoustic energy density E_{ac} vs. the frequency $f = \omega/2\pi$ of the oscillating velocity boundary conditions shown in the insets. f_1 and f_2 are the two resonance frequencies corresponding to the horizontal and vertical half-wavelength resonances, respectively. f_m indicates the middle frequency between the two resonance peaks. All walls have the same oscillation amplitude u_0 .

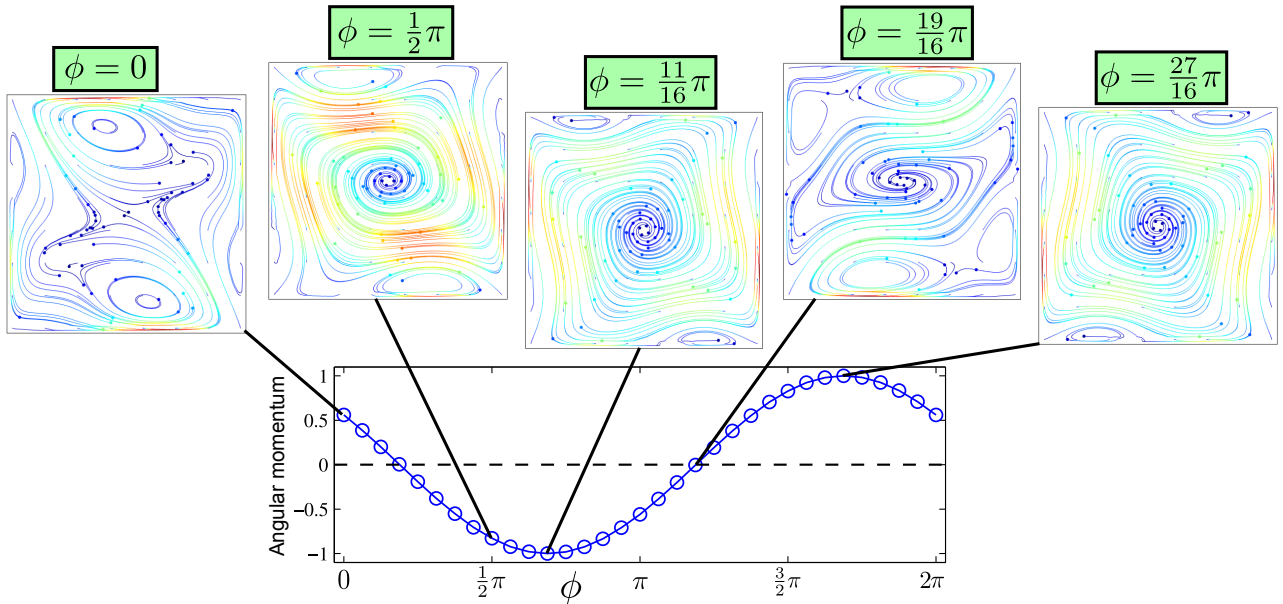


Figure 2: Simulated acoustophoretic trajectories of $0.5 \mu\text{m}$ particles in the vertical cross section of a microchannel along with a graph of the normalized angular momentum density of the fluid $\mathbf{L} = \mathbf{r} \times \rho_0 \langle \mathbf{v}_2 \rangle$ vs. the phase shift ϕ between the left/right wall pair and the top/bottom wall pair.

Results

Figure 1 shows the average acoustic energy density E_{ac} in the channel as function of the transducer frequency f for different velocity boundary conditions. Fig. 1(a) and (b) show the resonance curves for the horizontal and vertical half-wavelength resonances, respectively. Fig. 1(c) and (d) show a resonance curve with both peaks and a plateau in-between due to single-frequency simultaneous excitation of the two close-lying resonances. Even though the two-peak resonance curve is the same for the two different velocity boundary conditions with $\phi = 0$ and $\phi = \pi/2$, Fig. 1(c) and (d) respectively, the second-order steady streaming flow is significantly different. The simulated trajectories of $0.5 \mu\text{m}$ particles are shown in Fig. 2 for different values of the phase shift ϕ along with a graph of the normalized angular momentum density of the fluid $\mathbf{L} = \mathbf{r} \times \rho_0 \langle \mathbf{v}_2 \rangle$ perpendicular to the cross-sectional plane, which is seen to correlate well with the focussability of the particles. Continuous flow acoustophoresis experiments with a square $230\text{-}\mu\text{m}$ -by- $230\text{-}\mu\text{m}$ cross section demonstrated focusing of $0.5 \mu\text{m}$ particles and *E. coli* bacteria, which exerted a spiraling motion towards the channel center (results not shown, see Ref. [3]).

Conclusion

We have shown how simultaneous excitation of the two close-lying half-wavelength resonances of a nearly-square channel may generate a single-vortex streaming pattern. This enables focusing of sub-micrometer particles by the primary radiation force, following a spiraling motion towards the center of the channel, which is not possible with the usual quadrupolar vortex streaming of the half-wavelength resonance of a rectangular channel. The single-vortex streaming flow has been optimized numerically by changing the phase shift between the oscillating boundary velocity conditions. We demonstrate two-dimensional acoustophoretic focusing of *E. coli* bacteria and $0.5 \mu\text{m}$ polystyrene particles with high recovery. The ability to manipulate bacteria and other sub-micrometer particles in a bulk acoustic standing wave field opens up the acoustophoresis research field to new applications in microbiology.

References

- [1] P. B. Muller, R. Barnkob, M. J. H. Jensen, and H. Bruus, *Lab Chip* **12**, 4617-4627 (2012).
- [2] D. J. Collins, T. Alan, and A. Neild, *Lab Chip* **14**, 1595-1603 (2014)
- [3] M. Antfolk, P. B. Muller, P. Augustsson, H. Bruus, and T. Laurell, *Lab Chip* (2014), DOI: 10.1039/c4lc00202d.



Efficiency Assessment of Acoustic Solid-Particle Separation in Gases

Ramin J. Imani¹, Etienne Robert²

¹Department of Mechanics
Royal Institute of Technology(KTH)
KTH Mekanik, Osquare Backe 18
10044 Stockholm, Sweden
Email: ramin@mech.kth.se

²Departement of Mechanics
Polytechnique Montréal
C.P. 6079, succ. Centre-Ville
Montréal, Québec, Canada, H3C 3A7
Email: etienne.robert@polymtl.ca /etienne@mech.kth.se

Introduction

Separation of submicron particles suspended in gases is of great importance for both industrial and scientific applications. For instance, the particles produced through the combustion of hydrocarbons are known to pose serious health threats [1, 2]. Although submicron particles are produced in great numbers and penetrate deeper into the lungs, they still remain largely unregulated in current emission standards that focus on the total mass of particles produced. This situation is changing, motivating a need for robust particle separation techniques effective for submicron particles and capable of operating under harsh conditions in industrial applications such as biomass gasification [3], electronic waste recycling [4] and municipal waste incineration [5]. Established separation techniques are available (cyclones, electrostatic precipitators, scrubbers and filters), but each comes with its own set of limitations and all have reduced capabilities for the handling of submicron particles [6]. The objective of the work presented here is to investigate the potential of gas-phase acoustophoresis as a driving force for novel particle separation techniques, with an emphasis on submicron particles.

During the last decade, rapid developments in acoustic particle manipulation techniques in aqueous media have greatly benefited several microfluidics-based applications, essentially in the life sciences. These techniques exhibit several advantageous features that would be beneficial for aerosol treatment: physical barriers (subject to clogging) are not needed, nor are chemical additives, for separation of fine particles. Additionally, acoustics can separate particles based on their physical properties such as particle size, compressibility or density. The acoustic separation techniques developed in the liquid phase can potentially be adapted to particles suspended in gases. In this work we investigated the effect several key parameters (flow, acoustic and geometrical) on the particle separation efficiency in a simple rectangular channel seeded with submicron solid particles suspended in air.

Experiment

The separation channel used features an adjustable height of up to 20mm and an electrostatic broadband transducer (operated in the 50-100 kHz range) is used as an excitation source. This allows the investigation of the excitation frequency and the number of nodes on particle separation. The efficiency of the process is measured by seeding the gas flow through the channel with TiO₂ particles (300nm nominal diameter) and observing the distribution of particles using a light scattering technique. A thin laser sheet parallel to the flow direction is inserted through the downstream opening of the channel and a camera positioned perpendicular to the flow is used to capture the scattered light. The acquired images are then processed using Matlab to yield a value that can be used to assess the effect of different flow and acoustic parameters on separation efficiency. The efficiency metric used here is the ratio of the collected light intensity downstream of the transducer within the nodal bands to the collected light intensity upstream of the channel. Fig.1(a) illustrates the particle distribution with and without the acoustic excitation inside the separation channel.

Results

Using this experimental setup we have investigated the effect of sound pressure amplitude on the separation efficiency, with the results shown in Fig.1(b). As expected, the separation efficiency

increases with sound pressure amplitude. If we consider only the efficiency value corresponding to the optimum resonant frequency (ORF) in each frequency scan and plot them versus sound pressure amplitude, there is a trend that deviates slightly from the power-law growth expected from the axial component of primary radiation force. In Fig.1(c) the effect of channel velocity on the separation efficiency is depicted. The efficiency value corresponding to the ORF is inversely proportional to the gas velocity; it is therefore as expected proportional to the residence time of particle in the standing wave. The effect of frequency on the acoustic separation efficiency is also investigated and shown in Fig.1(d) where the result follow the trend expected from the dependence of the axial primary radiation force on the frequency. The effect of the parallelism of the reflector wall with respect to the channel base was also studied. The result showed that the average tolerance necessary to maintain 90% of the optimum separation efficiency was about $11\mu\text{m}$ (corresponding to an angle of 0.4 minute of arc) for channel height equal to 5.71mm. The alignment tolerance for 90% efficiency increased as the channel height decreased. In Fig.1(a) the visualization of particles in the presence of the acoustic excitation shows an unexpected distribution of particles inside the channel. When two nodes are present in the channel, they are located at a distance less than a half wavelength away from each other. An accumulation of particles at the transducer and reflector walls was also observed. This is at odds with the expectation that there is a pressure antinode at the walls and that solid particles suspended in air should move to the pressure nodes.

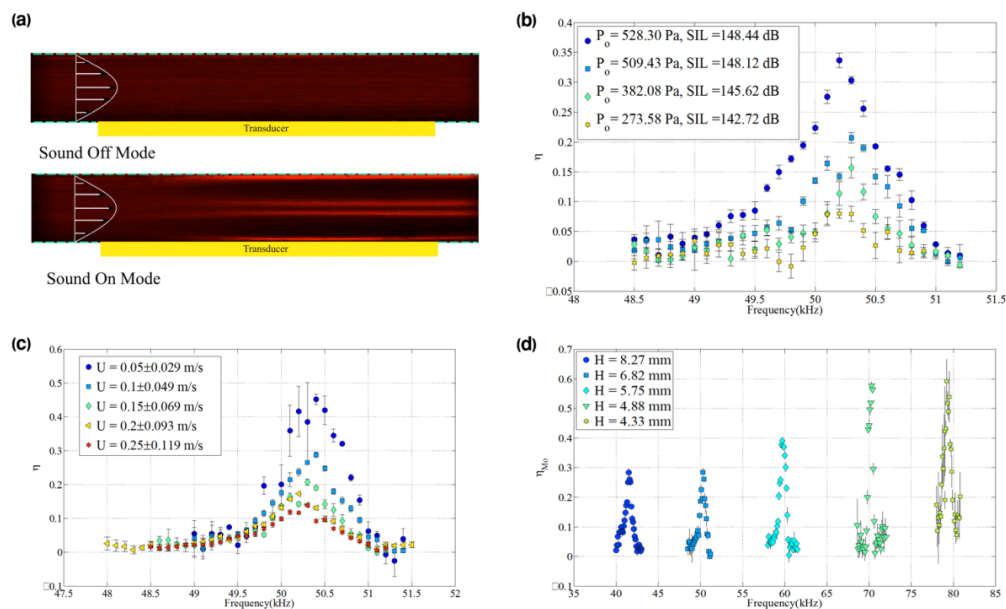


Fig. 1. (a) Visualization of acoustic particle separation with and without sound source in the separation channel using laser light scattering. (b) Separation efficiency as a function of sound pressure amplitude. (c) Separation efficiency as a function of velocity inside the channel. (d) Separation efficiency as a function of frequency

Conclusion

We have calculated the separation efficiency as functions of several key parameters in designing an acoustic separation channel. The results were mainly in agreement with the expected theory in which the acoustic axial component is considered as the dominant force in driving the particle to the nodal planes. The unexpected distribution of particles inside the channel, in presence of the acoustic excitation, has been observed. We have not found a satisfactory explanation for these observations so far and further investigations are underway.

References

- [1] Debra T. Silverman et.al, *The Diesel Exhaust in Miners Study: A Nested Case-Control Study of Lung Cancer and Diesel Exhaust*, JNCI J Natl Cancer Inst, Vol 104 (11), 1-14 (2012).
- [2] Attfield, M.D et.al, *A Cohort Mortality Study With Emphasis on Lung Cancer*, J. Nat. Cancer Inst, Vol 104 (11), 869-883 (2012).
- [3] Knoef H. and Jesper A. *Handbook biomass gasification*. BTG biomass technology group, 2005.
- [4] Deng, W. J. et.al, "Atmospheric levels and cytotoxicity of PAHs and heavy metals in TSP and $PM_{2.5}$ at an electronic waste recycling site in southeast China." *Atmospheric Environment* 40.36 (2006): 6945-6955.
- [5] Linak, William P., and Jost OL Wendt. "Toxic metal emissions from incineration: mechanisms and control." *Progress in Energy and Combustion Science* 19.2 (1993): 145-185.
- [6] Peukert, W., and C. Wadenpohl. "Industrial separation of fine particles with difficult dust properties." *Powder technology* 118.1 (2001): 136-148.

A novel combination of an optical trap with an acoustofluidic device to provide direct acoustic force measurements

Andreas Lamprecht¹, Stefan Lakämper¹,
Iwan Schaap², and Jurg Dual¹

¹ Center of Mechanics
Swiss Federal Institute of Technology
Tannenstrasse 3, Building CLA
CH-8092 Zurich, Switzerland
Email: lamprecht@imes.mavt.ethz.ch
URL: www.zfm.mavt.ethz.ch

² Drittes Physikalisches Institut
Georg-August Universität
Wilhelmsplatz 1
37073 Göttingen, Deutschland
Email: iwan.schaap@phys.uni-goettingen.de

Introduction

Due to its characteristics one appealing method for contact-free particle manipulation is the use of acoustic standing waves. It is becoming of particular interest at the interface of engineering and biological research, i.e. biomedical engineering, applied micro-technology and life science.

For a full acoustic characterization of an acoustofluidic device it is necessary to know the spatial distribution of the acoustic pressure within the fluid chambers. In an indirect way of measurement Barnkob et al.^[1] had shown that it is possible to estimate the local acoustic pressure amplitudes by particle tracking and a subsequent fitting to a theoretical model. Therefore the particle trajectory of an arbitrarily placed particle within the device was observed while it was moving to its equilibrium position at an acoustic pressure node. An alternative method was shown by Thalhammer et al.^[2] by locating the particles with a long-range optical trap at a defined starting position before the particle motion was initiated by ultrasound. A novel direct method to predict the spatial acoustic pressure distribution in acoustofluidic devices is realized here by the use of a single-beam gradient laser trap.

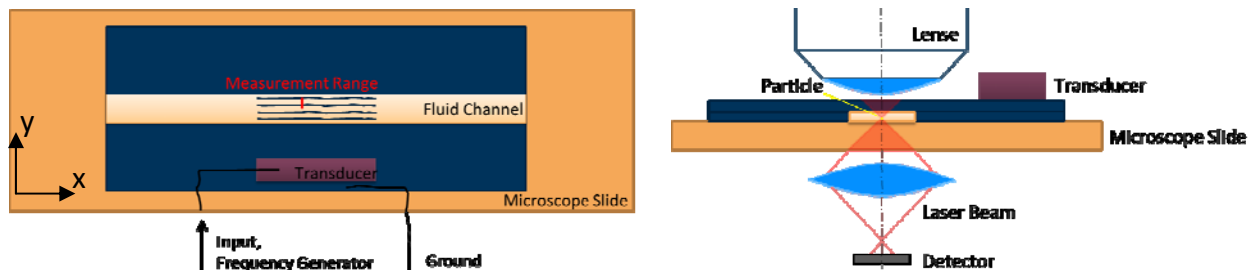


Fig. 1. Schematic illustrations of the acoustic device and the simplified main optical components. A standard microscope slide carries a cut coverslip as spacer for a 4 mm wide channel which is covered with another coverslip. A piezo-electric transducer of about 2x1x8 mm in size was glued to it with conductive epoxy parallel to the channel-length (x). The channel width of 4mm is due to the high numerical aperture objective needed for the optical trapping and position detection to avoid optical scattering on the channel walls. The laser trap is driven by a tightly focused laser-beam of 980nm wavelength which is collimated and projected in a slightly defocused manner on a quadrant photo detector to derive the trap stiffness by Brownian Motion.

Measurement Concept

This concept provides the possibility to do direct 3D acoustic force measurements at defined positions on dielectric spheres in the ray optics regime. Therefore transparent devices were built out of standardized microscope coverslips and a well-defined sharp edged fluid channel was made by the use of a dicing saw. A schematic illustration of a single-beam gradient laser trap and of the used device is shown in Fig.1. In the experimental setup a dielectric particle was suspended by the single-beam gradient trap of 980nm wavelength and moved to a specified position in the center of the channel to avoid boundary effects. While applying ultrasonic frequency sweeps around known eigen frequencies, we monitored the displacement of the particle from the trap center. The trap stiffness for the observed displacement was derived by measuring the Brownian motion of the particle in the optical trap potential. Knowing the stiffness of the trap we subsequently calculated

the time averaged forces in dependence of the frequency and the position along the direction of wave propagation, which was varied with a translation stage. Fig. 2a. shows the directly measured force field on a 7.61 μm Silica particle at an eigen frequency of 1510kHz.

Acoustic Pressure Prediction

Yosioka et al.^[3] gives the relation between the acoustic force amplitude A_F and the acoustic pressure amplitude A_P and is defined for the time averaged acoustic force $\langle F \rangle$ on a spherical particle as

$$\langle F \rangle = \pi \rho_f A_P^2 (k_F r_s)^3 F_y \sin(2 k_F y_s)$$

where, ρ_f is the fluid density, k_p is the wave number of the acoustic pressure field, r_s the radius of the sphere, y_s the position of the sphere within the pressure field and F_y is the acoustic contrast factor defined by Yosioka^[3]. Here, the pressure amplitude A_P is the only unknown parameter because the particle position y_s is defined by the position of the optical trap within the fluid chamber as well as the wave number k_F of the acoustic force curve. Under the assumption that this relation holds for each single point of the averaged acoustic force curve of multiple measurements, it is straightforward to calculate the acoustic pressure for $\lambda_P = 2 \lambda_F$. Subsequent averaging of the calculated pressure distributions of the investigated measurement range along the y -direction (Fig.2a) leads to the acoustic pressure amplitude for the eigen modes as shown in Fig. 2b. The results are compared to Comsol simulations.

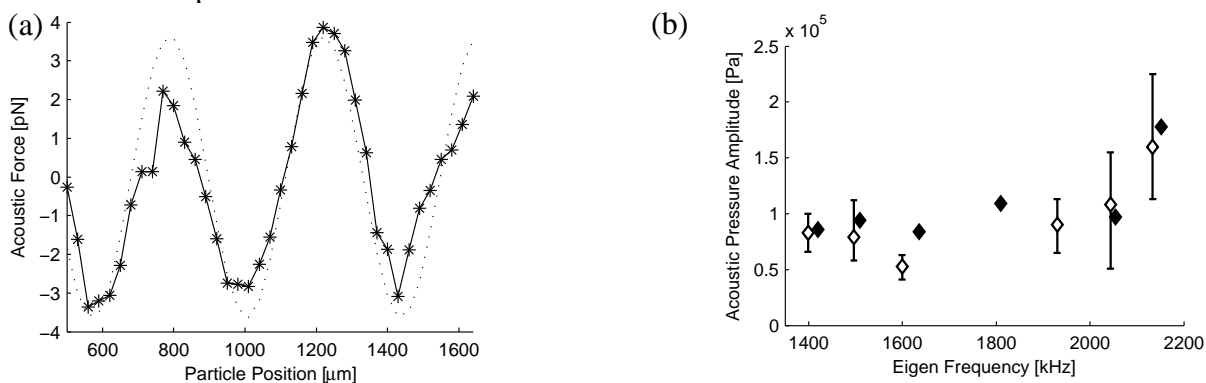


Fig. 2. (a) The connected Asterisk symbols indicate the observed force as calculated from the bead displacement and the trap-stiffness as a function of the y -position at 1510kHz. 7.61 μm Silica particles were used and the channel was filled with water. The dotted line shows the resulting sinusoidal fitting curve of the measurements ($\lambda_F=500\mu\text{m}$, $A_F=3.75\text{pN}$) (b) comparison of acoustic pressure amplitudes experimentally determined (open squares) and numerically calculated (filled squares). Error bars indicate the absolute range of experimental data.

Conclusion

Based on the current models we calculate the resulting acoustic pressure field properties. By use of a laser trap, we suspend a sound-hard spherical particle at a specified position within a fluid chamber. While applying ultrasonic frequency scans, we monitored the displacement of the particle from the trap center and subsequently calculated the time averaged forces in dependence of the position along the direction of wave propagation and the frequency. From the obtained quantitative data from both the device characterization and the sinusoidal position dependence, we were able to determine the pressure distribution within the device. The obtained data corresponds exquisitely well with predictions from theory and modeling. The method allows to be readily adjusted to other particle-, chamber-, and fluidregimes and will be combined with other imaging techniques, for example Schlieren-imaging to visualize the acoustic waves directly. Thus, this new and direct measurement opens up the possibility to quantify so far inaccessible small scale phenomena such as the effects of local and global acoustic streaming, effects of boundaries or near objects as well as non-linear fluids.

References

- [1] R. Barnkob, P. Augustsson, T. Laurell and H. Bruus, *Measuring the local pressure amplitude in microchannel acoustophoresis*, Lab Chip, 2010, 10, 563-570.
- [2] G. Thalhammer, R. Steiger, M. Meinschad, M. Hill, S. Bernet and M. Ritsch-Marte, *Combined acoustic and optical trapping*, Biomed Opt Express, 2011, 2, 2859-2870.
- [3] K. Yosioka and Y. Kawasima, *Acoustic radiation pressure on a compressible sphere*, Acustica, 1955, 5.



Acoustic trapping for sepsis diagnosis using MALDI-MS

B. Hammarström¹, B. Nilson^{2,3}, T. Laurell^{1,4,5}, J. Nilsson¹ and S. Ekström^{1,5}

¹ Department of Biomedical Engineering, Lund University, SWEDEN

² Clinical Microbiology, Labmedicin, Region Skåne, Lund, SWEDEN

³ Department of Laboratory Medicine, Division of Medicinal Microbiology, Lund University, Sweden

⁴ Department of Biomedical Engineering, Dongguk University, KOREA

⁵ CREATE Health, Lund University, SWEDEN

Acoustic trapping is here used to automate and speed up the sample preparation needed for MALDI-MS bacteria typing from blood-culture flasks. Automation is here enabled by using acoustic trapping to replace the standard centrifugation-based method. The presented technology addresses a number of current challenges and provides a possibility to handle microbial pathogens that are difficult to lyse, or have lots of peptidoglycans, as well as handling complex backgrounds (blood/urine) and leaves the potential for developing methods to quickly deduce antibiotics resistance.

Identification of bacteria species with MALDI-MS is becoming a new standard in clinical practice for microbial pathogen diagnosis [1], used in more than 1000 microbiology labs around the world with more than 20 million analyses were performed last year. These analyses all require time consuming manual sample preparation of hazardous samples. The current standard protocol for sepsis involves overnight culturing in blood culture flasks to increase the bacteria concentration, followed by manual sample preparation in form of selective-lysis and several cumbersome centrifugation steps. Our improved method for bacteria purification is based on a microfluidic platform for seed-particle aided acoustic trapping of the bacteria, enabling non-contact enrichment in low-cost disposable glass capillaries with efficient washing capability

Experimental

Escherichia coli was spiked in whole blood and cultivated using the clinically used blood culture flask-incubator. At an approximate concentration of 10^7 mL⁻¹ the presence of bacteria was detected by the incubator. The blood cells were selectively lysed using a lysis buffer from the Bruker-Sepsityper kit (20 μ L buffer in 1 mL blood). The lysate was directly aspirated in an acoustic trap arranged in a glass capillary (200x2000 μ m² cross-section) [2]. The trap was preloaded with a small number of seed-particles [3] allowing for acoustically trapping of the bacteria and subsequent aspiration and dispensing of deionized water enabled efficient removal of plasma proteins. The trapped bacteria were released by dispensing a 10 μ L water volume containing the bacteria cluster. The cluster was released into the previously presented ISET SPE sample preparation platform [4] packed with 10 μ m RP beads, in order to decrease the sample volume, concentrate and purify the bacterial proteins, as well as form a crystal for the MALDI-detection.

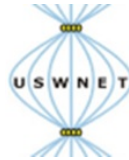
Results and discussion

The bacteria were successfully identified with MALDI-MS as *E. coli* using the standard Bruker-Biotyper software correlating the obtained spectra with the reference database. The presented microfluidic technology replaces five centrifugation steps and provides successful typing of bacteria from blood culture. This automated microfluidic assay can improve bacterial identification using only a very small sample, and provides help for clinical microbiology laboratories that are in dire need of fast and reliable methods to analyze bacteria in order to provide the correct choice of infection therapy.

References

- [1] S. Sauer, M. Kliem, "Mass spectrometry tools for the classification and identification of bacteria," *Nat. Rev. Microbiol.*, vol. 8, pp. 74-82, 2009.
- [2] B. Hammarström, M. Evander, H. Barbeau, M. Bruzelius, J. Larsson, T. Laurell, J. Nilsson, "Non-contact acoustic cell trapping in disposable glass capillaries," *Lab on a Chip*, vol. 10, pp. 2251-2257, 2010.
- [3] B. Hammarström, T. Laurell, J. Nilsson, "Seed particle-enabled acoustic trapping of bacteria and nanoparticles in continuous flow systems," *Lab on a Chip*, vol. 17, pp. 2251-7, 2012.
- [4] S. Ekström, L. Wallman, D. Hök, G. Marko Varga and T. Laurell, "Miniaturized solid-phase extraction and sample preparation for MALDI MS using using a microfabricated integrated selective enrichment target," *Journal of Proteome Research*, vol. 5, pp. 1071-1081, 2006.

Poster Abstracts



Acoustophoretic particle focusing in a square glass capillary: a 3D quantification

Rune Barnkob, Álvaro G. Marín, Massimiliano Rossi, and Christian J. Kähler

Institute of Fluid Mechanics and Aerodynamics
Bundeswehr University Munich
Neubiberg, Germany

Email: barnkob@unibw.de

Introduction

The manipulation of fluids and particles using ultrasound in microsystems is a rapidly expanding field. The use of bulk-acoustic-actuated glass capillaries is receiving increasing interest as mass-produced glass capillaries provide a cheap and efficient alternative to clean-room-fabricated chips. For example, glass capillaries have been used for acoustic trapping and separation purposes¹ and recently, Evander and Tenje presented the idea of using polymeric fluidic connectors to open up for the use of single-use glass capillaries with complex microfluidic systems². Alongside, more and more acoustofluidics applications are using two-dimensional acoustic focusing for improved manipulation and separation³, and recently, Antfolk *et al.*⁴ presented the use of simultaneously actuating two perpendicular acoustic resonances in a square microchannel to significantly enhance the separation of sub- μm -sized particles. In this work we present a quantitative study of the three-dimensional acoustophoretic particle motion in a square glass capillary. The motivation for this work is to understand and enhance the separation and manipulation of μm -sized and sub- μm -sized particles in such simple and versatile systems.

Theory

A square glass capillary is sketched in Fig. 1(a) and shown in Fig. 1(c). Considering only the two-dimensional liquid domain surrounded by hard walls and without losses, a horizontal half-wave resonance $p_{1y} = p_{ay} \sin[(\pi/w)y]$ and a vertical half-wave resonance $p_{1z} = p_{az} \sin[(\pi/h)z]$ are located at the exact same frequency $f_{10} = f_{01}$. However, the actual system includes viscous and dissipative losses leading to finite-width resonances. Furthermore, the actual system contains asymmetries in the capillary dimensions due to fabrication precision as well as asymmetries in actuation conditions and as a result the two resonances f_{10} and f_{01} will be separated by Δf . Thus, sweeping in frequency we expect a vertical pressure nodal line at f_{10} , a horizontal pressure nodal line at f_{01} , and a diagonal pressure nodal line at f_m being the frequency where the two resonances are present with the same acoustic energy, see Fig. 1(b). In Antfolk *et al.*⁴, this is simulated by finite element modeling by actuating the horizontal and vertical solid/liquid side walls simultaneously either in or out of phase, resulting in a steady or rotating diagonal nodal line, respectively. However, this is a simplified model of the actual actuation displacement at the solid/liquid interface. In this work we will clarify this by tracking the 3D position of particles being focused to the pressure nodal lines by the acoustic radiation force.

Experiments

The system is a 50-mm-long square glass capillary with nominal 400- μm -inner width and 800- μm -outer width. The capillary is filled with a neutrally-buoyant suspension of 5- μm fluorescent polystyrene particles in a glycerol:water (20:80) solution, see Fig. 1(c). The flow is stopped and the capillary is acoustically actuated via a piezo transducer while the three-dimensional particle trajectories are determined in a 3.3-mm-long field-of-view using astigmatic particle tracking

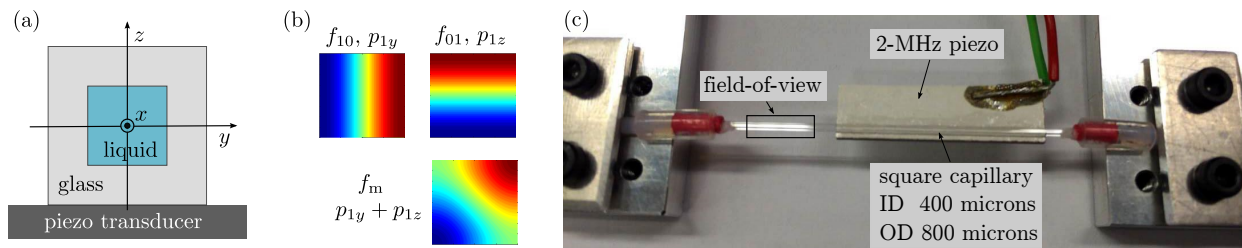


Figure 1: (a) Sketch of a liquid-filled square glass capillary attached to a piezo transducer. (b) Pressure modes p_{1y} and p_{1z} and their superposition in the square capillary. (c) Photograph of the square glass capillary.

velocimetry⁵. The actuation frequencies range from 1840 kHz to 1900 kHz at temperature $(25.2 \pm 0.2)^\circ\text{C}$. The actual channel is measured to have a width $w = (426 \pm 10) \mu\text{m}$ and height $h = (434 \pm 10) \mu\text{m}$ by forcing a Poiseuille flow through the channel and making a fit to find the walls. These channel widths correspond to $f_{10} \approx 1860$ kHz and $f_{01} \approx 1830$ kHz.

Results

Fig. 2 shows the obtained particle trajectories. Note that the acoustic resonances do also vary along x , but in this work the variation along x is weak and not investigated in detail. The observed results are as following; (a) at 1840 kHz the particles focus towards a horizontal nodal line as for the f_{01} resonance, (b) at 1865 kHz the particles focus to the channel center, (c) at 1890 kHz the particles focus to a diagonal nodal line as for f_m where the f_{10} and f_{01} modes are approximately equal, and finally (d) at 1900 kHz the particles focus to a vertical nodal line as for the f_{10} resonance. These results indicate a resonance splitting of $\Delta f \approx 60$ kHz.

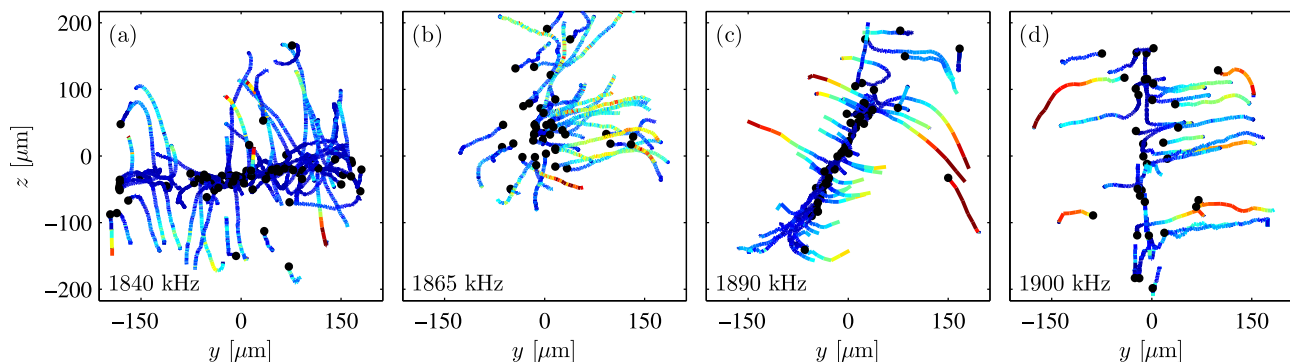


Figure 2: (y, z) -projections of experimental particle trajectories along a 3.3-mm field-of-view along x for four acoustic actuation frequencies, (a) 1840 kHz, (b) 1865 kHz, (c) 1890 kHz, and (d) 1900 kHz. The black dots show the trajectory endpoints and the absolute particle velocities are illustrated in colors from 0 (dark blue) to 80 % of the maximum particle velocity for each frequency (dark red).

Conclusions and outlook

Our quantitative measurements of radiation-dominated acoustophoretic particle motion in a square glass capillary agree qualitatively well with basic theoretical predictions. The final aim of this work will be to perform a full quantitative comparison with numerical models in order to improve our understanding of the acoustic resonances. To achieve this aim, better statistics on radiation-dominated as well as streaming-dominated particle motion will be obtained.

References

- [1] B. Hammarström, T. Laurell, and J. Nilsson, *Lab Chip* **12**, 4296 (2012).
- [2] M. Evander and M. Tenje, *J. Micromech. Microeng.* **24**, 027003 (2014).
- [3] P. Augustsson, C. Magnusson, M. Nordin, H. Lilja, and T. Laurell, *Anal. Chem.* **84**, 7954 (2012).
- [4] M. Antfolk, P.B. Muller, P. Augustsson, H. Bruus, and T. Laurell, *Lab Chip*, *online* (2014).
- [5] C. Cierpka, M. Rossi, R. Segura, and C. J. Kähler, *Meas. Sci. Technol.* **22**, 015401 (2011).

SAW-microchannel fluid mixing in simulation and experiment

Stefan Wege*, Andreas Winkler, Raimund Brüinig, and Hagen Schmidt

*IFW Dresden, SAWLab Saxony
 PF 270116, 01171 Dresden, Germany
 Email: S.Wege@ifw-dresden.de

Introduction

Surface acoustic wave (SAW) devices can be applied for mixing as well as for heating at low Reynolds numbers in order to increase sensor signals [1,2] or to speed up synthetic chemistry [3]. Concerning SAW-based mixing in microchannels only very few results are published yet, but mostly large SAW wavelengths (200 - 500 μm) are applied for this purpose [4-7]. Here, we present our investigations of mixing in a rectangular microfluidic channel using travelling SAWs and the associated fluid temperature development. Using finite element modelling of SAW induced streaming and mixing in microchannels, we identified wavelengths suitable for efficient mixing. Our results reveal the influences of the fluid velocity in the channel, the wavelength and the load power on the mixing efficiency. We show that efficient mixing can be achieved even at low power levels accompanied by a temperature increase of less than 5K if appropriate wavelengths, with respect to the channel dimensions, are chosen.

Experiment

Comsol Multiphysics FEM simulations were carried out in order to estimate three-dimensional concentration profiles of two aqueous fluids along the channel actuated/mixed by a volume force corresponding to the SAW amplitude. At fixed channel dimensions with a cross section of (500 x 500) μm^2 , SAW wavelength and power level as well as fluid flow rate in the channel were varied to identify the most appropriate wavelength for efficient mixing. To evaluate the simulations, tailored experiments were carried out: Impedance-matched interdigital transducers (IDT: 1 mm aperture; $\lambda_{\text{SAW}} = 20, 30, 60 \mu\text{m}$) were fabricated on 128°YX LiNbO₃ together with meander resistors for temperature measurement using Al/Ti-metallization and lift-off technology. Subsequently, SiO₂ (1000 nm) and Al₂O₃ (10 nm) layers were deposited on the device surface as passivation. Electrical connection was established via spring-pin electrodes on a customized chip holder and high frequency input signals ($P_{\text{Load}} = 0...2 \text{ W}$) were supplied (PowerSAW3 signal generator, Belektronik GmbH [8]). Y-shaped channels in PDMS (see Fig. 1) were mounted on the substrate and connected to a 12-roll rotary pump (Reglo Digital, Ismatec). To ensure efficient SAW excitation and prevent energy absorption in the PDMS, an air gap was kept above the IDT leaving only a 100 μm wide sealing strip (i.e. one of the channel walls) between IDT and the fluid filled channel. Equal volume flow rates were set for both channel inlets in 10 steps (10 to 600 $\mu\text{l}/\text{min}$), correlating to fluid velocities of $v_{\text{Fluid}} = 0.67...40 \text{ mm/s}$ in the acoustofluidic interaction zone of the main channel. The aqueous model fluids consisted of an acetate buffer (fluid 1) and a NaOH solution with Bromthymol blue (BTB) dye (fluid 2). The reaction of both fluids triggers a color-change reaction, which allows determination of the achieved mixing efficiency using a CCD camera.

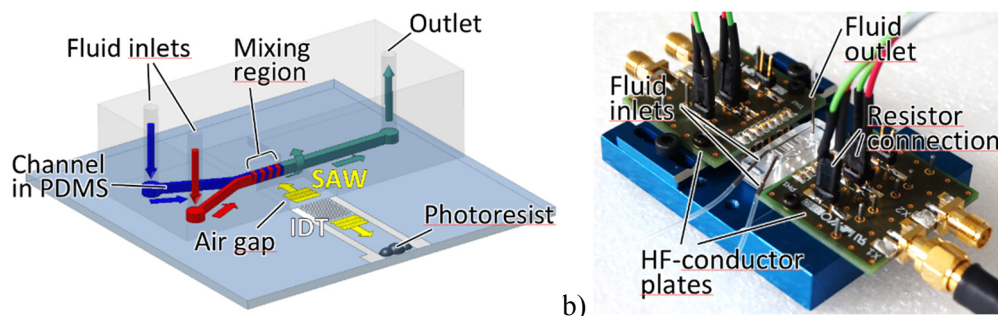


Fig. 1: a) Sketch of the experimental setup (arrows indicate SAW path and fluid flow directions); b) Photograph of the experimental setup showing the PDMS channel block with two stainless steel media inlets and one outlet on the SAW chip together with high-frequency spring pin conductor plates (PCB, green) and 4-wire resistor connections for temperature measurement in the channel

Results

According to our experiments and simulation results, efficient mixing can be achieved in microchannels using SAW devices with appropriate wavelengths at a large range of fluid flow rates (up to 600 $\mu\text{l}/\text{min}$). As the penetration depth of acoustic streaming is wavelength dependent [9], for efficient mixing the SAW wavelength should neither be too small (Case I) nor too large (Case II) with respect to the channel dimensions: Case I is limited by technological means and is - in the case of microchannels - a minor problem. Case II is determined by parasitic energy absorption in the channel wall material leading rather to heating of the wall material than to efficient mixing. In order to minimize this effect and, thus, to increase mixing efficiency, the SAW should be almost completely converted into a longitudinal pressure wave when propagating across the channel. As the amplitude of Rayleigh SAWs is attenuated to $1/e$ of its initial value in water after a length of about 11 wavelengths [9] and as the associated SAW power is proportional to the squared amplitude, a 90% (95%) power conversion is ensured at a channel width of approx. 13 (18) wavelengths. For the setup used in this study, the wavelengths of 20 and 30 μm fulfil this requirement. When such appropriate wavelengths are used, the increase in temperature can be as low as 5K for efficient mixing of two aqueous fluid streams. With increasing wavelength, a drastic increase of temperature can be measured (e.g. for the used 60 μm device), which can be related to energy absorption in the PDMS channel walls and associated local heating.

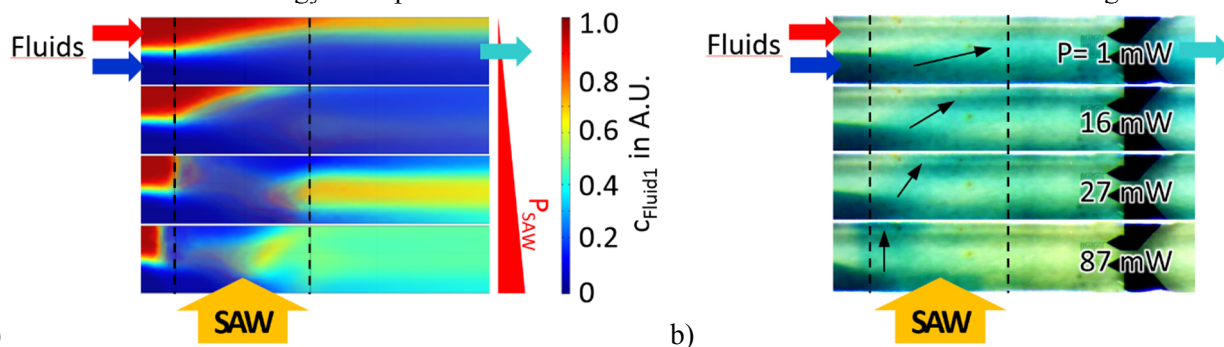


Fig. 2: **a)** Results of FEM simulation of fluid flow in microchannels (top view): concentration profile of fluid 1 with increasing SAW power (SAW aperture indicated by dashed lines, P increases from top to bottom); **b)** Fluid flow as seen in optical microscope (top view) for different power levels (fluid1 = transparent, fluid2 = blue, mixed fluid = yellow; $f_0=195$ MHz, 1 mm aperture, 150 $\mu\text{l}/\text{min}$ fluid flow rate; streaming direction indicated by arrow)

Conclusion

In summary, we present simulations and corresponding experimental results regarding fluid mixing in microchannels using SAWs. We investigated the dependencies of mixing efficiency and fluid temperature on SAW wavelength, input power and fluid flow rate. Hereby, the ratio of wavelength to channel width plays a crucial role for the mixing efficiency and the amount of energy absorption in the channel wall material. Using appropriate IDTs, we show efficient mixing at low power with a low temperature increase, even for high flow rates.

References

- [1] F. Kardous, A. Rouleau, B. Simon, R. Yahiaoui, J. F. Manceau, and W. Boireau, *Improving immunosensor performances using an acoustic mixer on droplet microarray*, Biosens. Bioelectron. **26**, 1666 (2010).
- [2] O. Ducloux, E. Galopin, F. Zoueshtiagh, A. Merlen, and V. Thomy, *Enhancement of biosensing performance in a droplet-based bioreactor by in situ microstreaming*, Biomicrofluidics **4** (2010).
- [3] K. P. Kulkarni, S. H. Ramarathinam, J. R. Friend, L. Y. Yeo, A. W. Purcell, and P. Perlmutter, *Rapid microscale in-gel processing and digestion of proteins using surface acoustic waves*, Lab on a Chip **10**, 1518 (2010).
- [4] M. C. Jo and R. Guldiken, *Dual surface acoustic wave-based active mixing in a microfluidic channel*, Sensors and Actuators A-Physical **196**, 1 (2013).
- [5] T. D. Luong, V. N. Phan, and N. T. Nguyen, *High-throughput micromixers based on acoustic streaming induced by surface acoustic wave*, Microfluid. Nanofluid. **10**, 619 (2011).
- [6] W. K. Tseng, J. L. Lin, W. C. Sung, S. H. Chen, and G. B. Lee, *Active micro-mixers using surface acoustic waves on Y-cut 128° LiNbO₃*, J. Micromech. Microeng. **16** (2006).
- [7] Q. Zeng *et al.*, *Milliseconds mixing in microfluidic channel using focused surface acoustic wave*, Sensors and Actuators B-Chemical **160**, 1552 (2011).
- [8] R. Brunig, A. Winkler, G. Guhr, and H. Schmidt, *Active Mixing in Microfluidic Systems Using Surface Acoustic Waves*, 2011 IEEE International Ultrasonics Symposium Proceedings, 794 (2012).
- [9] M. Dentry, L. Y. Yeo, and J. R. Friend, *Frequency effects on the scale and behavior of acoustic streaming*, Physical Review E **89** (2014).

Financial support by German BMBF (InnoProfile-Transfer grant 03IPT610A) is gratefully acknowledged.

A microfluidic musical instrument for making cells dance

David Rabaud¹, Jean-Philippe Kleman¹, Vivian Aubert¹, Philippe Marmottant², Ianis Bernard², Jean-Gael Vuillermet¹, Pierre Thibaut² and Cedric Poulain¹

¹ Univ. Grenoble Alpes, F-38000 Grenoble France
CEA, LETI MINATEC Campus, F-38054 Grenoble, France
Email : cedric.poulain@cea.fr

²Univ. Grenoble Alpes Savoie
LIPHY
F-3800 Grenoble, France
Email : pierre.thibault@ujf-grenoble.fr

Introduction

It is well known that acoustic radiation forces arise from the transfer of linear momentum carried by a pressure wave. An acoustic wave can also carry angular momentum and transfer it to matter in order to create a torque. Different approaches can be followed to create an acoustic torque by means of acoustics. In this talk, we will report on the use of acoustic streaming at low frequency to make cells spin at a constant angular velocity relying on two orthogonal out of phase standing waves to induce a stationary rotation of a particle or a living cell in a microchannel. The acoustic torque being a decreasing function of the sound frequency, we have designed an acoustorotation chip that is design to operate at low frequency (typ. $f_0 \leq 300 \text{ kHz}$). Indeed, the acoustic channel size is $300 \mu\text{m}$, much smaller than the sound wavelength λ so that the channels behave as sound waveguides and make the chip act like a musical horn. The low frequency regime is also interesting for cell mechanics study but as we will show, it is a challenging goal because of the necessity to achieve independant actuation in order to ensure the correct phase shift required for acoustorotation.

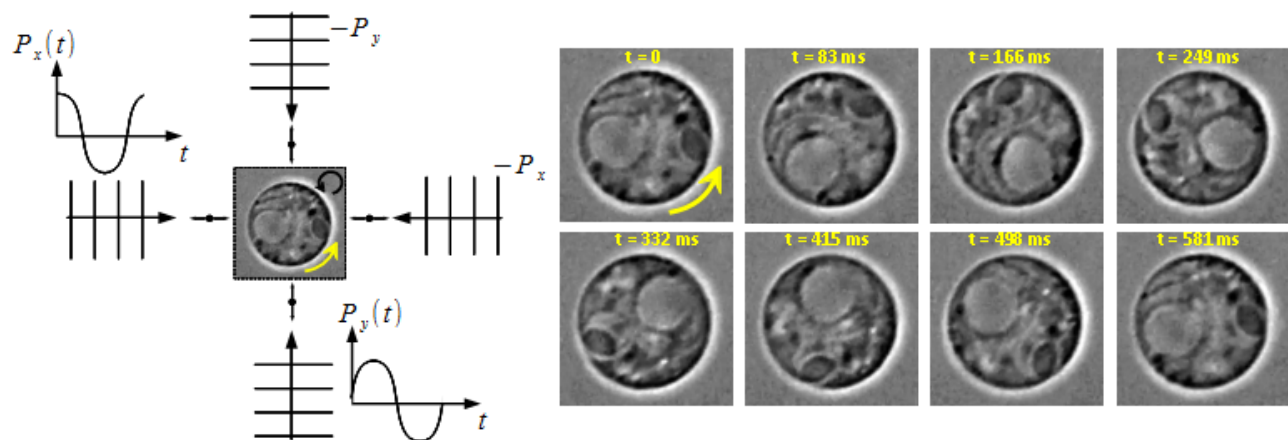


FIGURE 1: (a) Sketch of a typical acoustorotation protocol (b) Monocyte cells (THP1) spinning in an acoustic field for $f_0 = 36 \text{ kHz}$.

Framework

Consider two orthogonal plane standing acoustic waves :

$$P_x(x, t) = A_x \cdot \cos(k_0 x) \cdot \cos(\omega_0 t)$$

$$P_y(y, t) = A_y \cdot \cos(k_0 y) \cdot \cos(\omega_0 t + \phi)$$

Assuming a spherical particle of radius $a \ll \lambda_0$, the acoustic torque Γ_{acous} exerted upon a particle has been calculated in [1] and worth : $\Gamma_{acous} = \frac{3}{2} \frac{A_x A_y}{2\rho_0 c_0^2} \delta_\nu 4\pi a^2 \sin(\phi)$ where $\delta_\nu = \sqrt{\nu/\pi f_0}$ is the streaming boundary layer thickness. For a particle far from the walls, the viscous drag torque is $\Gamma_d \approx -8\pi\mu a^3 \Omega$ yielding to a stationary angular velocity

$$\Omega = \frac{3\delta_\nu A_x A_y \sin(\phi)}{2a\mu\rho_0 c_0^2} \propto \sqrt{\frac{1}{\omega_0}}$$

For the typical values used in this work, this lead to $\Omega \sim 1Hz$ which is of the same order as the observed rate of rotation (see Fig.1). To take advantage of the $1/\sqrt{\omega_0}$ dependance, we have designed a low frequency acoustofluidic chip.

Sound waveguide and horn design

To validate the concept of waveguide effect at low frequency, an aluminium waveguide has first been designed, simulated and manufactured. The chip design is shown on figure 2. It is composed of two facing acoustic cavities prolonged by an exponential-shape horn at each end of the microchannel waveguide (of constant width : $l = 300\mu m$). FEM numerical simulations of the acoustic field for different frequencies have confirmed that this chip acts as a waveguide with resonant frequencies typical of musical acoustics determined by the waveguide length (see Fig. 2). In a second step, this waveguides geometry will be implemented in order to achieve two orthogonal waves on a silicon chip. We will discuss the advantages and drawbacks of this set up that has been designed to achieve single cell spinning on a large cell population.

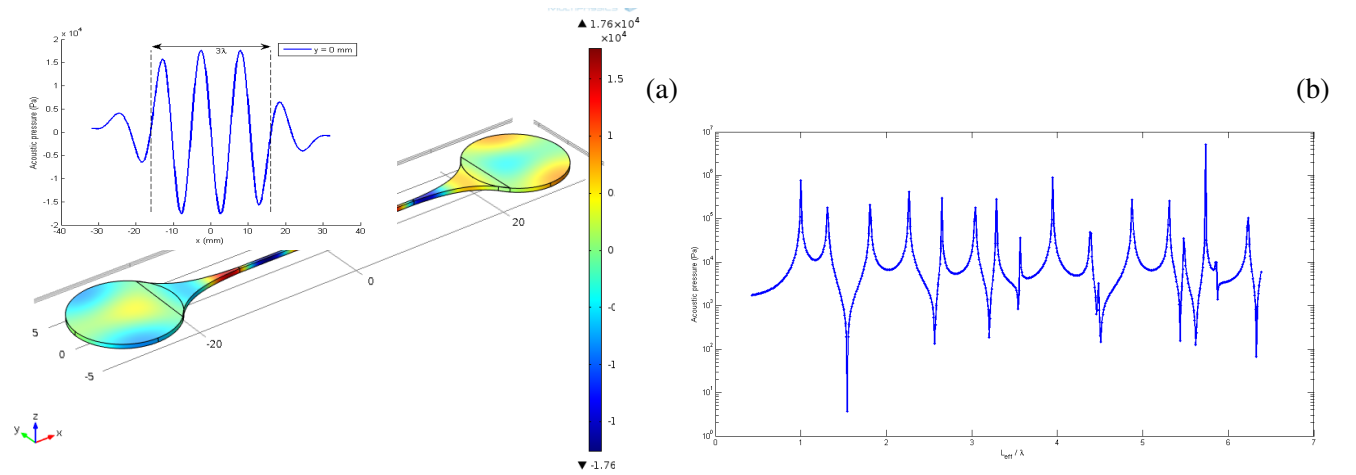


FIGURE 2: (a) Acoustic pressure field in the low-frequency waveguide chip (FEM estimation, hard wall assumption). $f_0 = 141kHz$ corresponding to $L_{eff}/\lambda \approx 3$ (cf insert showing a plot of the pressure along the center line of the channel). (b) Resonances in the waveguide (maximum pressure in the channel along the non-dimensional frequency λ/L_{eff} where $L_{eff} = 33mm$ is the effective resonance length).

Références

- [1] F. H. Busse and T. G. Wang. Torque generated by orthogonal acoustic waves-theory. The Journal of the Acoustical Society of America, 69(6) :1634–1638, 1981.

Electronic Sonotweezers – Ultrasonic particle manipulation with FPGA embedded systems

Han Wang¹, Christine Demore¹, Sandy Cochran¹

¹Institute for Medical Science and Technology, University of Dundee, United Kingdom

Email: hywang@dundee.ac.uk

URL: <http://www.imsat.org/>

<http://medicine.dundee.ac.uk/medical-research-institute/divisions/division-imaging-technology>

Introduction

Recent research in acoustic tweezing has mainly focused on the behaviour of devices for specific applications and the fundamental theories of the forces exerted on the target particles, e.g. dealing with particle - particle interactions. However, compared to optical tweezers [1], there have been only limited reports about developments and applications of acoustic tweezers at the system level. These offer the potential to meet demand for small, low cost and portable systems to allow accurate, robust and dexterous control with multi-element ultrasonic particle manipulation devices [2][3]. This paper reports the results of the development of a low-cost, low power consumption, fully programmable and bench top size electronic system for research applications of “Sonotweezer” devices.

Design and Experiment

The electronic system is designed to provide 16 channels of independently controlled signals in the form of continuous waves with approximately sinusoidal characteristics. For each channel, the signal frequency, phase and amplitude can be controlled individually. The system incorporates both programmable digital electronics based on FPGA (Field Programmable Gate Array), and bespoke analogue electronics, in a form that can be easily expanded to deal with a higher channel count.

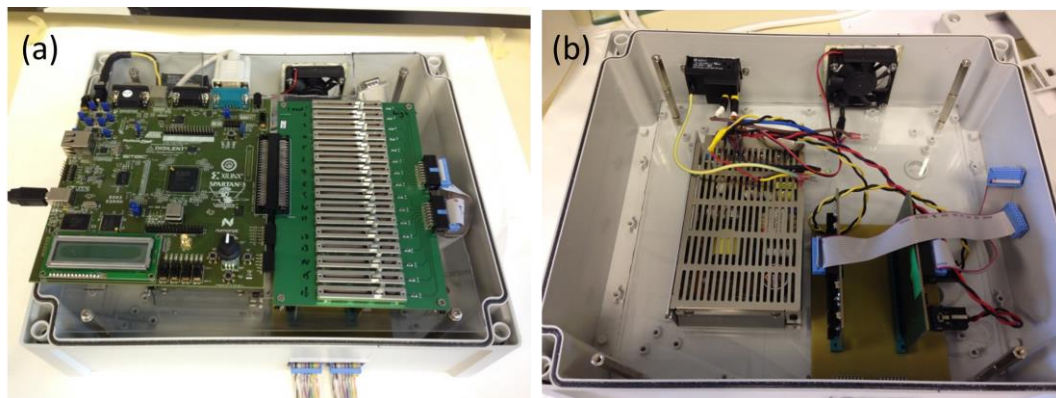


Fig. 1. Photographs of the 16 channel Sonotweezers control system. The pictures show the system electronics incorporated inside a chassis with the dimension of 334 mm (length) × 289 mm (width) × 117 mm (height). (a) Top layer electronics with FPGA development board and signal conditioning circuitry (b) Bottom layer electronics with customized amplifier array and 60-watt power supply.

A customized FPGA soft core is designed to generate 16 channels of independent digital signals with frequencies and phases which can be adjusted in real time from a PC within the MATLAB (Mathworks, Cambridge, UK) environment. Off-the-shelf Spartan 3A FPGA development board (Xilinx Inc., San Jose, CA, USA) with immediate available signal input/output ports is used to shorten the design period. MATLAB is used because of the ease of adopting the Sonotweezers

device models and the convenience of communicating with the hardware through established toolboxes. Bespoke analogue electronics were constructed in two parts, one for signal conditioning and the other for amplification. The signal conditioning stage is designed to provide an arbitrary amplitude attenuated bipolar signal from CMOS logic signals (0 to 3.3 V typically) generated from the digital stage. The 16-channel analogue amplifier array was designed with a fixed gain of 10 for direct amplification of the attenuated digital signal for transducer actuation.

Results

The electronics have been used successfully to demonstrate the capability to manipulate microparticle clusters for different array-based ultrasonic manipulation devices. Each channel could independently generate approximate sinusoidal signal with the maximum voltage amplitude of $25 V_{pp}$ without saturation and maximum current amplitude of about 100 mA with full voltage swing range. This report particularly discuss the manipulation of particles within a 16-element circular array reported previously [3]. The phase quantization control of the array elements was applied through the electronic system to generate acoustic pressure nodes to trap an aggregate of $10 \mu m$ diameter polystyrene microspheres, and the “acoustic trap” was manipulated dynamically following the route predefined by computer programs.

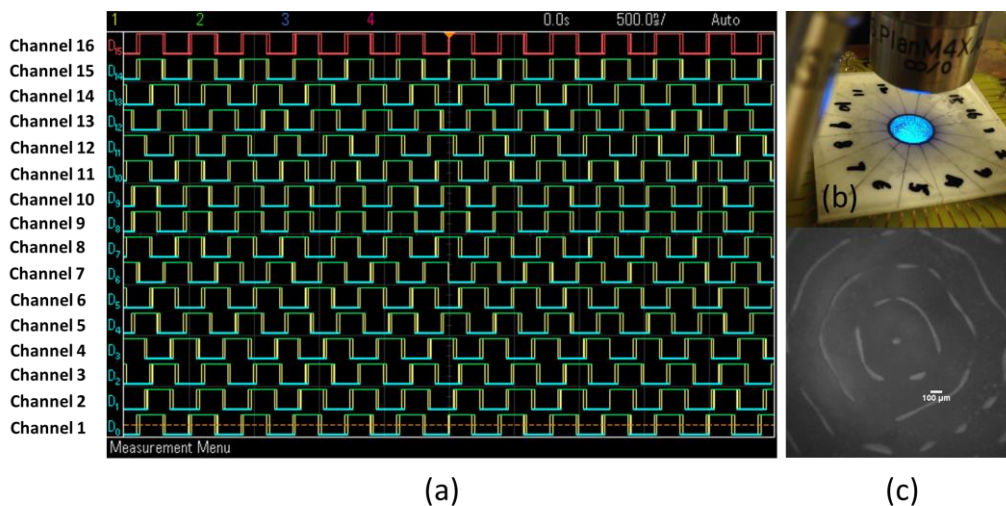


Fig. 2. (a) An Oscilloscope image: 16 channels of CMOS voltage signals for transducers actuation generated from FPGA digital circuit stage. (b) 16-element circular array device with $10 \mu m$ fluorescent polystyrene particles filled inside the cavity. (c) A microscopic image: Acoustic field in the shape of concentric circles illustrated by the trapping of $10 \mu m$ polystyrene microspheres.

Conclusion

This report introduced a novel design of electronics and control programs that could be used to control array based acoustic manipulation devices. The feasibilities of phase quantization control of a Sonotweezer based on a circular piezoelectric array have been demonstrated with this system. Further improvements of the system will emerge from work on diverse applications as well as enhanced packaging of the FPGA IP core and user friendly interface development.

References

- [1] R. Bowman, G. Gibson, D. Carberry et al., “iTweezers: optical micromanipulation controlled by an Apple iPad”, *Journal of Optics*, vol. 13, issue 4, pp. 044002, 2011.
- [2] P. Glynn-Jones, C. Demore, C. Ye et al., “Array-controlled ultrasonic manipulation of particles in planar acoustic resonator”, *IEEE Trans. Ultrason. Ferroelectr. Freq. Control*, vol. 59, issue 6, pp. 1258-66, 2012.
- [3] C. Courtney, B. Drinkwater, C. Demore et al., “Dexterous manipulation of microparticles using Bessel-function acoustic pressure fields”, *Applied Physics Letters*, vol. 102, issue 12, pp. 123508, 2013.



Sorting of CD8+ lymphocytes from peripheral blood progenitor cell products using affinity bead acoustophoresis

Anke Urbansky¹, Andreas Lenshof¹, Josefina Dykes², Thomas Laurell¹, and Stefan Scheduling³

¹Department of Biomedical Engineering
Lund University
S-221 00 Lund, Sweden
Email: Anke.Urbansky@bme.lth.se

²Division of Clinical Immunology and Transfusion Medicine
Skåne University Hospital
S-221 00 Lund, Sweden

³Lund Stem Cell center
Lund University
S-221 00 Lund, Sweden

Introduction

Processing of peripheral blood progenitor cells (PBPC) for clinical transplantation or research applications aims to effectively isolate or deplete specific cell populations. Here, we investigated the performance of microfluidic acoustophoresis for the separation of lymphocyte subsets from PBPC, and present a method for affinity-bead-mediated acoustic separation of cells which can otherwise not be acoustically discriminated. In an acoustic standing wave field radiation forces induce movement of particles depending on particle and medium properties as for example particle size, density and compressibility. Targeting of cells by affinity specific beads will generate cell-bead complexes that exhibit distinct acoustic properties relative to non-targeted cells and are, thus, possible to isolate. We have shown before that it is possible to separate CD4+ lymphocytes using affinity acoustophoresis. Here, we investigated the performance of the acoustic setup to isolate CD8+ lymphocytes which are lower in cell number in the PBPC compared to CD4+ cells.

Experiment

PBPC samples were obtained from patients and healthy donors. Following density gradient centrifugation, cells were labelled with anti-CD8 magnetic beads (Dynal) and sorted by acoustophoresis and, for comparison, standard magnetic cell sorting technique in parallel. For acoustic sorting a silicon chip with two inlets and two outlets and with 2D pre-focusing abilities was used¹ (Figure 1). The cell suspension was injected through the sample inlet and passed the pre-focusing channel at a flow rate of 60 $\mu\text{L}/\text{min}$. Histopaque-1077 as a wash buffer entered through the centre inlet at 120 $\mu\text{L}/\text{min}$. The bead-bound CD8+ cells were collected in the centre outlet at 60 $\mu\text{L}/\text{min}$ and non-target cells through the side outlet at 120 $\mu\text{L}/\text{min}$. PBPC samples, target and non-target fractions were analysed for purity, separation efficiency, recovery, T-cell function and progenitor cell content.

Results

Targeted CD8+ lymphocytes were acoustically isolated with a mean (\pm SD) purity of $92 \pm 7\%$, compared to $90 \pm 16\%$ for magnetic sorting (Figure 2a). Viability of sorted cells was $97 \pm 4\%$ (acoustic) and $97 \pm 3\%$ (magnetic), respectively (Figure 2b). The mean separation efficiency of acoustic sorted CD8+ cells was $65 \pm 19\%$ of the total CD8+ cells compared to a mean recovery of magnetic sorted CD8+ cells of $34 \pm 11\%$. Functional testing of sorted CD8+ lymphocytes showed unimpaired mitogen-mediated proliferation capacity after 2-day, 4-day and 6-day stimulation with CD3/CD28 (Figure 2c). Furthermore, hematopoietic progenitor cell assays revealed a preserved colony forming ability of post-sorted non-target cells.

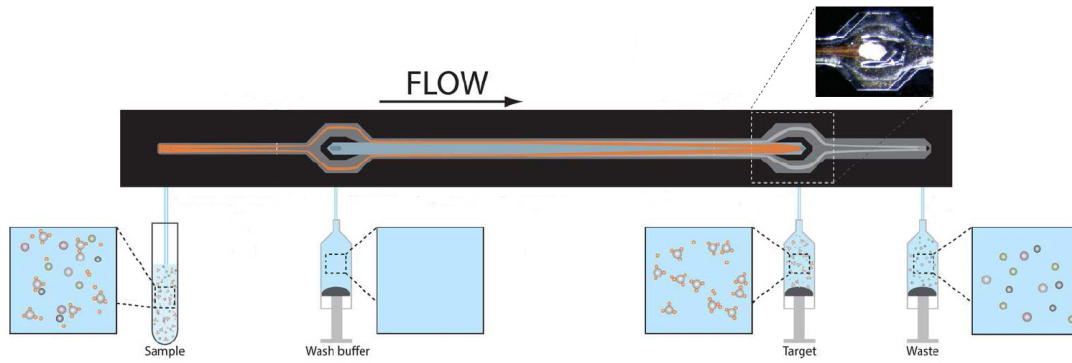


Figure 1. Picture of the acoustophoresis platform. The cell suspension with bead-labeled CD8+ cells enters through the side inlets while the wash buffer (Histopaque-1077) is injected through the center inlet. Radiation forces in the acoustic standing wave field move the cell-bead complex faster to the center compared to non-target cells and can be separated in the center outlet of the channel. Non-target cells exit through the side outlets.

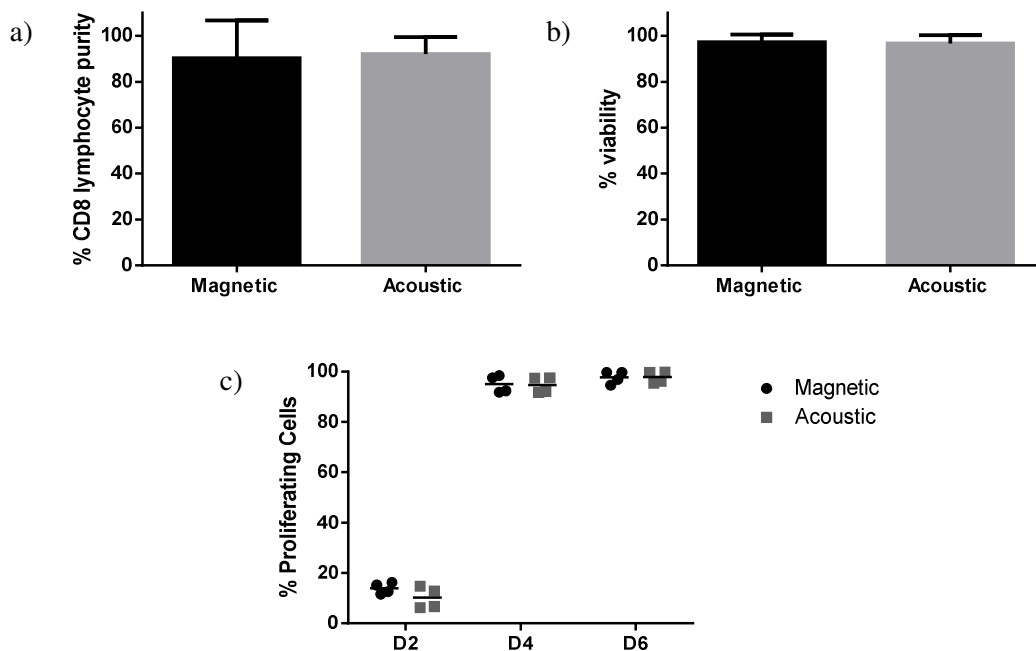


Figure 2. a) Comparison of CD8+ lymphocyte purities obtained with magnetic and acoustic enrichments are shown (n=16). b) The viability between both separation methods is comparable (n=16). c) Proliferation experiments with stimulated CD8+ cytotoxic T-cells show no difference between acoustic and magnetic sorted cells at different time points (n=2).

Conclusion

The acoustophoresis platform can be utilized to efficiently isolate bead-bound CD8+ lymphocytes from PBPC samples which can otherwise not be acoustically discriminated. A high separation purity, with preserved functional capacity of both target and non-target cells in a continuous flow format could be achieved. Compared to the separation of CD4+ lymphocytes we optimized the acoustic separation purity. Using the acoustic platform resulted in a higher separation efficiency compared to magnetic cell sorting. In a next step we want to be able to isolate hematopoietic stem and progenitor cells for stem cell transplantation which are even lower in cell number. Affinity-bead acoustophoresis is, thus, an interesting technology for PBPC processing and opens up for simultaneous separation of multiple cell population.

References

- [1] Augustsson, P., et al., *Microfluidic, label-free enrichment of prostate cancer cells in blood based on acoustophoresis* Analytical Chemistry, 2012. **84**(18): p. 7954-62

Improved chip based Coulter counting using 2D acoustophoretic particle prefocusing

Carl Grenvall¹, Christian Antfolk¹, Christer Zoffmann Bisgaard², Steen Kjær Andersen² and Thomas Laurell¹

¹Division of Nanobiotechnology
Department of Medical Engineering
Lund University
S-221 00 Lund, Sweden
Email: carl.grenvall@bme.lth.se

²FOSS Analytical A/S
Foss Allé 1
DK-3400 Hillerød, Denmark
Email: CZB@foss.dk

Introduction

Here we present how 2-dimensional acoustic prefocusing drastically improves the performance of a novel microfluidic chip Coulter counter (MCC), by prealignment of cells, in an upstream acoustophoretic zone. By appropriate design of the acoustically actuated channel the sample particles flowing in the prefocusing zone are simultaneously aligned vertically and laterally before entering the MCC chip zone, leading to improved Coulter Counter measurement performance since they are now flowing through the same electric field density. This addresses known MCC sensitivity issues, caused by varying particle positions in the flow channel, which other groups have also tried to solve using different techniques, including sheath flow alignment and intricate multilayer microchip structuring [1-4]. When compared to earlier solutions, our acoustic approach allows for a less complicated chip fabrication and can be used for on-chip sample preparation in addition to the prefocusing of the target particles [5]. Our proof-of-concept data, using polystyrene beads and whole blood, shows that on-chip acoustophoretic prefocusing of particles can be used to improve MCC performance.

Experiment

The ability to separate, focus or trap cells using acoustophoresis has opened up new micro-analytic possibilities. Meanwhile, MCC's have allowed thorough investigations of cell populations and single cell properties. In an attempt to combine these technologies and solve the need for accurate particle positioning in MCC's we developed an MCC chip with an integrated acoustic prefocusing zone. The microfluidic glass chip was designed in Lund and fabricated by Micronit Microfluidics BV using a two step wet etching process followed by patterning of planar platinum electrodes across a narrow flow channel (35x80 μm) in order to allow impedance measurements, Figure 1.

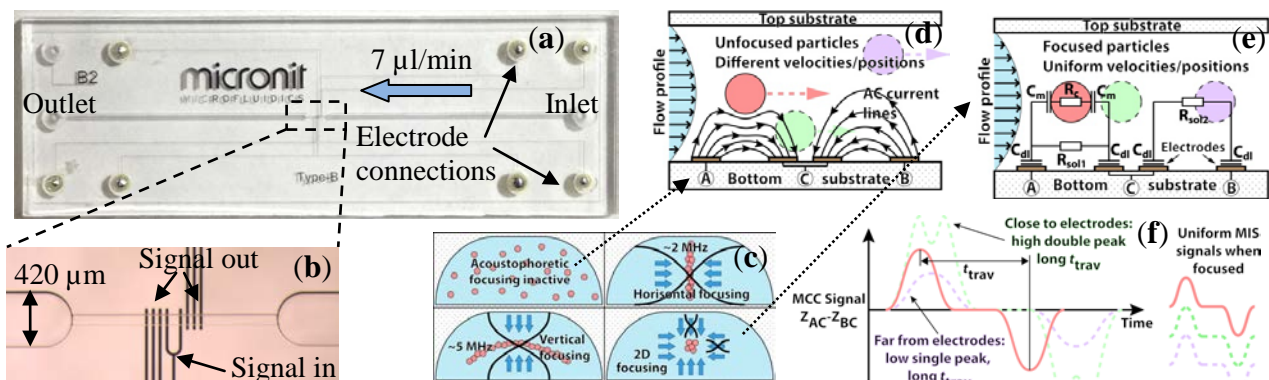


Fig. 1. (a) The glass chip containing a prefocusing channel, width 420 μm and height 150 μm , and an (b) MCC zone, width 80 μm and height 35 μm , where prefocused particles can be detected using planar electrode impedance cytometry. (c) By actuating the prefocusing channel using two transducers, operated at ~ 2 and ~ 5 MHz, a stream of particles/cells can be precisely positioned in the centre of the channel before entering the downstream MCC-zone. (d) While an unfocused stream of same size particles will induce different MCC pulse amplitudes, (e) prefocusing of the particles will result in uniform pulse amplitudes, creating possibilities for more correct particle counts and detailed impedance based cytometry. (f) By analysing the raw pulse data in terms of electrode-electrode travelling time (t_{trav}) and pulse shapes it is possible to determine how well the particles were prefocused.

Planar electrode configurations in microfluidic Coulter Counters are relatively easy and cheap to fabricate but sensitive to varying particle positions, which make them a good candidate for improvement if a simple particle prefocusing technique can be employed. To address this need we added an acoustic prefocusing zone to focus particles using standing wave ultrasound at 5 (vertically) and 2 (laterally) MHz respectively. Comsol simulations were used in order to optimize for standing wave ultrasound at these frequencies and resulted in a 420 μm wide and 150 μm deep channel. In order to evaluate the system two different suspensions were used. A mixture of 5, 7 and 10 μm polystyrene beads suspended in 0.9 % NaCl MQ water and whole blood diluted 10000 times in PBS with 7 μm ps beads added in order to provide a baseline for the pulse data. Flow was set to 7 $\mu\text{l}/\text{min}$. Differential impedance spectroscopy was performed at 1.1 MHz and 2 V output. Acoustic standing wave forces were induced by piezoelectric transducers attached to the bottom of the chip, beneath the flow channel, actuated by signal generators. The raw data was analysed using Matlab and electric pulse amplitudes were extracted together with differential (+)pulse to (-)pulse travel time for each particle to estimate transition time between the two measuring electrode areas in the MCC, Figure 1f. The sample data from the MCC was compared with data using a Multisizer 3 Coulter counter in order to further evaluate MCC performance.

Results

Confocal microscopy of the channel with polystyrene beads show particles distributed across the channel with ultrasound inactive, Figure 2a (upper), and can then either be acoustophoretically focused laterally (middle right), vertically (left) or into a well-defined centre point (lower). Pulse data further shows that the prefocusing improved the MCC performance. Pulse amplitude histograms suggest good correlation between particle volume and pulse amplitudes for both the 5, 7 and 10 μm bead populations and the blood/ps mix which was also confirmed in the Multisizer data, Figure 2b-g. When prefocusing was activated the distribution of pulse amplitudes for each particle size was significantly improved, matching the reference Multisizer data.

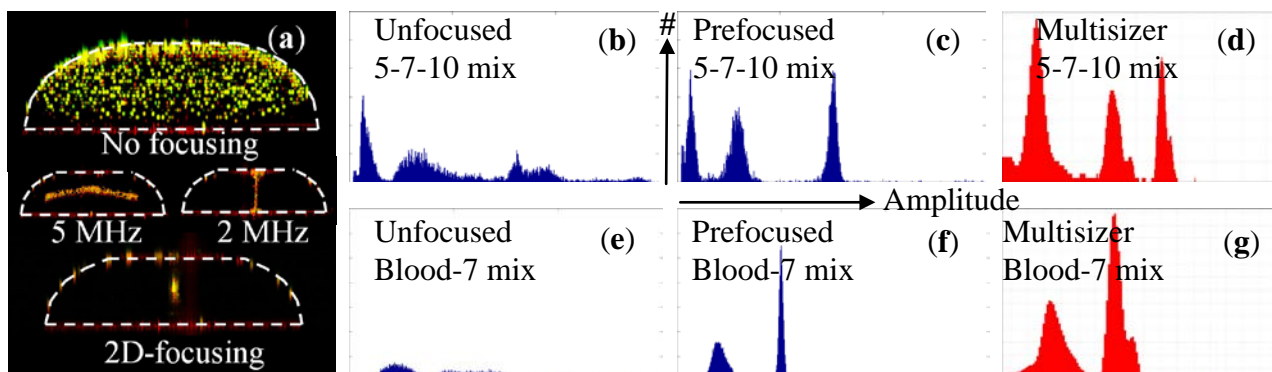


Fig. 2. (a) Confocal imaging of the channel show that the particles could be prefocused into a well-defined position in the channel centre. It should be noted that the top-bottom 5 MHz ultrasound induced a curved focusing field, never before reported, corresponding to tapered wall acoustic simulations in Comsol. (b) With no prefocusing there were some overlaps between pulse amplitudes in the 5-7-10 μm bead mix histogram. (c-d) With 2D prefocusing active the amplitude data improved significantly and corresponded well to Multisizer measurements of the same sample. (e) In the blood-7 μm ps mix it was also hard to distinguish between cells (RBC's) and beads without the prefocusing. (f-g) With prefocusing active each population was easily resolved and the relative number of particles in each population corresponded well with Multisizer data.

Conclusion

We have shown that 2-dimensional acoustic particle prefocusing can vastly improve the performance of a planar electrode impedance based cytometer. We now aim to develop an integrated device with acoustophoretic pretreatment of a sample, for example raw milk, with particle sorting, prefocusing and cytometry on a single chip.

References

- [1] S. Gawad, Ph. Renaud et al., *Micromachined impedance spectroscopy flow cytometer for cell analysis and particle sizing*, Lab Chip, 1, 76-82 (2001)
- [2] D. Spencer and H. Morgan, *Positional dependence of particles in microfluidic impedance cytometry*, Lab Chip, 11, 1234-1239 (2011)
- [3] R. Rodriguez-Trujillo, G. Gomila et al., *High-speed particle detection in a micro-Coulter counter with two-dimensional adjustable aperture*, Biosens Bioelectron, 24, 290-296 (2008)
- [4] K Cheung, A. Tárnok et al., *Microfluidic impedance-based flow cytometry*, Cytometry A, 77, 648-66, (2010)
- [5] C. Grenvall and T. Laurell et al., *Harmonic microchip acoustophoresis: a route to online raw milk sample precondition in protein and lipid content quality control*, Anal Chem, 81, 6195-6200 (2009)



Microchannel Geometry Dependent Acoustofluidics and Whole Blood Manipulation in Surface Acoustic Wave Counterflow Devices

Marco Travagliati^{1,2}, Richie J. Shilton², Marco Pagliuzzi¹, Ilaria Tonazzini¹,
Fabio Beltram^{1,2}, Marco Cecchini¹

¹Laboratorio NEST
Scuola Normale Superiore and Istituto Nanoscienze - CNR
Piazza San Silvestro 12, 56127 Pisa, Italy
Email: marco.cecchini@nano.cnr.it

²Center for Nanotechnology Innovation @ NEST
Istituto Italiano di Tecnologia
Piazza San Silvestro 12, 56127 Pisa, Italy
Email: marco.travagliati@iit.it

Introduction

Acoustic counterflow [1] has been demonstrated to generate efficient integrated fluid pumping in closed microchannels allowing true device portability. Development of on-chip functional blocks for sample pre-processing is necessary in view of its application for micro-total analysis systems (μ TAS). Here, we investigated the microparticle and whole blood manipulation capabilities of these devices as a function of microchannel geometry. Here we show that, depending on the microchannel height h compared with the ultrasound wavelength λ_f scattered by the SAWs in water, it is possible to switch from an acoustic streaming dominated regime ($h \gg \lambda_f$) to an acoustic radiation force dominated one ($h \leq \lambda_f$). We then exploited these two regimes separately for whole blood manipulation.

Experiment

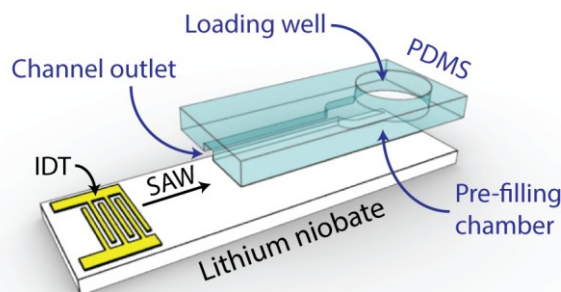


Fig. 1. Schematic of the SAW counterflow device (not to scale).

Our experimental devices (Figure 1) are composed of a lower 128° XY lithium niobate substrate with a patterned interdigital transducer for SAWs excitation at 100 MHz and an upper polydimethylsiloxane microchannel layer. Devices with microchannel heights ranging from 14 μm to 70 μm were tested. The SAW amplitude was calibrated as a function of the operating power by laser Doppler vibrometry. 10 μL of fluid was pipetted into the reservoir and pumped via SAW counterflow at fixed SAW amplitudes, ranging from 800 pm to 1.4 nm. The channel filling was recorded with a brightfield inverted microscope equipped with a fast camera and analyzed using a μPIV software. Whole blood experiments were carried out using mouse blood diluted 1:10 in sodium citrate 3.8% in PBS to prevent coagulation. Adult wild type mice (CS7BL/6J strain, Jackson Laboratory) were treated in accordance with the ethical framework of FP7 and with the guidance of the Animal Protection Law of the Italia Republic (D.L. 16/1992). Detailed fabrication and operation protocols can be found in [2].

Results

By seeding the fluid with 500 nm particles, we observed two completely different acoustofluidic behaviours depending on the ratio h/λ_f (Figure 2). When $h \leq \lambda_f$, as reported in Figure 2a, we observed beads collection within a two dimensional periodical pattern, that matches the simulated distribution of semi-nodes of the partially standing ultrasound wave scattered in water by SAWs. Conversely, when $h \gg \lambda_f$ we observed that the particles are dragged into a double vortical pattern (shown in Figure 2d) which evolves through different phases during the initial channel filling. Hence, we can tune the balance between the acoustic radiation force and the acoustic streaming (Stokesian) drag force by simply varying the microchannel height. Changing the beads size, we observed that the transitional height between these two regimes depends on the microparticle size with respect to λ_f . Finally, we investigated the effect of these regimes on whole blood in 14 μm ($h \sim \lambda_f$) and 70 μm ($h \gg \lambda_f$) high channels. In the 14 μm high channels, we observed that complete plasma separation can be obtained between periodic accumulation lines in proximity to the meniscus (Figure 2b). When acoustic streaming dominates, however, we can generate a cell concentration gradient located in the vortical area which is independent of the device operating power (Figure 2d and 2e).

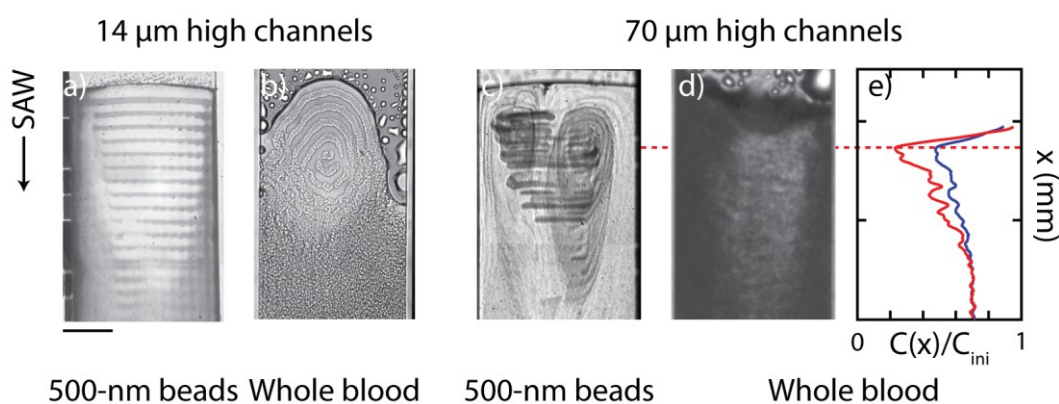


Fig. 2. Representative images during pumping in the 14 μm high and 70 μm high channels with 500 nm particles and whole blood. Panel a) shows particle collection resulting from the dominant action of the acoustic radiation force in 14 μm high channels. Panel b) illustrates the consequent complete separation of plasma from the blood cells obtained in the semi-antinodes of the acoustic wave during pumping. Panel c), d) and e) refer to the 70 μm high channel case. Panel c) shows an image of the streaming pattern obtained with 500 nm beads which highlights the connection between the streaming and the relevant gradient features observed in blood manipulation. Panel d) shows a representative micrograph of the whole-blood dilution gradient. The corresponding cell concentration as a function of distance from the meniscus is reported in panel e) averaged within the jet area (red curve) and the whole channel width (blue curve). All the figures are aligned and the scale bar is 100 μm .

Conclusion

We have demonstrated microchannel dependent acoustophoresis and the resulting whole-blood manipulation driven by surface acoustic wave counterflow. We have shown that the ratio of microchannel height, h , with respect to the ultrasound wavelength, λ_f , scattered by SAWs triggers a transition between two particle dynamics regimes, each associated with the dominance of one of the two primary acoustic forces—the acoustic radiation force and the acoustic streaming drag force. In the acoustic radiation force dominated regime (where $h \lesssim \lambda_f$), microparticles down to 500 nm diameter are collected in a periodic pattern whose dimension can be controlled tuning the SAW operating frequency. This configuration can be exploited to achieve a complete on-chip separation of the plasma from blood cells in a pre-determined area during the channel filling. In the acoustic streaming dominated regime (where $h \gg \lambda_f$), the microbeads instead follow symmetrical vortical streamlines that changes within three different phases. Within this regime, a cell concentration gradient generates in whole blood samples during whole blood pumping associated with the vortex geometry. Switching between these two regimes is possible by careful design of the microchannel dimensions enabling the integration of different whole blood manipulation capabilities in portable μTAS devices.

References

- [1] M. Cecchini, S. Girardo, D. Pisignano, R. Cingolani, and F. Beltram, *Acoustic-counterflow microfluidics by surface acoustic waves*, *Appl. Phys. Lett.*, **92**, 104103 (2008).
- [2] M. Travagliati, R. Shilton, F. Beltram, and M. Cecchini, *Fabrication, Operation and Flow Visualization in Surface-acoustic-wave-driven Acoustic-counterflow Microfluidics*, *J. Visualized Exp.*, **78**, e50524 (2013).



Automatic Device Design by Numerical Optimization

Philipp Hahn, Olivier Schwab, and Jurg Dual

Institute of Mechanical Systems
Dept. of Mechanical and Process Eng.
ETH Zurich
CH-8092 Zurich, Switzerland
hahnp@ethz.ch

Introduction

With the growing performance of computing hardware and the increasing user-friendliness of simulation software, numerical simulations are widely used to design new particle manipulation setups. We demonstrate how the combination of simulation and numerical optimization routines can be used to automatically design devices that utilize acoustic radiation forces. We present the structure of the numerical routine and illustrate its performance with two examples. The planar resonator provides a first validation of the automatic design results whereas the automatic design of a 3D microdevice shows that any desired acoustic mode shape can be generated at maximum pressure amplitude. The presented approach is of great practical relevance for the development of highly optimized microdevices and it can speed up and facilitate the design-process.

Method

In order to generate reasonable design recommendations, any simulation-based design procedure requires an accurate simulation model. Therefore, the numerical model requires special attention and, if possible, validation to make sure that the model contains all relevant physics. Once a the numerical device model is set up, it is easy to change the device dimensions and other attributes with the aim of achieving improved device performance. In principle, this procedure is already a manual and iterative approach to solve the optimization problem shown in Fig. 1(a) [1].

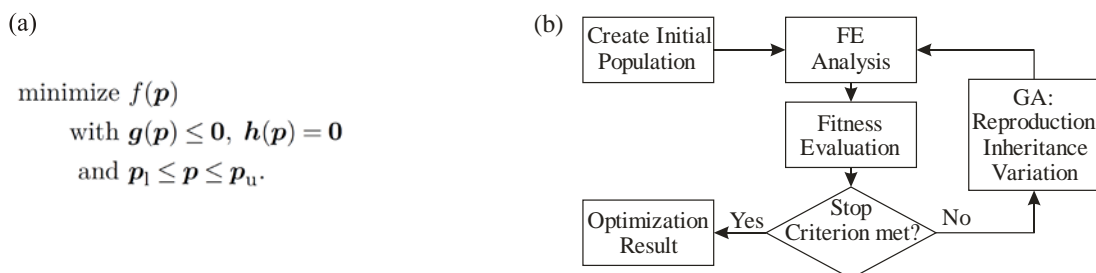


Fig. 1. (a) Mathematical representation of the optimization problem whereas the objective function $f(\mathbf{p})$ is to be minimized by changing the parameter vector \mathbf{p} within the parameter space between the lower bound \mathbf{p}_l and the upper bound \mathbf{p}_u . The inequality conditions $\mathbf{g}(\mathbf{p}) \leq \mathbf{0}$ and the equality conditions $\mathbf{h}(\mathbf{p}) = \mathbf{0}$ enforce geometric constraints. (b) Flowchart of the automatic genetic algorithm (GA) optimization loop. After the finite element (FE) analysis of all parameter combinations in one generation, there is a fitness evaluation based on the objective function. The population of individuals (i.e. parameter combinations) is modified by the GA until a satisfactory solution is found. The GA uses reproduction, inheritance, and variation to create a new population of individuals.

An automatic solution of the optimization problem is possible with established global optimization routines like genetic algorithms (GA), as depicted in Fig. 1(b). However, two key questions need to be solved. First, the device design needs to be parametrized, and second, the simulated device performance needs to be quantified by the so-called objective function in order to compare different designs. To avoid over-complex designs, it makes sense to prescribe the device topology and only modify the dimensions or the shape of individual parts. With an increasing number of optimization parameters grows the flexibility of the optimization to develop a good design. On the other hand, the more parameters, the higher the computational effort to search the parameter space for the optimal solution. Clearly, a trade-off needs to be found here. The fitness evaluation based on the

objective function (see Fig. 1 (b)) is one of the most important steps since it defines which simulation result will be considered optimal. Depending on the task of the device, different objective functions are conceivable. For a 1D planar resonator it might be sufficient to evaluate only the maximum radiation force. For more complex acoustic fields we suggest an objective function based on the Gor'kov potential U ,

$$f(\mathbf{p}) = -\frac{1}{V} \int_V U(\mathbf{p}) \hat{U} dV, \quad (1)$$

which is essentially a linear integral transform with the kernel \hat{U} . It evaluates both, shape and magnitude of the simulated force potential $U(\mathbf{p})$ whereas the integration is performed over the fluid volume V . The kernel \hat{U} is chosen to be the desired normalized force potential. In this way, the objective function becomes minimal for a $U(\mathbf{p})$ of high magnitude and of similar shape as \hat{U} .

Results

As a prove of concept, we analyse the planar resonator since it is the only acoustofluidic device type for which a detailed optimization has been published [2]. For the automatic GA optimization, the material properties and the parameter space are adopted from [2]. Indicating that the optimization code is working properly, our automatic approach leads to an equally high radiation force and very similar layer thicknesses as the once presented in [2]. In order to prove that the automatic design is also applicable in more complex situations, a 3D microdevice for positioning of hollow glass particles, similar to the one in [3] is chosen. Here, the parameters to be optimized are the frequency, the position and size of the piezoelectric transducer as well as the length of the inlet channels to both sides of the fluid cavity. As depicted in Fig. 2(a), the desired acoustic field is the so-called (1,1)-mode which defines the integration kernel \hat{U} in the objective function (eqn. 1). Figure 2(b) shows the simulated fields and the device geometry after 42 hours of numerical optimization. It delivers an exceptionally strong acoustic field and, by comparison with Fig. 2(a), it becomes evident that the optimization produces the desired mode shape.

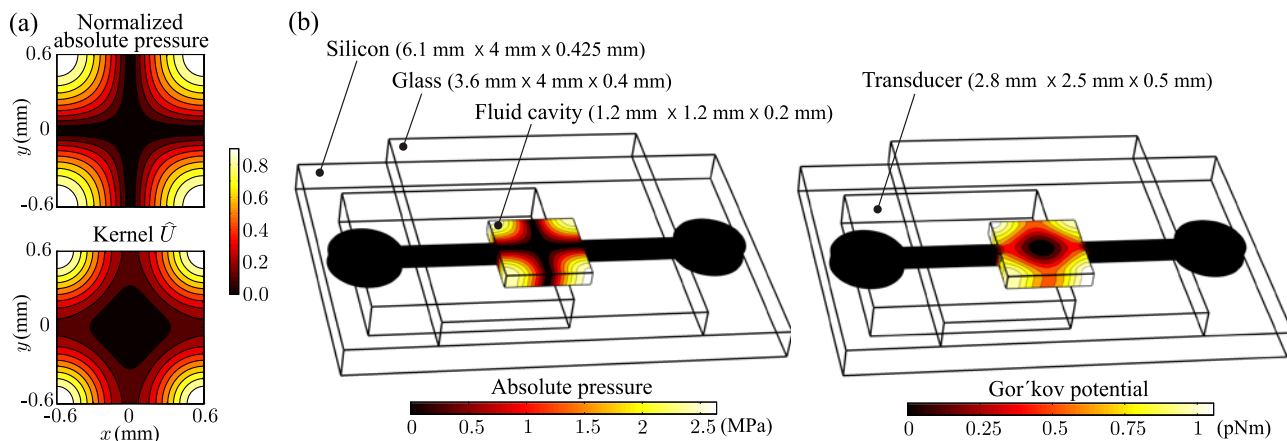


Fig. 2. (a) The normalized absolute pressure field and the kernel \hat{U} of the objective function. They are both calculated based on the theoretically optimal pressure field which is defined by the (1,1)-mode. (b) The simulated absolute pressure field and Gor'kov potential $U(\mathbf{p})$ for the optimized device design. Material and dimensions of the major device components are indicated. Comparing \hat{U} in (a) with the simulated Gor'kov potential $U(\mathbf{p})$ in (b), shows that the automatic design by optimization provides the desired force potential. Despite the low driving voltage of 5 Vpp and realistic damping, the absolute pressure field has a high amplitude.

Conclusion

Design by optimization is a numerical tool for the automated development of particle manipulation devices. Its utility has been proven in two practical examples in which devices have been designed to maximize the radiation forces. As the field of acoustofluidics is moving towards commercial lab-on-a-chip applications, optimal device performance becomes increasingly important whereas our approach is a flexible and powerful method to achieve this goal in a time-efficient manner.

References

- [1] C. T. Leondes, *Structural Dynamic Systems Computational Techniques and Optimization*, CRC Press, 1999, vol. 7.
- [2] P. Glynne-Jones, R. J. Boltryk, and M. Hill, *Lab Chip* **12**, 1417-1426 (2012), DOI: 10.1039/C2LC21257A.
- [3] I. Leibacher, W. Dietze, P. Hahn, J. Wang, and J. Dual, *Microfl. Nanofl.* **16**, 513-524 (2014), DOI: 10.1007/s10404-013-1240-7



Reduction in biofilm formation through the continuous use of ultrasonic standing waves in polymer devices.

Michael Gedge¹, Martyn Hill¹, Dyan Ankrett¹, Peter Glynn-Jones¹.

¹Engineering Sciences,
University of Southampton,
United Kingdom
Email: m.gedge@soton.ac.uk

Introduction

Polymer sensors left in a marine environment suffer from the effects of biofilm accumulation. Biofilms are comprised of microorganisms and extracellular polymeric substance (EPS) and are formed when bacteria adhere to a wetted surface. The bacteria then excrete slime like EPS which aids the adherence of other microorganisms such as fungi, yeast, algae and other bacterial species [1]. The presence of biofilms will have detrimental effects on the performance of marine sensors. Mechanical and chemical cleaning options exist but are either expensive or likely to reduce the working life of the system. The formation of biofilms in microfluidic channels will also have detrimental effects on flow rates and could eventually lead to clogging. For these reasons it is important to protect *in-situ* oceanographic sensors from biofouling. Ultrasonic standing wave technology has been applied to polymer channels and has been shown to lead to a reduction in biofilm formation.

Designing ultrasonic devices in polymer differs from more conventional ceramic designs, the acoustic quality factor of the materials will not be as high but devices are less sensitive to small changes in dimensions. The difficulty is in designing and manufacturing the polymer layers so that the node is positioned correctly and so that no antinodes are present in the channel, as this would lead to enhanced biofilm growth at the boundaries. As the acoustic impedances of PMMA and water are not too dissimilar, they act almost as one continuous material, allowing any fraction of a standing wave to be set up in the fluid cavity. This differs from the more conventional half wave and quarter wave designs of ceramic devices. Efficiency gains can be made by reducing the volume of plastic used in comparison to the fluid volume, as excess plastic will dissipate energy. Modelling and experimental work has shown that as the volume of plastic decreases the flexibility increases which can produce complex modal patterns and poor repeatability.

Experiment

Polymer channels were milled into sheets of polymethylmethacrylate (PMMA) and were bonded together using a 1:2 solution of acetone and ethanol, [2]. Lead zirconium titanate (PZT) transducers were clamped to half the channels and all were connected in parallel to a solution of sterile artificial seawater called minimal marine media with nutrients (3MN) seeded with *Vibrio natriegens*, [3]. Four polymer devices were used per experiment, half of which were ultrasonically powered. Three experiments were run in series, each of which lasting 1 week. At the end of each experiment individual channels were flushed with distilled water prior to fluorescent labelling with CTC and DAPI to identify actively respiring and the total number of cells respectively. Images were captured along the length of each chip and image analysis was carried out in CellProfiler, [4]. Excitation voltages ranged from 0.5 – 4 V_{pp} and each experiment had two control channels.

Results

The majority of the bacteria identified in all 12 channels were not actively respiring. As expected, ultrasonic excitation led to a decrease in the quantity of bacteria adhered to the inner surfaces of the devices observed in both the CTC and the DAPI images. Particularly low voltages (0.5 V_{pp}) did not lead to any significant reduction in biofilm formation. The effects of ultrasonic excitation were seen at voltages as low as 1 V_{pp} . Higher excitation voltages (4 V_{pp}) led to a reduction in biofilm formation of over 60% in the respiring cells and 20% in the total number of cells, Figure 1.

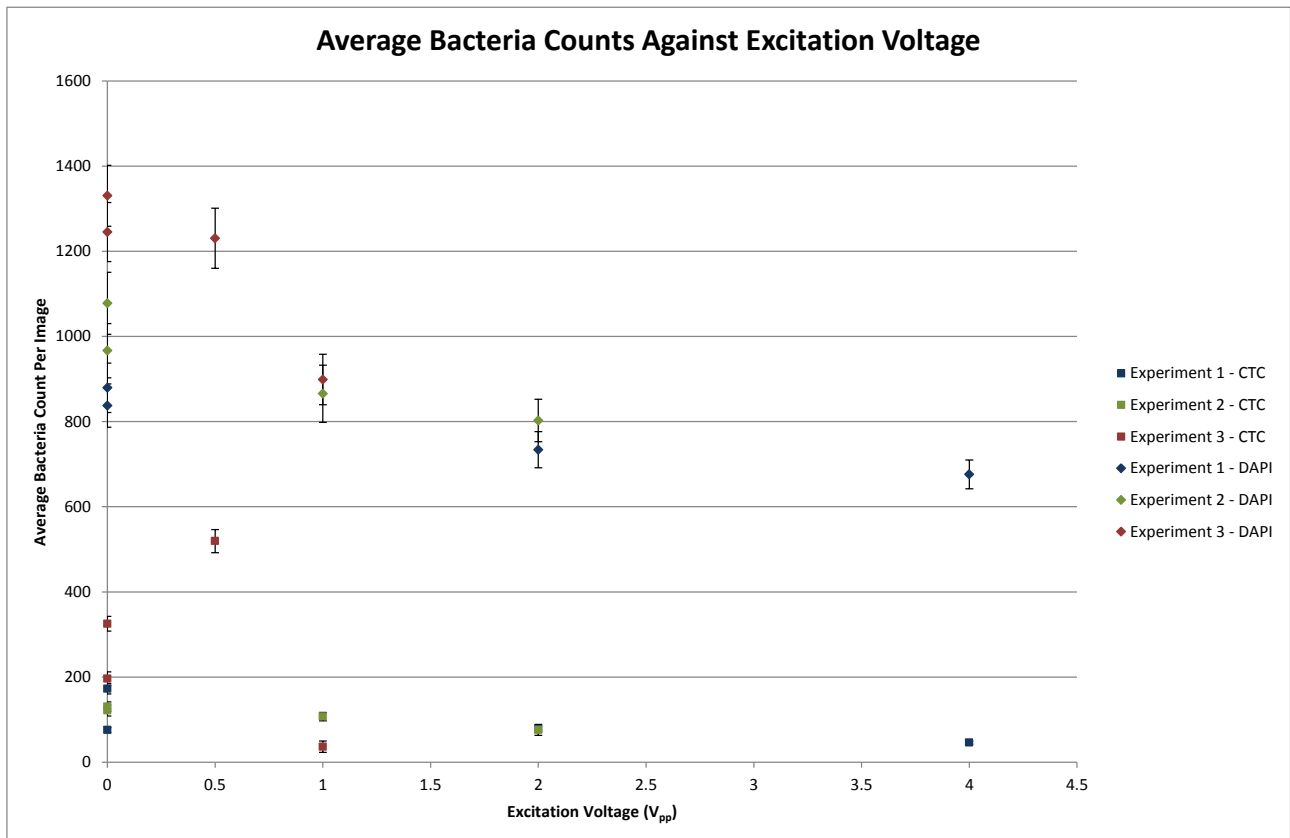


Figure 1: Excitation voltage is plotted on the abscissa and the ordinate refers to the average number of bacteria identified in each chip/dye combination. Error bars are defined as \pm the standard error. Readings of the same dye type share shape and readings from the same experiment share colour. DAPI readings indicate total cell count whilst CTC readings indicate respiring cells. Ultrasonic excitation led to a reduction in biofilm formation in every slide. Every experiment also showed a drop in the number of actively respiring cells, excluding the chip powered at 0.5 V_{pp} .

Conclusions

Ultrasonic excitation has been shown to reduce the number of bacteria that adhere and grow in a polymer microfluidic device. Excitation voltage of 0.5 V_{pp} lead to a noticeable increase in actively respiring cells but the total quantity of bacteria observed was reduced. Once excitation reached 1 V_{pp} a reduction in biofilm formation was seen at every level of excitation in both dye sets. This data demonstrates the potential of low power ultrasonic excitation as an anti-biofouling methodology. It is hoped that further optimisation of this methodology will lead to more significant, and consistent reductions in biofouling. This work also shows that robust ultrasonic devices can be made from polymers and can operate for relatively long time periods.

References

- [1] Z. Lewandowski, *Fundamentals of Biofilm Research*: CRC Press, 2007.
- [2] N. Harris, A. Keating, and M. Hill, "A Lateral Mode Flow-through PMMA Ultrasonic Separator.," presented at the APCOT2010, Perth, Western Australia., 2010.
- [3] R. G. Eagon, "Pseudomonas Natriegens, A marine bacterium with a generation time of less than 10 minutes.," *J. Bacteriology.*, vol. 83, pp. 736-737, 1962.
- [4] A. Carpenter, T. Jones, M. Lamprecht, C. Clarke, I. Kang, O. Friman, *et al.*, "CellProfiler: image analysis software for identifying and quantifying cell phenotypes," *Genome Biology*, vol. 7, p. R100, 2006.

Imaging cytometer with acoustic focussing

Robert Žmijan, Yu Kochi,
Martyn Hill, and Peter Glynn-Jones

Engineering Sciences
University of Southampton
University Road
Southampton
SO17 1BJ
Email: r.zmijan@soton.ac.uk

Introduction

Due to the short exposure time of the sample to a photosensitive element, characterisation of fluorescent objects in flow cytometry usually requires high sensitivity sensors, for example photomultipliers. In general, image flow cytometry has the potential to offer better specificity than conventional flow cytometry, however, the limiting factor is the sensitivity of the CCD element of the camera. The high throughput and high sensitivity of flow cytometers is especially desired in detection and identifying circulating tumour cells (CTC) in blood. Recently, an approach to implement imaging cytometry for CTC detection in blood used a TDI (Time Delay and Integration) CCD camera observing a moving tray containing a single layer of blood cells [1]. Performance of a cytometer device depends of the quality of the particle focussing mechanism, with single file coaxial hydrodynamic focussing still being the most widely used approach. Acoustic streamline particle focussing has already been employed in commercial cytometer devices such as Attune NxT [2]. Our approach also uses acoustic forces, specifically, focussing flowing particles into a single plane.

Experiment

We use acoustic manipulation to focus beads or cells into a single layer as they flow through a rectangular channel. Figure 1 presents the optical schematics of the system. The acoustic focussing maintains the flowing objects in the focal plane of the objective of the camera enabling many particles to be imaged simultaneously.

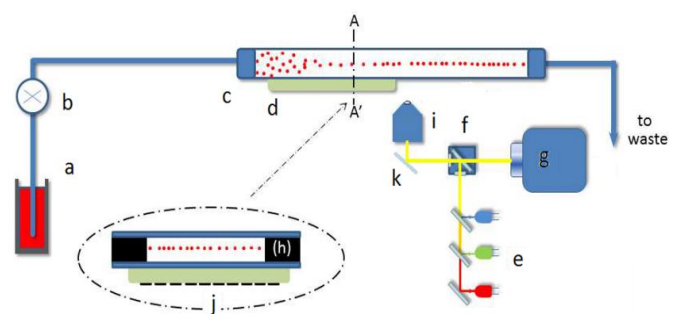
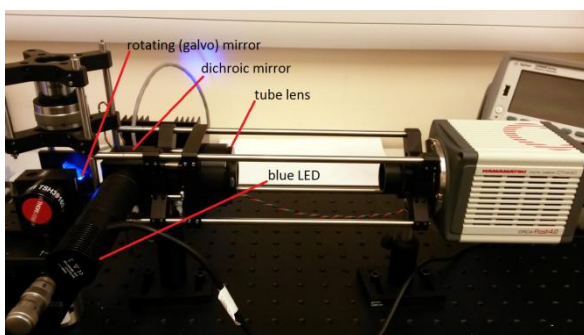


Fig. 1. Photograph of the existing experimental setup, system schematic and operating principle. Diluted sample (a) is pumped (b) through the ultrasonic focus unit (c) which comprises a chamber and piezoelectric transducer (d). The aligned particles are imaged using a CMOS camera (g), with three colour excitation light (e) via a triple-band filter cube (f). Apart from the infinity focused objective (i), lenses are not shown. In cross section A-A' the acoustically matched rubber (h) forms the sides of the chamber to prevent acoustic edge effects and in combination with an electrode array (j) ensures planarity in the acoustic alignment. Rotating mirror (k) is synchronised with the velocity of the particles to increase exposure time.

In order to increase the exposure time, a rotating (galvo) mirror is synchronised with the velocity of the particles in the flow cell. The setup consists of a 400 nm collimated LED light source, dichroic mirror, the rotating mirror, 4x microscope objective, a tube lens, and Hamamatsu Flash 4 camera. The rotating galvo mirror is driven from an arbitrary signal generator using a linear tooth saw pattern and adequate frequency to match the velocity of the fluorescent particles in the flow cell. For simplicity we have only used one excitation and one fluorescence wavelength (FITC), however the system can be easily upgraded to detect

other fluorescence wavelengths. The device is compatible with a variety of transparent flow cells. We have tested a commercial rectangular 6x0.3mm glass capillary [3] (figure 2) combined with a piezo-transducer.



Fig. 2. Flow cell made of a commercial rectangular glass capillary with PDMS connectors and PTFE tubing.

The piezo element was driven from a signal generator at 2.32 MHz and sinusoidal waveforms in the range 1-10 V_{pp} to focus in flow 10 μm FITC fluorescent particles into a single layer. The images of the particles flowing at 10 ml/h through the capillary were taken at 30 fps, resulting in a real field of view approximately 3.2x3.2 mm.

Results

The image data were studied using particle image velocimetry (MPIV) toolbox in Matlab [4] (figure 3a). Figure 3 shows the particle velocities in the field of view of the camera for two devices, the commercial capillary, and a micro-milled rectangular channel of similar dimensions. Noticeably, the flow profile of the capillary is more parabolic than it would otherwise be for a perfect rectangular channel of 6x0.3 mm. We have discovered that the capillary has a more elliptical cross section, about 30% wider at the centre compared to the width at the sides. This explains why the velocity flow profile is more parabolic for the capillary in comparison to the other device with the same size of rectangular channel (figure 3b).

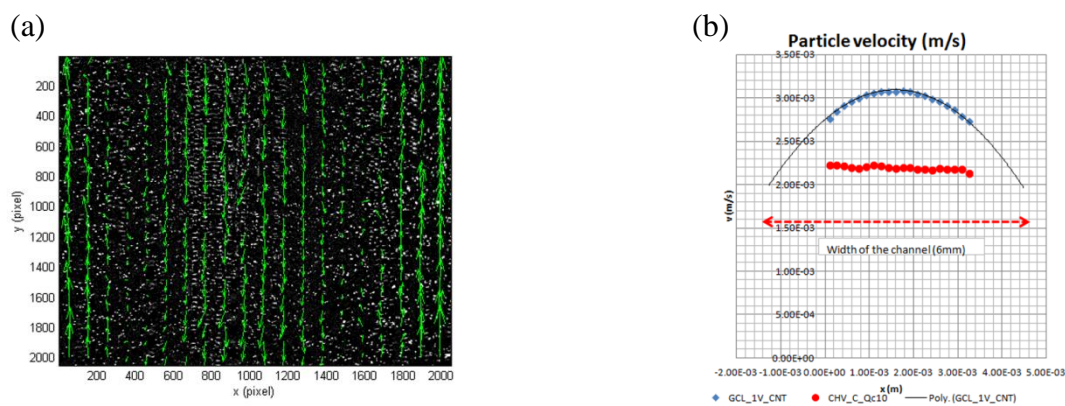


Fig. 3. Superimposed images of flowing particles (top view of the capillary) including velocity vector field calculated using Matlab MPIV library (a), Comparison of velocity profiles of both flow cells, the capillary (blue) and the rectangular channel (red) of similar dimensions (b).

Conclusion

The device has a future potential to become deployed at point of care diagnostics, for routine CTC screening of blood of patients. Future work will focus on upgrading the existing optical setup to include two additional excitation light sources, and LabView software for image acquisition and analysis.

References

- [1] Scholtens, T.M., et al., CellTracks TDI: An image cytometer for cell characterization. *Cytometry Part A*. 79A(3): p. 203-213
- [2] <http://www.lifetechnologies.com/uk/en/home/life-science/cell-analysis/flow-cytometry/flow-cytometers/attune-acoustic-focusing-flow-cytometer.html>
- [3] Hammarstrom, B., et al., Non-contact acoustic cell trapping in disposable glass capillaries. *Lab on a Chip*. 10(17): p. 2251-2257
- [4] Nobuhito Mori and Kuang-An Chang (2003) "Introduction to MPIV", user reference manual, 14p.

Acoustic radiation force of a single beam: towards three-dimensional non-contact manipulation

Diego Baresch^{1,2}, Régis Marchiano² and Jean-Louis Thomas¹

¹Institut des Nanosciences de Paris
 Université Pierre et Marie Curie
 4, Place Jussieu
 75005, Paris, FRANCE
 Email: diego.baresch@upmc.fr
jean-louis.thomas@upmc.fr

²Institut Jean Le Rond D'Alembert
 Université Pierre et Marie Curie
 4, Place Jussieu
 75005, Paris, FRANCE
 Email: regis.marchiano@upmc.fr

Introduction

Standing acoustic waves are a powerful tool to levitate single or multiple particles [1]. In particular ultrasonic acoustophoresis has proven to assist with the challenges of complex microfluidic environments [2,3]. However in these strategies the actuation is in general unidirectional and environment dependant. A single ultrasonic beam is appealing for accurate manipulation at the single particle level but despite early attempts [4,5] elastic particles have the propensity to be expelled from the focus of such beams. We present a theoretical analysis of the trapping behaviour of particular beams, acoustic vortices [6], selected candidates to achieve three-dimensional particle manipulation. Preliminary insights on their experimental synthesis are given.

Acoustical radiation force of a vortex beam.

We have calculated the radiation forces exerted on a small polystyrene sphere by an incident vortex beam. This is achieved with a recent three-dimensional framework developed in acoustics [7,8]. In Fig. 1(a), the incident pressure is modelled by Rayleigh's integral with a pupil function varying with the azimuthal angle φ . The acoustic intensity vanishes on the propagation axis as a consequence of a phase singularity and helicoidal wavefronts. This singularity gives unique features to the radiation force vector (Fig. 1(b)) where both radial and axial components act as restoring forces and bear witness of a three-dimensional trap for elastic particles.

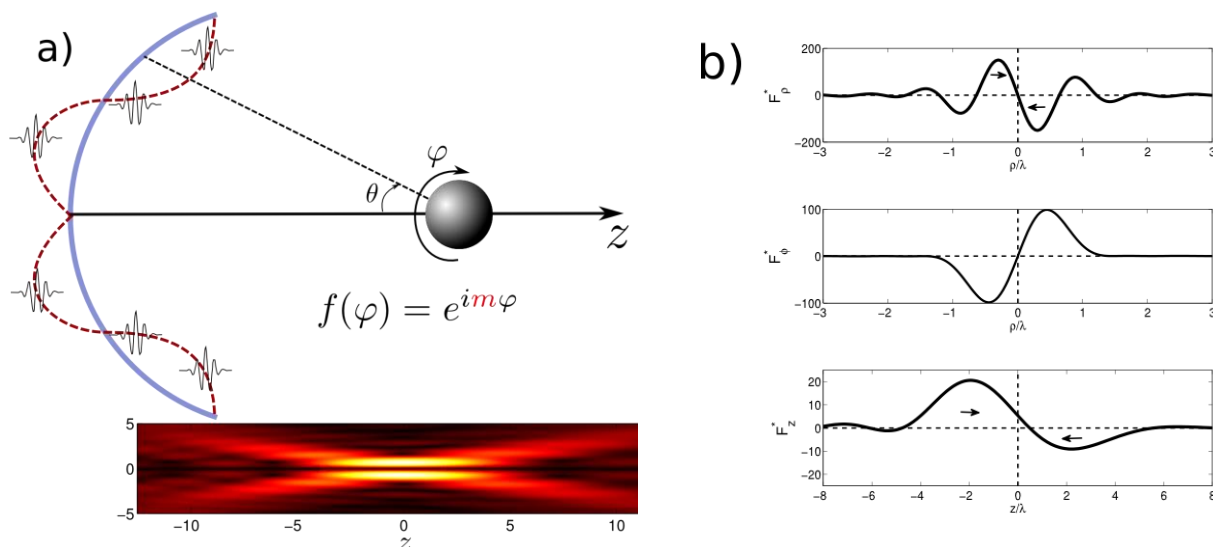


Fig. 1. (a) The incident wavefront is tailored at the focused emitter's surface to obtain an incident helicoidal vortex beam. The theoretical incident beam is represented in a plane in the direction of propagation by a colorplot. (b) The radial, azimuthal and axial

components of the force (nN) acting on a polystyrene sphere of radius 200 microns. They are functions of the displacement of the particle away from the focus.

It has already been experimentally observed and predicted that a simply focused beam, to say a Gaussian beam, generally violently pushes solid particles away from the focus. This problem has only been circumvented by counter propagating two beams in opposite direction [5] or blocking the axial force with a polyethylene film [6]. Here the results suggest the existence of a negative axial force attracting the particle towards the focus.

Experimental synthesis of a vortex beam

In Fig.2.a), a sketch of the experimental set-up is shown. An ultrasonic array of 127 transducers is immersed in a water tank. Each transducer can be driven independently by a multiple output generator at their central frequency $f=1\text{MHz}$. An acoustic lens (carved in PMMA) ensures tight focusing of the ultrasonic beam. A membrane hydrophone mounted on a three axis motorized positioning system scans the acoustic pressure field. We use a versatile and robust method to synthesize complex wavefronts [6]. In Fig.2.b), we scanned the incident beam in the direction of propagation (axis z) and represented the absolute value of the pressure field. It can be seen that our experimental beam reproduces the modelled acoustic vortex with fidelity.

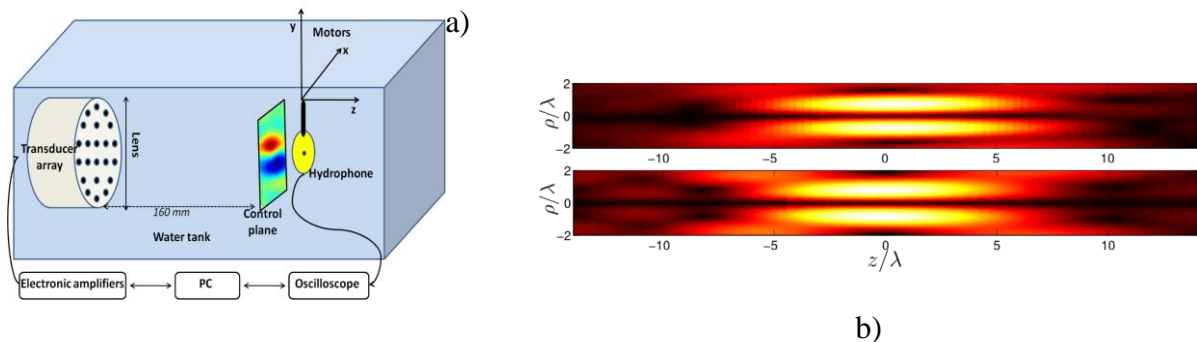


Fig. 2. (a) A sketch of the experimental set-up comprising an array of ultrasonic transducers, a focusing lens, and a membrane hydrophone. (b) Scanned (upper colorplot) and theoretical (bellow) vortex beams in the direction of propagation. The absolute value of the pressure is represented.

Conclusion

We have analysed the acoustic radiation force exerted by an incident ultrasonic vortex beam on an elastic particle. Theory supports the existence of a three-dimensional trapping behaviour of these peculiar wavefields that will attract elastic particles towards the focus. Preliminary experimental results demonstrate that the versatile synthesis method is capable of generating such beams and we expect to affect the dynamics of elastic particles in a manner consistent with our predictions. Single beam acoustical tweezers will become a powerful tool for non-contact manipulation tasks and may be scaled to higher frequencies in the perspective of assisting in complex microfluidic environments.

References

- [1] D. Foresti et al., *Acoustophoretic contactless transport and handling of matter in air*, P.N.A.S, **10**, 1073, (2013).
- [2] T. Laurell et al, *Chip integrated strategies for acoustic separation and manipulation of cells and particles*, Chem.Soc.Rev, **36**, (2007).
- [3] P.B. Muller et al., *Ultrasound-induced acoustophoretic motion of microparticles in three dimensions*, Phys. Rev. E, **88**, 023006 (2013).
- [4] J. Wu, *Acoustical Tweezers*, J. Acous. Soc. Am. **87**, 997 (1991).
- [5] J. Lee et al., *Single-beam acoustic trapping*, Appl. Phys. Lett. **95**, 0737701 (2009).
- [6] J-L. Thomas et al, *Pseudo angular momentum and topological charge conservation for nonlinear acoustical vortices*, Phys.Rev.Lett. **91**, 24 (2003).
- [7] D. Baresch et al, *Three dimensional acoustic radiation force on an arbitrarily located elastic sphere*, J. Acous. Soc. Am. **133**, 25 (2013).
- [8] D. Baresch et al, *Spherical vortex of high radial degree for enhanced single-beam tweezers*, J. App. Phys. **113**, 184901 (2013).

3D printing of metamaterials for use at ultrasonic frequencies

Simon Leigh¹, Stefano Laureti^{1,2}, Peter Morrison¹, David Hutchins¹ and Marco Ricci²

¹School of Engineering
University of Warwick
Coventry
CV4 7AL, UK
Email: S.J.Leigh@warwick.ac.uk
URL: ww2.warwick.ac.uk/fac/sci/eng/research/sensors/dmtl

²Polo Scientifico Didattico di Terni
Università degli Studi di Perugia
05100 Terni
ITALY
Email: marco.ricci@unipg.it

Introduction

There has been a significant increase in research into acoustic metamaterials in the last few years. This is primarily because they can provide characteristics that are very difficult to produce in any other way. Examples include cloaking (*i.e.* the ability to bend signals around an object rather than reflect from it), and the ability to design new lens structures without using classical refraction. There are two basic types of acoustic metamaterial. The first uses scattering from periodic structures to achieve effects such as focussing at specific frequencies. These materials are sometimes referred to as phononic crystals [1]. The other approach includes structures through which signals are transmitted along carefully-designed channels, often employing resonance within them [2]. There are challenges in fabricating such structures, especially as there is much interest in extending their operation to ultrasonic frequencies. This paper reports that such structures can potentially be fabricated using 3D printing.

Formation of an array of scattering spheres

We have performed experiments using ultrasonic particle manipulation to fabricate regular arrays of polystyrene microspheres, whose size distribution is shown in Fig. 1(a). These will form the primary scattering mechanism for metamaterial operation. The polystyrene microspheres were suspended in water, and trapped between two glass slides. An ultrasonic transducer was then operated continuously at frequencies which could be varied over the 200–900 kHz range using the experimental arrangement shown in Fig. 1(b). This created a regular pattern of spheres. This pattern could then be recorded as either the thickness of the liquid layer or the excitation frequency was adjusted. The result of such an experiment at 750 kHz is shown in Figure 2, where it can be seen that the particles have formed into a periodic structure. Currently, water is being replaced by liquid polymer; a micro-stereolithography (MSL) process can then be used to solidify individual metamaterial layers.

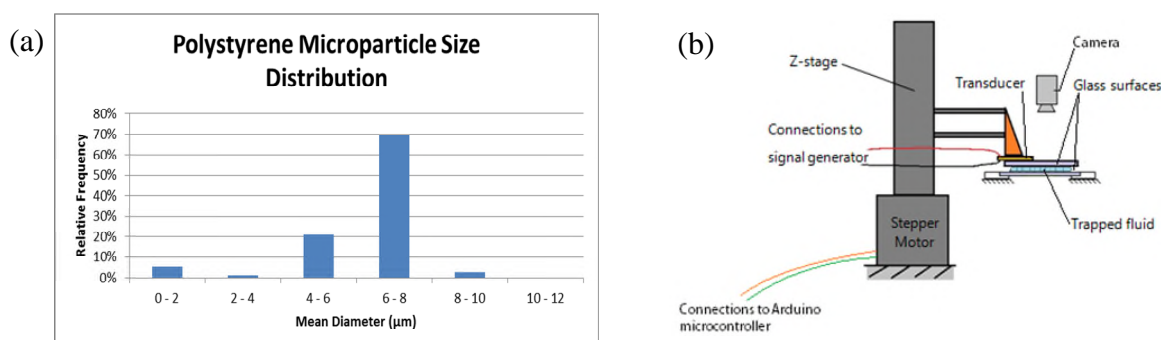


Fig. 1. (a) Size distribution of polystyrene microspheres used in the experiment. (b) Experimental arrangement, with the polystyrene microspheres suspended in water between two glass slides.

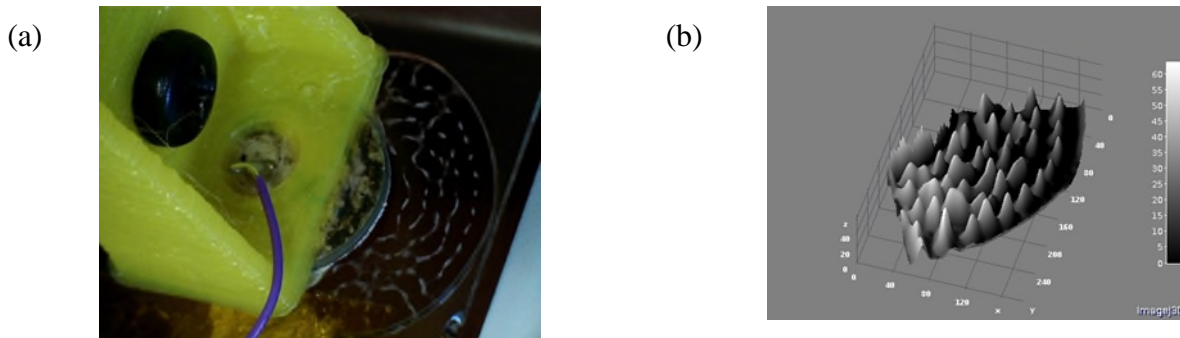


Fig. 2. (a) Pattern caused by ultrasonic excitation. (b) 3D surface plot of the particle distribution derived from the optical data.

3D-printed metamaterials

The alternative design of metamaterial uses channels through which the ultrasound propagates. Here, the aim is to create an array of Fabry-Perot resonant cavities, each with a sub-wavelength aperture. The waves emanating from these structures then interact to give interesting behaviour. The current work has constructed a single channel using fused deposition modelling (FDM), with the design shown in Fig. 3(a). This was then tested using a carefully-designed ultrasonic source and a vibrometer receiver (via a thin polymer film stretched across the output). The results are shown as the dotted line in Fig. 3(b) for a swept-frequency (chirp) excitation (shown as the solid line). Three clear resonant peaks are shown, these being the fundamental resonance and subsequent harmonics.

Analysis shows that the number of resonances available is limited by the need to have a sub-wavelength width to the channels, with the thickness of the material giving the fundamental resonant frequency. Theoretically, it should be possible to generate signals at much higher harmonic numbers than shown here. This is currently being investigated.

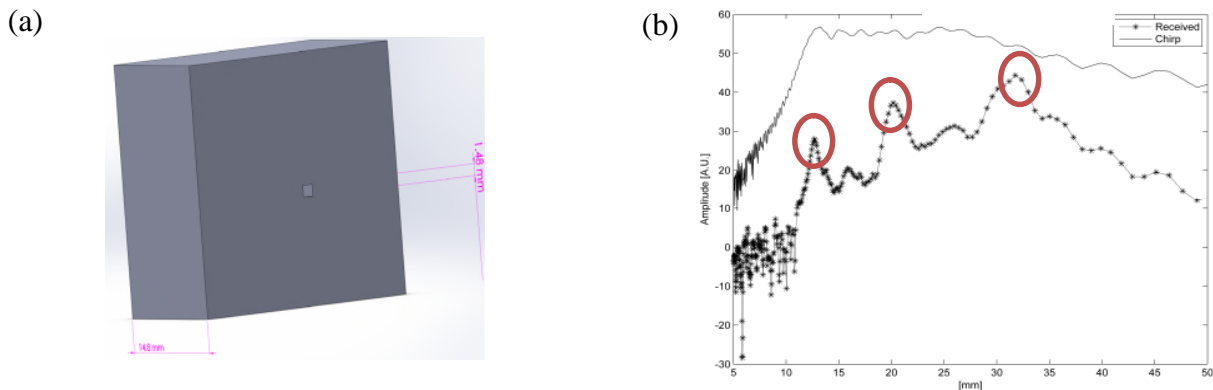


Fig. 3. (a) The single channel model. (b) The through-transmitted signal in air, showing the expected Fabry-Perot resonances.

Conclusions

It is possible to use various 3D printing strategies to produce different types of metamaterial structures. Such structures could be very useful in future for many applications of ultrasound, as they provide characteristics that are not possible using conventional ultrasonic components.

References

- [1] N. Fang, D. Xi, J. Xu, M. Ambati, W. Srituravanich, C. Sun, and X. Zhang, "Ultrasonic metamaterials with negative modulus.," *Nat. Mater.*, vol. 5, no. 6, pp. 452–456, 2006.
- [2] S. Yang, J. Page, Z. Liu, M. Cowan, C. Chan, and P. Sheng, "Ultrasound Tunneling through 3D Phononic Crystals," *Phys. Rev. Lett.*, vol. 88, no. 10, p. 104301, 2002.



Hydrodynamic particle interactions in liquid suspensions acoustically induced in microchannels

Almudena Cabañas¹, Itziar González¹

¹Group of ultrasonic Resonators
Institute of Physical Technologies ITEFI
CSIC, Serrano 144,
28006 Madrid, Spain
Email: iacgg38@ia.cetef.csic.es
URL: <http://www.csic.es/web/guest/centros-de-investigacion1>

Introduction

We present an analysis of micron-sized particles immersed in water interacting under the action of ultrasounds in a single half-wavelength cavity. The experiments show different interacting behaviour depending on their location with respect to the pressure node position of the standing wave. Different second-order hydrodynamic mechanisms seem to govern their motion that can be associated to the disturbances of the axial and lateral radiation force components respectively.

Experiment

We have used a microfluidic square capillar of 700 μm inner width and depth (Fig. 1.a). It was mounted on a square piezoelectric transducer pz26 with a 1mm thickness.



Fig. 1. a) The square capillar with a length $l = 40$ mm, inner width $w = 0.7$ mm, and inner height $h = 07$ mm. It is glued to a piezoelectric ceramic pz26 (30.0 mm \times 30 mm \times 1.0 mm) and mounted under the microscope attached to a high-speed CCD camera. The piezo has the dimension. b) Both small and large particles collect almost perfectly aligned at the channel center driven by the primary radiation force, generating a 1D chain along the channel length

Dilute aqueous bidisperse suspensions ($C_v < 0.1$ g/mL) containing 6 μm and 20 μm -diameter polystyrene microbeads were injected into the microchannel and subjected to a plane standing wave at a frequency of $f = 1.154$ MHz at which the channel cross square section acts as a half-wavelength resonator, providing a pressure node at the centre along the channel length, where the particles collect in a single line due to the primary radiation force (Figure 1.b) exerted in both x-z dimensions .

The particle dynamics was analyzed from the observed motion of the microbeads recorded by a high-speed CCD camera, during their drift motion toward the node of pressure established at the centre of the channel and after it, once collected along a single line. Special attention was paid on pairs of particles that experienced approaching processes with and without collision. Hydrodynamic mechanisms governing these interactions could be identified by the particle center-line orientations with respect to the acoustic axis at the given driving frequency f of resonance.

Results

Once collected, the particles experience a second order lateral radiation force exerted along the pressure node line, giving rise to their longitudinal displacements toward certain locations of acoustic equilibrium within it. The particles coming from both sides are pushed to a single central point and are forced to break partially their line-formation. As this motion is not exactly symmetrical due to the physical features of the device, some of these aligned particles jump out breaking the linearity of the particle chain. As a result of the two orthogonal forces appearing perpendicular to the chain line a rotation is generated around it (reminding that the resonance is exerted across both the y and z-direction of the channel square cross section). The filmed images of Figure 3.a, taken from a single movie evidences this over-induced motion.

Interaction between single particles

Hundreds of movies show weak particle interaction processes developed in water always from distances not much larger than their diameters. This behavior is quite different than those of aerosols, in which hydrodynamic attraction processes developed at low frequencies have been observed from much larger distances, up to 20 times their diameters [1,2]. Not any attraction process has been observed between particles exactly aligned along the acoustic axis. However, angles slightly higher seem to be suitable in for some pairs of nearby particles that described in the experiments approach paths during their drift motion toward the pressure node from distances of the order of their diameters and with their center-lines almost aligned with acoustic axis. (Figure 3.b).

After their collection within the pressure node location, the particles develop several mutual approaching processes along this line, with their centre-line perpendicular to the acoustic axis. This type of interaction can answer to the Bjerkness forces, whose theoretical models predict maximal attractions at $\theta=90^\circ$.

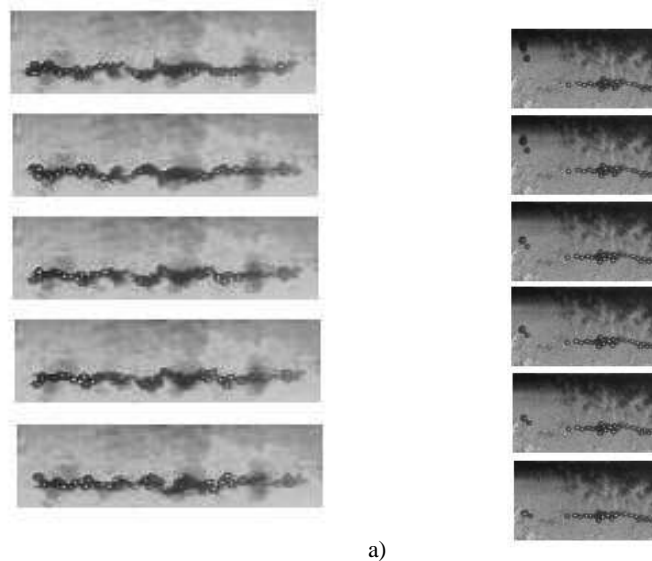


Fig. 3. a) reconstruction of a precession motion experienced by a particle chain around its axis due to the lateral radiation force. Once collected the particles experience a second order lateral radiation force displacing the chains of particles
b) reconstruction of an attraction process developed between two particles before reaching the pressure node (left side of the image)

Conclusion

We have analyzed the acoustically induced motion of microbeads in dilute, aqueous solutions in straight glass capillaries subject to piezo-induced ultrasound standing waves. The microbead paths have been recorded by a CCD and their dynamics have been analysed. Different mechanisms of interaction govern the particles before reaching the pressure and after collected there, that agree with the acoustic wake effect and mutual radiation force mechanisms respectively.

References

- [1] Hoffmann T. L. and Koopmann G. H., Visualization of acoustic particle interaction and agglomeration: Theory and Experiments, *Acoust. Soc. Am.* 99 (4) 1996, 2130-2141
- [2] I. González, T.L. Hoffmann, J.A. Gallego-Juárez, Visualization of hydrodynamic interactions: Validation of a numerical model, *ACUSTICA united with ACTA ACUSTICA* 88(1)19-26 (2002)
- [3] Song L. Modeling of **acoustic agglomeration** of aerosol particles,” Ph.D.Penns Univ. 1990



Schlichting streaming caused by Scholte waves in an electrochemical cell

Sabrina Tietze, and Gerhard Lindner

Institute of Sensor and Actuator Technology
Coburg University of Applied Sciences and Arts
Am Hofbräuhaus 1b
96450 Coburg, Germany
Email: sabrina.tietze@isat-coburg.de
URL: www.isat-coburg.de

Introduction

Aiming at an acceleration of electrochemical reactions by surface acoustic waves excited on the electrodes of an electrochemical cell different mechanisms have been observed so far [2]: In an electropolishing experiment the polishing current could be increased considerably by exciting surface acoustic waves on the anode. The dominating effect turned out to be the disturbance of the diffusion boundary layer by Scholte waves [1], which caused Schlichting streaming near the solid-liquid boundary [3, 4]. In a certain frequency range, however, a substantial additional increase of the electropolishing current has been observed [2], which was supposed to result from a characteristic electrode-transducer resonance. In order to obtain a better understanding of these processes, scanning laser vibrometer measurements of the system were compared with the camera observations of the streaming profiles.

Experiment

The experiments were performed in an electropolishing cell with copper electrodes and a high-viscous phosphoric acid electrolyte. Scholte waves have been generated on the anode of the system by a piezoelectric transducer glued to it. A camera with macrolens was used for recording the streaming pattern in the electrolyte near the electrode caused by the Scholte waves. Before starting the experiments the propagation of surface acoustic waves on the electrode was measured by a Scanning Laser Doppler Vibrometer (SLDV) out of the electrolyte and the frequency was identified, at which the highest amplitude occurred. Subsequently, in the electropolishing experiment, the electropolishing current was measured at different frequencies and streaming pattern at the solid-liquid boundary was recorded simultaneously.

Results

The measurements with the SLDV revealed the propagation surface acoustic waves across the whole area of the electrode with different wavelengths at frequencies of 710 kHz and 240 kHz, at which the giant enhancement of the electropolishing current has been observed, see Figure 1. Whereas at 710 kHz undisturbed plane waves were observed, there seems to be some interference disturbance at 240 kHz. The amplitudes could not be compared, however, since different transducers were used in both cases.

During the electropolishing process in the electrolytic cell vortices in the boundary layer caused by acoustic streaming became visible from the camera records at both frequencies (Figure 2). The extension of the vortices, however, changed with the wavelength of the acoustic waves. Since the acoustic streaming pattern could be observed along the whole length of the electrode it is attributed to Scholte waves, which can propagate along the solid-liquid boundary without major dissipation. The vortex pattern of the streaming profile is characteristic for Schlichting type streaming.

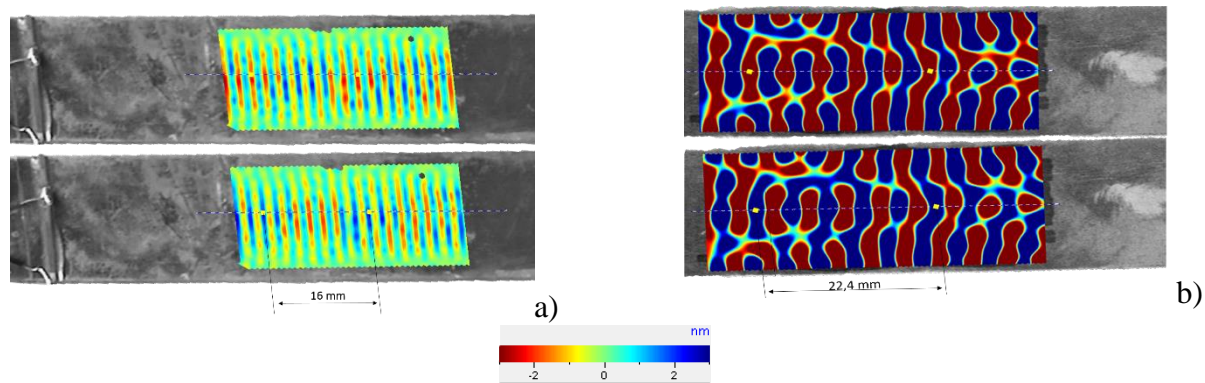


Figure 1. Visualization of the wave propagation on 1 mm thick copper electrodes (phase of vibration 0 and π) measured with the SLDV at (a) 710 kHz and (b) 240 kHz. The colours represent the amplitudes of the displacements on a nanometer scale.

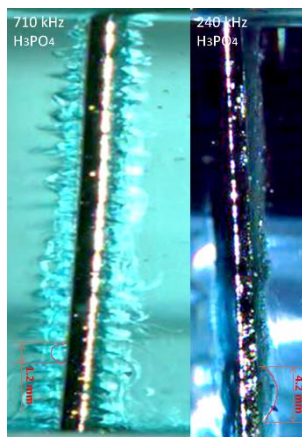


Figure 2. 1 mm thick copper electrodes of an electropolishing cell immersed into an phosphoric acid electrolyte in the polishing mode with surface acoustic waves at a frequency of 710 kHz (left) and 240 kHz (right) recorded by a camera with macro lens.

A comparison of the acoustic wavelengths calculated from the corresponding frequencies, the wavelengths measured by SLDV and the dimensions of the vortices is provided by Table 1. Whereas the calculated and measured acoustic wavelengths on one hand and the dimension of the vortices on the other hand are comparable at 240 kHz, they differ by a factor two in the case of 710 kHz.

Table 1. Comparison of calculated and measured acoustic wavelengths and vortex diameters

frequency	$\lambda_{\text{acoustic wave, theoretical}}$	$\lambda_{\text{acoustic wave, measured}}$	d_{vortex}
240 kHz	4.6 mm	4.5 mm	4.2 mm
710 kHz	2.4 mm	2.0 mm	1.2 mm

Conclusion

In an electrochemical cell the current in the electropolishing regime could be substantially enhanced by exciting surface acoustic waves on the anode. From the vortex-type acoustic streaming pattern observed along the electrode it is concluded that Schlichting type streaming has been excited by Scholte waves propagating along the solid-liquid interface causing an effective mixing of the diffusion boundary layer. At 710 kHz the vortex diameter became much smaller than the acoustic wavelength in contrast to lower frequencies.

Acknowledgements

This work has been supported by the government of the Federal Republic of Germany (“Forschungsinitiative Energiespeicher”, BMBF and BMU, project no. 03SF0437A). The experimental support from Sandra Ebert is gratefully acknowledged.

References

- [1] M. de Billy and G. Quentin, *Experimental study of the Scholte wave propagation on a plane surface partially immersed in a liquid*, J. Appl. Phys. 54(8), pp. 4314-4322 (1983).
- [2] S. Tietze, J. Schlemmer and G. Lindner, *Influence of surface acoustic waves induced acoustic streaming on the kinetics of electrochemical reactions*, Proc. SPIE 8923, 89231B (2013).
- [3] M. Wiklund, R. Green and M. Ohlin, *Acoustofluidics 14: Applications of acoustic streaming in microfluidic devices*, Lab Chip 12(12), pp. 2438-2451 (2012).
- [4] L. D. Rozenberg, *High-intensity ultrasonic field*, New York: Plenum Press (1971).



Low Frequency Capture of Nanoparticles

Prashant Agrawal^{1,2,3}, Prasanna S. Gandhi³, Adrian Neild¹

¹Laboratory for Micro Systems
Department of Mechanical & Aerospace
Engineering, Monash University, Clayton, 3800,
Vic, Australia
Email: adrian.neild@monash.edu.au
URL: <http://www.labformicrosystems.com/>

²IITB Monash Research Academy,
Indian Institute of Technology Bombay,
Mumbai,
Maharashtra, 400076, India

³Suman Mashruwala Advanced
Microengineering laboratory, Department
of Mechanical Engineering,
Indian Institute of Technology Bombay,
Mumbai,
Maharashtra, 400076, India

Introduction

At ultrasonic frequencies, the capture of sub-micron diameter particles is hindered by acoustic streaming, the same is true for low frequency vibration (in the order of 100Hz). The horizontal actuation of a fluid filled open rectangular chamber, results in the formation of capillary waves at the liquid-air interface, which is accompanied with a spatially varying flow field in the bulk fluid. This flow field can be used to collect particles at stable locations due to inertial effects, whereas it also gives rise to the rotational streaming flows. By considering the factors which reduce the streaming hindering this collection, we demonstrate the capture of particles as small as 50nm in diameter.

Results

Comsol Multiphysics has been used to model the first and second order fluid flow fields in an open chamber excited by low frequency vibration. It is well known that in such regimes, particles will collect at certain locations under the capillary wave which forms at the air-water interface due to the first order field. These locations depend on whether the excitation is horizontal¹ or vertical². By including analysis of the second order field, that termed acoustic streaming, we are able to distinguish whether a particle undergoing excitation will collect or follow the streaming trajectory.

Figure 1 shows the two flow fields. In the absence of the second order field, particles can be expected to collect beneath alternate nodes in the capillary wave, that is at locations of minimum horizontal velocity at the base of the chamber (labelled A, B and C)¹. Examination of the second order field shows that the horizontal component can act to enhance the particle collection at these locations. However the vertical component reaches a maximum upward value directly above the collection locations, and can act to lift the particles into the faster flowing fluid above the base of the chamber, from where they will follow a swirling trajectory in the second order flow field.

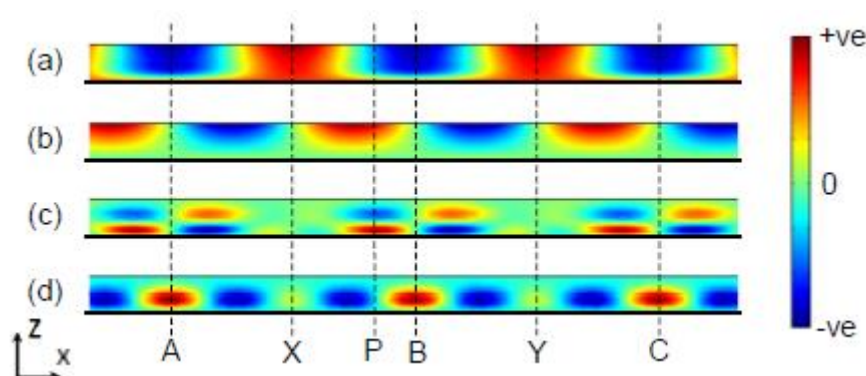


Fig. 1: First and second order fields in a horizontally actuated chamber (a) first order horizontal flow velocity, (b) first order vertical flow velocity, (c) second order horizontal flow velocity, (d) second order vertical flow velocity (The first order fields are shown at time $t=0$ with an excitation of $\cos(\omega t)$).

By using a particle tracing model, using viscous drag forces derived from the Khan and Richardson expressions³, our simulations show whether a particle collects or circulates. By running multiple simulations for a range of parameter sets, in terms of chamber size, height (both of which affect resonant frequency) and actuation amplitude, we are able to establish the critical particle density for a range of radii; above this density particles will collect, below it they will circulate. This data is presented in Figure 2.

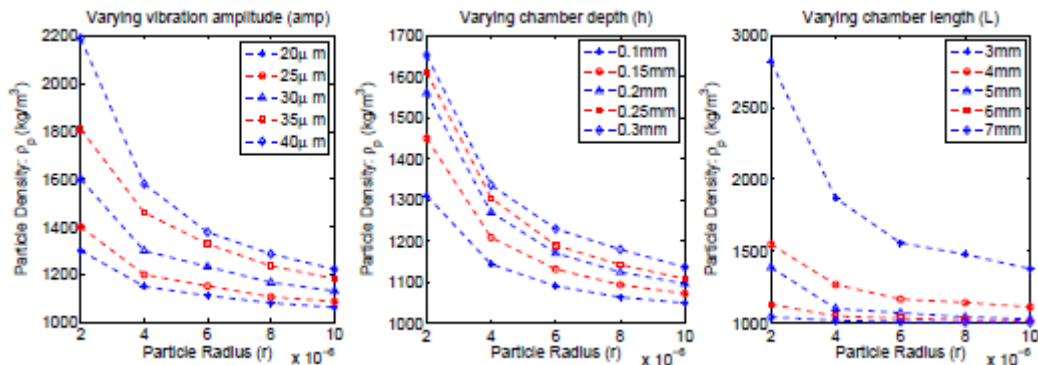


Fig. 2: Particle radius and density cut-offs are shown for varying (a) excitation amplitude, (b) chamber height and (c) chamber length. The data is collected from numerous simulations of the particle trajectory in the combined first and second order flow fields using COMSOL.

It can be seen from Figure 2 that for a particle of given density, in order to capture increasingly small particles, it is necessary to use a lower amplitude, applied to a chamber of shallower depth and longer length.

This information was used, and extrapolating beyond the simulation data set, we have captured particles as small as 50nm as shown in Figure 3.

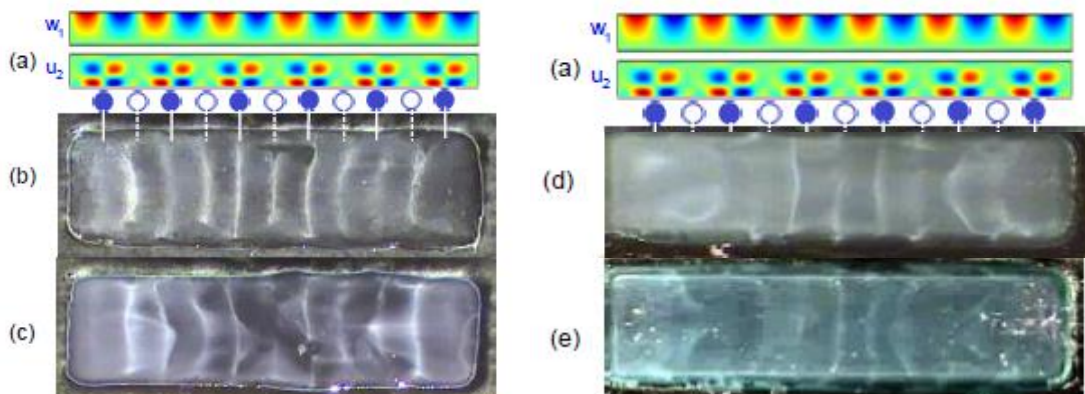


Fig. 3: Collection of Polystyrene particles (density: 1050kg/m^3) in a chamber measuring 8mm by 0.1mm, vibrating at 336 Hz, which corresponds to 6 wavelengths at the interface. The COMSOL plots (a) are shown to discern the position of nodes on the capillary wave (upper) and the collection locations (lower). The collection locations indicated by the solid circles correspond to collection at positions A, B, C in figure 1, and those indicated by the hollow circles correspond to collection at positions X, Y. The particles used have a diameter of (b) 1 μm , (c) 300nm, (d) 100nm, (e) 50nm.

CONCLUSION

Through the examination of the collection force and acoustic streaming, we have shown that vibration, in the horizontal direction, of an open fluid chamber, can result in the collection of sub micrometer sized particles.

References

- [1] P. Agrawal, P. S. Gandhi, A. Neild, The mechanics of microparticle collection in an open fluid volume undergoing low frequency horizontal vibration, *Journal of Applied Physics*, 114, 114904 (2013)
- [2] P. Agrawal, P. S. Gandhi, A. Neild, Quantification and comparison of low frequency microparticle collection mechanism in an open rectangular chamber, *J. Appl. Phys.* 115, (2014) 174505.
- [3] J.F. Richardson, J. H. Harker, J. R. Backhurst, *Particle Technology and Separation Processes* (Butterworth Heinemann, Woburn, MA, 2002) p. 153.



Manipulation of microbubbles in a microfluidic chip using a planar array

Agesinaldo Silva¹, Bruce Drinkwater¹,
Chris Fury^{2,3}, Philip H. Jones³ and Gianluca Memoli²

¹Department of Mechanical Engineering,
University of Bristol,
Bristol, BS8 1TR,
United Kingdom.
Email: b.drinkwater@bristol.ac.uk

² Acoustics and Ionising Radiation Division
National Physical Laboratory
Hampton Rd,
Teddington, TW11 0LW,
United Kingdom.
Email: gianluca.memoli@npl.co.uk

³ Department of Physics and Astronomy
University College London
Gower Street,
London, WC1E 6BT,
United Kingdom.
Email: chris.fury@npl.co.uk

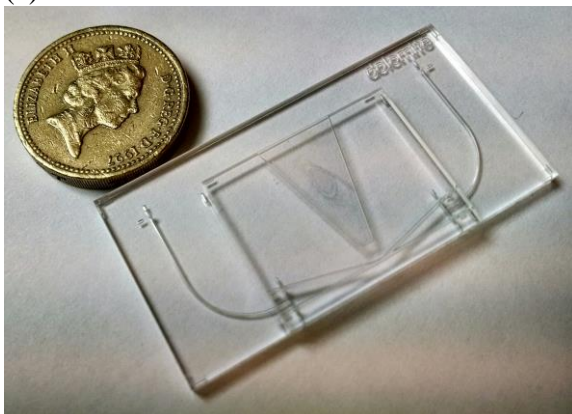
Introduction

Devices that combine optical and acoustic tweezing have recently attracted attention, due to their ability to manipulate objects over a large range of both lengths and forces [1-2]. This combined technology builds upon dexterous ultrasonic tweezer devices, which give an increasing spatial control [3]. In this paper we describe modelling and experimental validation of the performance of an ultrasonic manipulator, designed to accurately position microbubbles where the simultaneous use of optical tweezers is desired. This device is based on a glass microfluidic chip containing various micro channels along which the microbubbles are manipulated [4]. A planar array of piezoelectric elements [5] is used for manipulation, bringing microbubbles from an inlet to the centre of the chip, where the optical tweezer system is focused.

Experiment

The microfluidic glass chip, designed at NPL and assembled by Dolomite, contains a K-shaped manifold of microchannels as shown in Fig. 1(a). We inject a dilute, aqueous suspension of 10-15 μm diameter polymer coated microbubbles (ExpancelTM) into the microchannel. We have mounted a planar ultrasonic array on the front edge of the chip, Fig. 1(b). This array is connected to a signal generator and amplifier via a multiplex unit that enables a sinusoidal voltage to be applied to any of the elements on the array. By selectively exciting a single element, a localised resonance is excited in the microfluidic chip that acts to trap the microbubbles along the main channel.

(a)



(b)

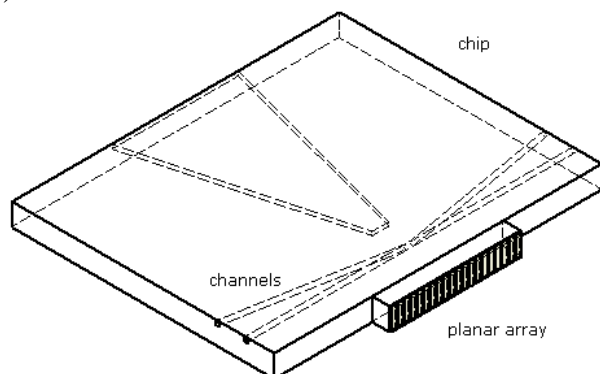


Fig. 1. (a) Photograph of the chip; (b) schematic diagram of the glass microfluidic chip with attached planar array.

Results

A 2D finite element model (COMSOL Multiphysics) was used to simulate pressures within a region close to the planar array. Absorbing layers with increasing damping are used to reduce the size of the model, shown in Fig.2. The planar array is modelled by a 9mm x 0.75mm plate of PZT

(NCE51). The system has been solved in a parametric study over a frequency range of 7.5-9.5 MHz comprising a response spectrum close to a high harmonic transducer resonance.

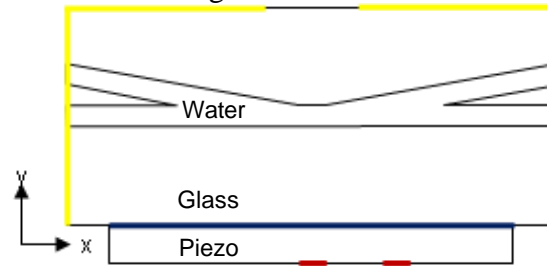


Fig. 2. 2D Finite element model of the glass chip with planar array attached (red = 1 V, blue = ground, yellow = absorbing layer).

Two characteristic modes within this range are discussed here and Fig. 3, which shows the potential energy density around 8.65 MHz by activating two different elements. Fig. 3a suggests that by driving the central piezo element there will be 4 different trapping positions in the central region of the K-shaped manifold (our area of manipulation interest). Fig. 3b, obtained in the simulations by driving a secondary element, suggests that manipulation across the channel is also possible with this transducer configuration. Images will be used to determine the positions of the air filled microbubbles as a function of driving voltage of each active element using image tracking software.

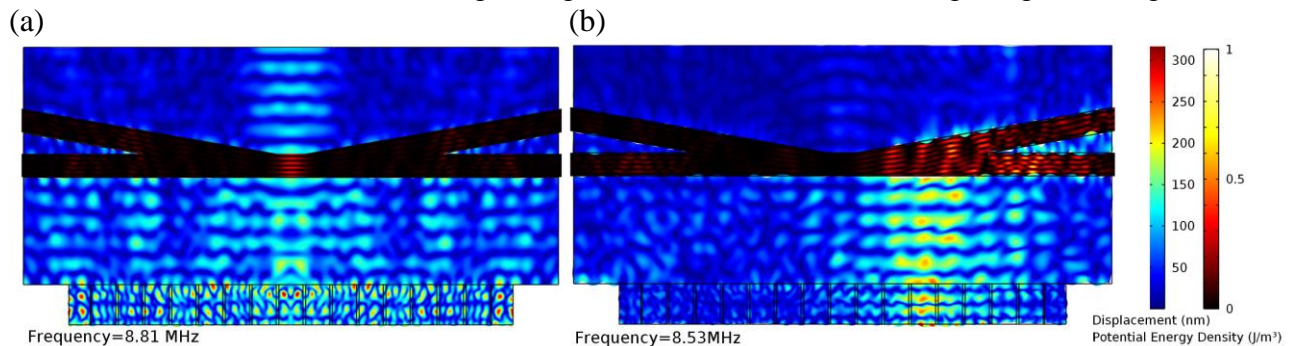


Fig. 3. Potential energy density in the fluid and the y-direction displacement in colour at 8.8 MHz with central element activated (a) and at 8.5 MHz with a secondary element activated (b).

Conclusion

The feasibility of microbubble manipulation has been investigated by exploiting characteristic resonating modes of a dedicated microfluidic chip with an attached planar array. An ultrasonic manipulator could be designed to operate on a fraction of the chip regardless of various geometrical features along the microchannels. Simultaneous optical and acoustic trapping (not described here) will be possible by insonating the microchannel in a small central area of interest.

References

- [1] Bassindale, P. G., Phillips, D. B., Barnes, a. C., & Drinkwater, B. W. (2014). Measurements of the force fields within an acoustic standing wave using holographic optical tweezers. *Applied Physics Letters*, *104*(16), 163504. doi:10.1063/1.4872462
- [2] Thalhammer, G., Steiger, R., Meinschad, M., Hill, M., Bernet, S., & Ritsch-Marte, M. (2011). Combined acoustic and optical trapping. *Biomedical Optics Express*, *2*(10), 2859–70. doi:10.1364/BOE.2.002859
- [3] Courtney, C. R. P., Demore, C. E. M., Wu, H., Grinenko, A., Wilcox, P. D., Cochran, S., & Drinkwater, B. W. (2014). Independent trapping and manipulation of microparticles using dexterous acoustic tweezers. *Applied Physics Letters*, *104*(15), 154103. doi:10.1063/1.4870489
- [4] Fury, C., Gélat, P. N., Jones, P. H., Memoli, G. (2014). Laser vibrometry characterisation of a microfluidic lab-on-a-chip device: a preliminary investigation. *Journal of Physics: Conference Series*, *498*, 012002. doi:10.1088/1742-6596/498/1/012002
- [5] Glynne-Jones, P., Demore, C., Ye, C., Qiu, Y., Cochran, S., & Hill, M. (2012). Array-controlled ultrasonic manipulation of particles in planar acoustic resonator. *IEEE Transactions on Ultrasonics, Ferroelectrics, and Frequency Control*, *59*(6), 1258–66. doi:10.1109/TUFFC.2012.2316